# DISSERTATION

Titel der Dissertation

## Pseudoscalar Fermion-Antifermion Bound States
——Analyzing the Salpeter Equation

angestrebter akademischer Grad

## Doktor der Naturwissenschaften (Dr. rer. nat.)

Verfasser:                      Mag. Zhifeng Li

Matrikel-Nummer:        0447015

Dissertationsgebiet:      Physik

Betreuer:                    Ao. Univ.-Prof. Dr. Franz Schöberl

Wien, am 31. January 2008

**Abstract**

In this thesis we introduce the exact quark propagator function for both the instantaneous Bethe-Salpeter equation and the reduced Salpeter equation. The stability of solutions of the exact-propagator full Salpeter equation and reduced Salpeter equation with various interaction kernels, including Lorentz-scalar, Lorentz-pseudoscalar, Lorentz-vector, time component Lorentz-vector and Böhm-Joos-Krammer (BJK) structure are analyzed. By expanding the Salpeter amplitude to a set of orthonormal functions, we present a numerical tool to transfer the Salpeter equation to a matrix form and obtain the eigenvalues and eigenfunctions for pseudoscalar fermion-antifermion bound states. Furthermore, by using 't Hooft's instanton-induced interaction and applying the numerical method to the study of pseudoscalar $\pi, K, D, D_s, B$, $B_s, B_c, \eta_c, \eta_b$ mesons, we obtain the mass eigenvalues and wave functions for these meson's ground state and excited states within the framework of both the free-propagator and exact quark propagator Salpeter equation. The calculation shows that the exact-propagator contributes non-neglectable effect on the numerical results. In addition, we calculate the decay constant of $\pi, K, D, D_s$ mesons with the exact quark propagator. Finally, we propose a differential equation approach to study the properties of solutions of the full Salpeter equation and reduced Salpeter equation for various Lorentz structures analytically.

# Zusammenfassung

In dieser Arbeit stellen wir die exakte Quark-Propagatorfunktion für die instantane Bethe-Salpeter Gleichung als auch für die reduzierte Salpeter Gleichung vor. Die Stabilität der Lösungen der vollen Salpeter Gleichung mit exaktem Propagator und der reduzierten Salpeter Gleichung mit verschiedenen Wechselwirkungskernen - einschließlich Lorentz-Skalar, Lorentz-Pseudoskalar, Lorentz-Vektor, Zeitkomponenten-Lorentz-Vektor und Böhm-Joos-Krammer (BJK) Struktur - wird analysiert. Durch Entwickeln der Salpeter Amplitude in eine Reihe orthonormaler Funktionen stellen wir ein numerisches Werkzeug vor um die Salpeter Gleichung auf Matrixform zu bringen und um Eigenwerte und Eigenfunktionen der pseudoskalaren Fermion-Antifermion Bindungszustände zu erhalten. Durch die Verwendung von 't Hooft's instanton-induzierter Wechselwirkung und durch Anwendung der numerischen Methode um $\pi, K, D, D_s, B, B_s, B_c, \eta_c, \eta_b$ Mesonen zu untersuchen, erhalten wir außerdem die Masseneigenwerte und Wellenfunktionen für Grundzustände und angeregten Zustände der Mesonen im Rahmen der freien Propagator als auch der Quark-Propagator Salpeter Gleichung. Die Berechnungen zeigen, dass der exakte Propagator zu den numerischen Resultaten einen nicht vernachlässigbaren Beitrag liefert. Darüber hinaus berechnen wir die Zerfallskonstante von $\pi, K, D, D_s$ Mesonen mit Hilfe des exakten Propagators. Schließlich schlagen wir eine Methode mit Differentialgleichungen vor, um die Eigenschaften der Lösungen der vollen und der reduzierten Salpeter Gleichung für verschiedene Lorentz Strukturen analytisch zu untersuchen.

# Contents

# Chapter 1

# Introduction

The understanding of hadronic states' properties is one of the challenging tasks in strong interaction physics research. For more than half a century, the theory about strong interaction physics has been well established and investigated by physicists. A phenomenological theory, quantum chromodynamics (QCD), has obtained great success in describing the hadron's structure and dynamic properties. Although this theory has been well established and developed since 1960s, there is still no consistent and straight way to describe the hadronic properties. Practical calculation can only be performed for some special cases. Due to the large QCD coupling constant, the perturbation theory which is quite successful in QED is not valid for the strong interaction physics at low and intermediate energies.

Therefore as an alternative approach to describe the structure of hadrons - quark models were proposed by Gell-Mann [1] and Zweig [2] as a realization of the basic representation of SU(3) group. These models have been developed to simulate the features of QCD and to depict the hadronic substructure. With numerical calculation, one can use these models to reproduce experimental data of the hadrons such as masses and decay ratio, and describe the observations properties such as confinement in QCD. Some non-perturbative methods, such as lattice QCD calculations, have also been developed.

One of the successful models in describing the properties of heavy mesons and baryons is the nonrelativistic constituent quark model [1, 3]. But it fails to describe the properties of light mesons and baryons since the relativistic effects have to be considered for light constituent masses. Therefore relativistic methods of the quark dynamics are developed in order to describe hadronic properties better.

The Bethe-Salpeter equation is the most general tool for describing the relativis-

tic system in the framework of quantum field theory. It was first proposed by Nambu [10] more than half a century ago, and then was extended to the general form by Bethe and Salpeter [4] based on the Feynmann graph analysis. The Bethe-Salpeter equation was also independently proposed by Schwinger [5] using the functional-derivative formalism, and by Kita [6] employing the S-matrix method. Since then, the study of Bethe-Salpeter equation has been developed and widely discussed in many aspects.

Because the time variable appears in the Bethe-Salpeter equation, it is difficult to solve the general Bethe-Salpeter equation by using either numerical or analytical approach. Therefore some simplification treatments for the Bethe-Salpeter have been proposed. The most popular approach is the so called instantaneous simplification proposed by Salpeter [7]. This approximation scheme is based on two assumptions: instantaneous interaction and free propagator, i.e., the interactions between the constituents of bound state are instantaneous, and every constituent of the bound state propagates as a free particle. With these two assumptions the Bethe-Salpeter equation is reduced to the instantaneous Bethe-Salpeter equation, or Salpeter equation. The instantaneous Bethe-Salpeter equation represents a simplification from four-dimensional space to three dimensional space and avoids the difficulties of the relative time degree of freedom.

Reduced Salpeter equation: Several years ago, Lagaë presented a systematic investigation of the instantaneous Bethe-Salpeter equation [8]. A straightforward reduction method which transforms the instantaneous Bethe-Salpeter equation to a set of coupled equations for Salpeter radial wave functions was also proposed in [8]. Using this method the full instantaneous Bethe-Salpeter equation can be easily transformed to reduced Salpeter equation. Subsequently, employing Lagaë's method Olsson et al. [17, 18] explored the properties of full and reduced Salpeter equation. For several kinds of interaction kernel, such as kernels of time component Lorentz scalar, vector, and full vector types, they investigated the validity of the reduced Salpeter equation. With an instanton-induced interaction, the mass spectra and the weak decays of mesons are investigated in [20, 21, 22, 80].

More recently an instantaneous approximation to the Bethe-Salpeter formalism which retains the exact propagators of the bound-state constituents has been proposed [14]. The relevant analysis shows that the influence of introducing exact quark propagators in the Salpeter equation can not be ignored. The application of the exact quark propagator to the investigation of pseudoscalar bound states with various interaction kernels has been performed in [95].

2

In this work, some new results on pseudoscalar fermion-antifermion bound state mass spectra and decay constant are discussed within the framework of Bethe-Salpeter model. By introducing the exact quark propagator assumption, we analyze the influence of exact-propagator on the mass spectrum and eigenfunctions for pseudoscalar mesons.

This thesis is organized as follows: in chapter 2, starting from Green function, the general properties of Bethe-Salpeter equation and instantaneous Bethe-Salpeter equation (Salpeter equation) are reviewed. The so called reduced Salpeter equation is introduced by using a type of reduction approach. In order to solve the Salpeter equation, by transforming it to a set of coupled equations and then to a relevant matrix problem, we obtain the corresponding eigenvalue equations which can be calculated numerically. Then we discuss the Bethe-Salpeter equation with various types of interaction kernels: the Lorentz scalar, Lorentz pseudoscalar, Lorentz vector, time-component Lorentz vector and BJK structure kernel. The exact-propagator full and reduced Salpeter equation for the pseudoscalar fermion-antifermion bound states are also introduced in this chapter.

In chapter 3, the behaviors of mass function and wave-function renormalization function of the exact quark propagator are discussed. By introducing the exact quark propagator to the Salpeter equation with time component Lorentz vector interaction structure for the pseudoscalar fermion-antifermion bound state, we numerically compute the spectra and plot the corresponding eigenfunctions with details. Furthermore, we also give the eigenvalues and eigenfunctions for the full and reduced Salpeter equation with other types of interaction kernels and compare the difference of results between the exact and free propagator cases.

In chapter 4, by adopting a residual interaction which is based on instanton effects [20, 21], we compute the masses of the pseudoscalar mesons for their three lowest states with a kernel of Böhm-Joos-Krammer (BJK) structure. We consider both the free and exact quark propagator and apply them to the Salpeter equation to study the properties of pseudoscalar mesons. The mass spectra and eigenfunctions of $\pi$, $K$, $D$, $D_s$, $B$, $B_s$, $B_c$, $\eta_c$, $\eta_b$ are obtained and compared with the results of Koll's model [20, 21, 22] and the newest data from Particle Data Group (PDG2007) [37]. In addition, the decay constants of $\pi$, $K$, $D$, $D_s$ mesons are also obtained and compared with Koll's model [22] and PDG2007 [37].

Chapter 5 presents a kind of analytical treatment for the free- and exact-propagator Salpeter eigenvalue equations with various kernels of interaction structures. For the harmonic oscillator potential, we transform the reduced Salpeter equation to the cor-

responding differential equation, specially to the standard Schrödinger type equation for the kernel of Lorentz-scalar and Lorentz-vector structure. Then we analyze the spectra and stability of the bound states solutions.

The appendix gives the metric tensor and $\gamma$ matrix relations used in this thesis. The generalized Laguerre basis for the radial functions and the corresponding formula for the relevant variables are also presented. The detailed calculations for the transformation from reduced Salpeter equation to Salpeter eigenvalue equation are also stated in the appendix. For the full Salpeter equation, as an example, we give the detailed calculation for the equation with kernel of Lorentz pseudoscalar interaction structure $\gamma_5 \otimes \gamma_5$. The plots of eigenfunctions for quark-antiquark bound states with different interaction kernels are also given in the appendix.

# Chapter 2

# The Salpeter Equation

The Bethe-Salpeter model for fermion-antifermion bound states will be described in this chapter. The general properties of the Bethe-Salpeter equation and its instantaneous approximation (instantaneous Bethe-Salpeter equation) are also presented. Furthermore, we introduce a reduction approach for the Salpeter equation and obtain the so called reduced Salpeter equation. A suitable extension to the case of exact-propagator [14] for the instantaneous Bethe-Salpeter equation and reduced Salpeter equation is also presented.

## 2.1   Introduction

In particle physics, most hadrons can be described by the quark model which is proposed in the 1960s by Gell-mann [1]. After several decades of development, quantum chromodynamics has been well established and widely accepted as the fundamental theory which describes the properties and dynamics of mesons and bayons. However, there are still some flaws in this strong interaction theory. For example, practical calculations can only be performed in some special limits. Unlike in QED, one cannot use perturbation method to make approximations for the interaction kernel in QCD. To understand the internal structure of hadronic bound states is still one of the main tasks in strong interaction physics. Since there is still no complete and uniform knowledge of the interaction between quarks, various phenomenological alternatives have to be developed and tested.

Since 1950's, a relativistic treatment for two-body bound states which is derived from Green's function has been proposed and developed within the framework of quantum field theory. This is the so called Bethe-Salpeter equation [4], which pro-

vides a suitable starting point to study the hadronic bound states. However, the general interaction kernels of the Bethe-Salpeter equation depend on the relative time variable, which leads to serious conceptional and practical problems. The retardation effects of a parametrization of confinement is also lacking. Therefore, it is necessary to make some simplification for the Bethe-Salpeter kernel to the three-dimensional space. After many efforts, it has been proved that the Bethe-Salpeter kernel can be approximated by an effective static interaction which is instantaneous in the rest frame of the bound state. Another approximation is the so called free-propagator assumption which means the constituent of bound state propagates as a free particle. With both of these two approximations, the Bethe-Salpeter equation reduces to the (full) Salpeter equation [7], which has been widely investigated for $q\bar{q}$ states by Llewellyn Smith [15], Le Yaouanc [16] and recently by Lagaë [8] and Koll [20]. Although the instantaneous Bethe-Salpeter equation avoids some crucial problems, there still exists some shortcomings, such as negative energy solutions and some solutions with zero norm.

For low binding energies, if at least one of the constituent masses in the bound states is infinite, a further approximation would lead to the so called reduced Salpeter equation [9, 18]. The reduced Salpeter equation has been widely used because of it's standard Hamiltonian form. In this chapter we will review the properties of Bethe-Salpeter equation and its instantaneous approximation form, then extend it to the case of exact propagator.

This chapter is organized as follows. In Sec. 2.2, we simply review the general properties of the Salpeter equation for fermion-antifermion bound states and then analyze the various interaction kernels between the quark and antiquark. A kind of simplification for Bethe-Salpeter equation are introduced in this section, where two assumptions, instantaneous interaction and free-propagator approximation are employed. These approximations result in the well-known Salpeter equation. In Sec. 2.3, by using Lagaë's method [8], we convert the Salpeter equation to matrix equation. In Sec. 2.4, we introduce the reduction of the Salpeter equation [8] and derive the reduced Salpeter equation which is of the standard eigenvalue type equation compared with the full instantaneous Bethe-Salpeter equation. In Sec. 2.5, the general instantaneous Bethe-Salpeter equation is extended to the exact-propagator case. Sec. 2.6 is the conclusion and summary of this chapter.

## 2.2 General Properties of the Salpeter Equation

### 2.2.1 From Bethe-Salpeter Equation to Salpeter Equation

Within elementary particle physics the Bethe-Salpeter equation has been widely applied to quantum electrodynamics (QED) and quantum chromodynamics (QCD). Unfortunately it faces problems of interpretation and of the ignorance of the full interaction kernel in QCD. Except for a very few special cases, such as the well-known Wick-Cutkosky model [29, 30] which describes the interaction of two scalar particles by exchange of a massless scalar particle, the Bethe-Salpeter equation is not easy to handle. The appearance of timelike variables in the equation of motion is one of the main reasons for this fact. Thus, simplifications of the Bethe-Salpeter equation in form of some three-dimensional reductions are highly desirable. The most popular among all proposals is known as instantaneous Bethe-Salpeter equation [7]. Its formulation is based on assuming all bound state constituents to interact instantaneously and to propagate as free particles. The specific relation between Bethe-Salpeter equations in the Minkowski space and Schrödinger equations in Euclid space was proposed by Salpeter who used the so called instantaneous approximation. The latter assumption leads to hard to implement effects such as spontaneous chiral-symmetry breaking, which is crucial for QCD. That is one of the reasons why we extend this free-propagator assumption to the exact-propagator case as we will see later on.

### 2.2.2 The Instantaneous Interaction and Free Propagator Approximation

In order to circumvent its complexity and problems of interpretation of (all) its solutions, Salpeter [7] proposed a simplification of the Bethe-Salpeter equation by using a three-dimensional reduction. Through this method, the Bethe-Salpeter equation is reduced to the so called instantaneous Bethe-Salpeter equation, which is frequently employed to study the phenomenology of mesons and even baryons as bound states of quarks [38, 39].

The Bethe-Salpeter equation reduces to instantaneous Bethe-Salpeter equation (Salpeter equation) under two assumptions [7]:

- All interactions between the constituents of the bound state are instantaneous in the center-of-momentum frame of the bound state; the corresponding momentum $P = (M, \mathbf{0})$;

- Within the bound state, every constituent propagates as a free particle with some effective mass.

The so called instantaneous approximations have been adopted widely in various applications of Bethe-Salpeter equations. With the aid of these approximations, one can simplify the calculation and express the Salpeter equation just in terms of the Salpeter amplitude $\Phi(\boldsymbol{p})$ instead of $\Phi(p)$.

### 2.2.3   Formulation of the Salpeter Equation

With these two assumptions stated above, the integration of the interaction kernel over the momentum coordinate produces the so called Salpeter equation. For fermion-antifermion bound states the Salpeter equation [7] reads

$$
\Phi(\boldsymbol{p}) \;=\; \int \frac{\mathrm{d}^3 p'}{(2\pi)^3} \Bigg[ \frac{\Lambda_1^+(\boldsymbol{p}_1)\gamma_0 [V(\boldsymbol{p}, \boldsymbol{p}')\Phi(\boldsymbol{p}')]\gamma_0\Lambda_2^-(\boldsymbol{p}_2)}{M - E_1(\boldsymbol{p}_1) - E_2(\boldsymbol{p}_2)}
$$
$$
- \frac{\Lambda_1^-(\boldsymbol{p}_1)\gamma_0 [V(\boldsymbol{p}, \boldsymbol{p}')\Phi(\boldsymbol{p}')]\gamma_0\Lambda_2^+(\boldsymbol{p}_2)}{M + E_1(\boldsymbol{p}_1) + E_2(\boldsymbol{p}_2)} \Bigg]. \tag{2.1}
$$

Here we use the Dirac Hamiltonian

$$
H_i(\boldsymbol{p}) = \gamma_0 \left[ \boldsymbol{\gamma} \cdot \boldsymbol{p} + m_i(\boldsymbol{p}) \right] , \quad i = 1, 2 \tag{2.2}
$$

and the one-particle energy

$$
E_i(\boldsymbol{p}) = \sqrt{\boldsymbol{p}^2 + m_i^2(\boldsymbol{p})} , \quad i = 1, 2, \tag{2.3}
$$

where $m_i(\boldsymbol{p})$ is the mass of constituent of bound state. The Hamiltonian satisfies $H_i^2(\boldsymbol{p}) = E_i^2(\boldsymbol{p})$ and $H_i(\boldsymbol{p})\gamma_0 = \gamma_0 H_i(-\boldsymbol{p})$. The energy projection operators for positive or negative energy of particle $i = 1, 2$ are given by

$$
\Lambda_i^\pm(\boldsymbol{p}) = \frac{E_i(\boldsymbol{p}) \pm H_i(\boldsymbol{p})}{2\, E_i(\boldsymbol{p})} , \quad i = 1, 2 \tag{2.4}
$$

which satisfies projection-operator relations

$$
\Lambda_i^\pm(\boldsymbol{p})\Lambda_i^\mp(\boldsymbol{p}) = 0, \;\; \Lambda_i^+(\boldsymbol{p}) + \Lambda_i^-(\boldsymbol{p}) = 1, \tag{2.5}
$$

$$
\Lambda_i^\pm(\boldsymbol{p})\Lambda_i^\pm(\boldsymbol{p}) = \Lambda_i^\pm(\boldsymbol{p}), \;\; \Lambda_i^\pm(\boldsymbol{p})\gamma_0 = \gamma_0\Lambda_i^\pm(-\boldsymbol{p}). \tag{2.6}
$$

## 2.2.4  Interaction Kernel

In the following we introduce the interaction kernel used in the Salpeter equation, i.e., the confining interaction.

Although lots of efforts over the last several decades have been done, the spin structure of the confining interaction is still not well established theoretically (at least for light quarks). That is why various phenomenological spin structures are considered for the calculations of the mass spectrum of the bound state in the framework of Bethe-Salpeter equation. In fact, only in the static limit of heavy quarks the confining interaction is understood. Within this limit the static potential between heavy quarks takes the linear form [18]

$$V_c(r) = a_c + b_c r, \tag{2.7}$$

where $a_c$ denotes the confinement offset, $b_c$ is the slope of the potential. For the light quarks there is still no extension of the confining potential beyond the static limit.

Concerning the interaction kernels of the Bethe-Salpeter equation, one should choose some special Lorentz spin structures $\Gamma \otimes \Gamma$ for the confining interaction. Spin structures used in this work are constructed by the following matrices:

$$\{I, \gamma_0, \gamma_\mu, \gamma_5\}.$$

Using these matrices one can build up several Lorentz spin structures as the following:

Lorentz-scalar structure $\qquad\qquad\qquad\qquad\qquad$ $\Gamma \otimes \Gamma = 1 \otimes 1$

Time-component Lorentz-vector structure $\quad$ $\Gamma \otimes \Gamma = \gamma_0 \otimes \gamma_0$

Lorentz-vector structure $\qquad\qquad\qquad\qquad\quad$ $\Gamma \otimes \Gamma = \gamma_\mu \otimes \gamma^\mu = \gamma_0 \otimes \gamma_0 - \boldsymbol{\gamma} \otimes \boldsymbol{\gamma}$

Lorentz-pseudoscalar structure $\qquad\qquad\quad$ $\Gamma \otimes \Gamma = \gamma_5 \otimes \gamma_5$

Böhm-Joos-Krammer (BJK) structure [25, 26] $\Gamma \otimes \Gamma = \frac{1}{2}(\gamma_\mu \otimes \gamma^\mu + \gamma_5 \otimes \gamma_5 - 1 \otimes 1)$.

The parameters of confinement potential $a_c$, $b_c$ and the different Lorentz structures influence the properties of bound states strongly as we will see later on. In the present work, in order to compare the calculational results with previous literature, we will appropriately choose the same parameter values used in Olsson's paper [17].

## 2.3 Converting Salpeter Equation to Matrix Equation

In order to overcome the difficulty of calculation, Lagaë proposed a method to deal with the Bethe-Salpeter equation [8, 9]. By expanding the Salpeter amplitude into a suitable set of basis matrices, the instantaneous Bethe-Salpeter equation can be transformed to a set of coupled equations for radial wave function [8]. In our work we adopt the generalized Laguerre basis to expand the Salpeter equation. In the following we briefly describe the basis matrices and transformation process.

### 2.3.1 Eigenvalue Equation

Following Lagaë [8] and Olsson [17]'s approach for pseudoscalar bound state, we use the Salpeter amplitude

$$\Phi(\boldsymbol{p}) = N\Big[S_\phi\Phi_1(\boldsymbol{p}) + C_\theta\Phi_2(\boldsymbol{p})\gamma_0 - C_\phi\Phi_1(\boldsymbol{p})\hat{\boldsymbol{p}}\boldsymbol{\gamma} - S_\theta\Phi_2(\boldsymbol{p})\hat{\boldsymbol{p}}\boldsymbol{\gamma}\gamma_0\Big]\gamma_0\gamma_5, \qquad (2.8)$$

where $N$ is the normalization factor, $\Phi_1(\boldsymbol{p})$ and $\Phi_2(\boldsymbol{p})$ are components of the Salpeter amplitude.

Comparing with the Salpeter wave function used in Lagaë's formalism [8], we make a substitution $\Phi(\boldsymbol{p}) \to \Phi(\boldsymbol{p})\gamma_0$ as that used in Olsson's work [17]. Therefore the corresponding eigenvalue equation reads

$$H[\Phi(\boldsymbol{p})\gamma_0] = M[\Phi(\boldsymbol{p})\gamma_0]. \qquad (2.9)$$

Here $M$ is the mass eigenvalue.

In order to solve the Salpeter equation, from Eq. (2.1) one can rewrite Eq. (2.9) as an eigenvalue equation

$$\begin{aligned}
M[\Phi(\boldsymbol{p})\gamma_0] &= H_1(\boldsymbol{p_1})[\Phi(\boldsymbol{p})\gamma_0] - [\Phi(\boldsymbol{p})\gamma_0]H_2(\boldsymbol{p_2}) \\
&+ \int \frac{\mathrm{d}^3p'}{(2\pi)^3}\Big[\Lambda_1^+(\boldsymbol{p_1})\gamma_0[V(\boldsymbol{p},\boldsymbol{p'})\Phi(\boldsymbol{p'})]\Lambda_2^-(\boldsymbol{p_2}) \\
&\quad -\Lambda_1^-(\boldsymbol{p_1})\gamma_0[V(\boldsymbol{p},\boldsymbol{p'})\Phi(\boldsymbol{p'})]\Lambda_2^+(\boldsymbol{p_2})\Big].
\end{aligned} \qquad (2.10)$$

By multiplying $\Lambda_1^{\pm}(\boldsymbol{p_1})$ from the left and $\Lambda_2^{\pm}(\boldsymbol{p_2})$ from the right, we find that half of the components of the instantaneous Bethe-Salpeter equation $\Phi(\boldsymbol{p})$ vanishes:

$$\Lambda_1^+(\boldsymbol{p_1})\Phi(\boldsymbol{p})\Lambda_2^+(\boldsymbol{p_2}) = \Lambda_1^-(\boldsymbol{p_1})\Phi(\boldsymbol{p})\Lambda_2^-(\boldsymbol{p_2}) = 0. \qquad (2.11)$$

That is,

$$\Lambda_1^+(\boldsymbol{p_1})\Phi(\boldsymbol{p})\Lambda_2^+(\boldsymbol{p_2}) - \Lambda_1^-(\boldsymbol{p_1})\Phi(\boldsymbol{p})\Lambda_2^-(\boldsymbol{p_2})$$

$$= \frac{1}{4E_1(\boldsymbol{p_1})E_2(\boldsymbol{p_2})}\Big\{[E_1(\boldsymbol{p_1}) + H_1(\boldsymbol{p_1})]\Phi(\boldsymbol{p})[E_2(\boldsymbol{p_2}) + H_2(\boldsymbol{p_2})]$$

$$-[E_1(\boldsymbol{p_1}) - H_1(\boldsymbol{p_1})]\Phi(\boldsymbol{p})[E_2(\boldsymbol{p_2}) - H_2(\boldsymbol{p_2})]\Big\}$$

$$= \frac{1}{4E_1(\boldsymbol{p_1})E_2(\boldsymbol{p_2})}[H_1(\boldsymbol{p_1})\Phi(\boldsymbol{p})E_2(\boldsymbol{p_2}) + E_1(\boldsymbol{p_1})\Phi(\boldsymbol{p})H_2(\boldsymbol{p_2})]$$

$$= 0. \tag{2.12}$$

From the above equation on can easily find that the Salpeter amplitude $\Phi(\boldsymbol{p})$ satisfies

$$\frac{H_1(\boldsymbol{p_1})}{E_1(\boldsymbol{p_1})}\Phi(\boldsymbol{p}) + \Phi(\boldsymbol{p})\frac{H_2(\boldsymbol{p_2})}{E_2(\boldsymbol{p_2})} = 0. \tag{2.13}$$

For a fermion-antifermion system in the rest frame, the instantaneous Bethe-Salpeter equation involves only the relative momentum $\boldsymbol{p} = \boldsymbol{p_1} = -\boldsymbol{p_2}$. Therefore Eq. (2.10) becomes

$$M[\Phi(\boldsymbol{p})\gamma_0] = H(\boldsymbol{p})[\Phi(\boldsymbol{p})\gamma_0] - [\Phi(\boldsymbol{p})\gamma_0]H(-\boldsymbol{p})$$

$$+ \int \frac{\mathrm{d}^3 p'}{(2\pi)^3}\Big[\Lambda^+(\boldsymbol{p})\gamma_0[V(\boldsymbol{p},\boldsymbol{p'})\Phi(\boldsymbol{p'})]\Lambda^-(-\boldsymbol{p})$$

$$-\Lambda^-(\boldsymbol{p})\gamma_0[V(\boldsymbol{p},\boldsymbol{p'})\Phi(\boldsymbol{p'})]\Lambda^+(-\boldsymbol{p})\Big]. \tag{2.14}$$

The formal product of $V\Phi$ in the above eigenvalue equations represents the sum of potentials $V_i$ and bilinear covariants:

$$V(\boldsymbol{p},\boldsymbol{p'})\Phi(\boldsymbol{p'}) \longrightarrow \sum_i V_i(\boldsymbol{p},\boldsymbol{p'})\Gamma_i\Phi(\boldsymbol{p'})\Gamma_i . \tag{2.15}$$

Therefore the eigenvalue equation (2.10) becomes

$$M[\Phi(\boldsymbol{p})\gamma_0] = H_1(\boldsymbol{p_1})[\Phi(\boldsymbol{p})\gamma_0] - [\Phi(\boldsymbol{p})\gamma_0]H_2(\boldsymbol{p_2})$$

$$+ \sum_i \int \frac{\mathrm{d}^3 p'}{(2\pi)^3}V_i(\boldsymbol{p},\boldsymbol{p'})\Big[\Lambda_1^+(\boldsymbol{p_1})\gamma_0\Gamma_i\Phi(\boldsymbol{p'})\Gamma_i\Lambda_2^-(\boldsymbol{p_2})$$

$$-\Lambda_1^-(\boldsymbol{p_1})\gamma_0\Gamma_i\Phi(\boldsymbol{p'})\Gamma_i\Lambda_2^+(\boldsymbol{p_2})\Big], \tag{2.16}$$

where the $\Gamma_i$'s are Dirac matrices.

This eigenvalue equation can be numerically calculated by transforming it to a set of matrix equations as we will see in the following.

### 2.3.2  The Generalized Laguerre Basis

We choose the basis states for the components of the Salpeter amplitude by the configuration-space representation [23]

$$\phi_i^{(l)}(r) = \sqrt{\frac{(2\mu)^{2l+3}i!}{\Gamma(2l+i+3)}}r^l\exp(-\mu r)L_i^{(2l+2)}(2\mu r), \quad i = 0, 1, 2, \dots , \tag{2.17}$$

where the generalized Laguerre polynomial $L_i^{(l)}(x)$ is given by [74]

$$L_i^{(\gamma)}(x) = \sum_{t=0}^{i}(-1)^t \begin{pmatrix} i+\gamma \\ i-t \end{pmatrix}\frac{x^t}{t!}, \quad i = 0, 1, 2, \dots , \tag{2.18}$$

which satisfies the orthonormal-relation [74]

$$\int_0^\infty \mathrm{d}x x^\gamma \exp(-x)L_i^{(\gamma)}(x)L_j^{(\gamma)}(x) = \frac{\Gamma(\gamma+i+1)}{i!}\delta_{ij}, \quad i, j = 0, 1, 2, \dots . \tag{2.19}$$

From this choice, the Salpeter amplitude will be expanded on the basis $\phi_i^{(l)}$. More details can be found in appendix B.

### 2.3.3  Salpeter Eigenvalue Equations for Various Kernels

In the instantaneous Bethe-Salpeter equation, various interaction kernels have been investigated in recent years. In this chapter we focus on Salpeter equation with time-component Lorentz-vector structure $\gamma_0 \otimes \gamma_0$ [17]. The calculation processes of Salpeter equation with other interaction kernels are similar.

As used in Ref. [8], considering constituent quarks of masses $m_i$, we are employing the following definition

$$S_\theta = \sin\theta = \sqrt{\frac{E_1E_2 - p^2 - m_1m_2}{2E_1E_2}}, \quad C_\theta = \cos\theta = \sqrt{\frac{E_1E_2 + p^2 + m_1m_2}{2E_1E_2}}, \tag{2.20}$$

$$S_\phi = \sin\phi = \sqrt{\frac{E_1E_2 - p^2 + m_1m_2}{2E_1E_2}}, \quad C_\phi = \cos\phi = \sqrt{\frac{E_1E_2 + p^2 - m_1m_2}{2E_1E_2}}. \tag{2.21}$$

Here, to simplify the description, we have made substitutions:

$$E_i(p) \rightarrow E_i, \; i = 1, 2, \tag{2.22}$$

$$S_\theta(p) \rightarrow S_\theta, \; S_\theta(p') \rightarrow S'_\theta, \; C_\theta(p) \rightarrow C_\theta, \; C_\theta(p') \rightarrow C'_\theta.$$

Starting from Eq. (2.16), for the kernel of the time-component Lorentz-vector structure $\Gamma_1 \otimes \Gamma_2 = \gamma_0 \otimes \gamma_0$, we transform the Salpeter eigenvalue equation to a set of coupled equations by two steps as shown in the following.

**The first step:** multiply $\gamma_5$ from the right side for both sides of Eq. (2.16) and calculate the corresponding *trace*.

The *trace* of the left side of Eq. (2.16) multiplying with $\gamma_5$ is:

$$
\begin{aligned}
Left &= \mathrm{tr}\Big\{ M\Phi(\boldsymbol{p})\gamma_0\gamma_5 \Big\} \\
&= M\,\mathrm{tr}\Big\{ \big[ S_\phi\Phi_1(\boldsymbol{p}) + C_\theta\Phi_2(\boldsymbol{p})\gamma_0 - C_\phi\Phi_1(\boldsymbol{p})\hat{\boldsymbol{p}}\boldsymbol{\gamma} - S_\theta\Phi_2(\boldsymbol{p})\hat{\boldsymbol{p}}\boldsymbol{\gamma}\gamma_0 \big]\gamma_0\gamma_5\gamma_0\gamma_5 \Big\} \\
&= -4MS_\phi\Phi_1(\boldsymbol{p}).
\end{aligned}
\tag{2.23}
$$

The *trace* of the right side of Eq. (2.16) multiplying with $\gamma_5$ involves two parts:

$$
\begin{aligned}
Right &= \mathrm{tr}\Big\{ \underbrace{H_1(\boldsymbol{p_1})\Phi(\boldsymbol{p})\gamma_0\gamma_5 - \Phi(\boldsymbol{p})\gamma_0 H_2(\boldsymbol{p_2})\gamma_5}_{kinetic\ part} \Big\} \\
&\quad + \mathrm{tr}\Big\{ \big[\underbrace{\Lambda_1^+(\boldsymbol{p_1})\gamma_0\gamma_0\Phi(\boldsymbol{p}')\gamma_0\Lambda_2^-(\boldsymbol{p_2})\gamma_5 - \Lambda_1^-(\boldsymbol{p_1})\gamma_0\gamma_0\Phi(\boldsymbol{p}')\gamma_0\Lambda_2^+(\boldsymbol{p_2})\gamma_5}_{potential\ part}\big] \Big\}.
\end{aligned}
\tag{2.24}
$$

For the *kinetic part*:

$$
\begin{aligned}
&\mathrm{tr}\Big\{ H_1(\boldsymbol{p_1})\Phi(\boldsymbol{p})\gamma_0\gamma_5 - \Phi(\boldsymbol{p})\gamma_0 H_2(\boldsymbol{p_2})\gamma_5 \Big\} \\
&= \mathrm{tr}\Big\{ \gamma_0(\boldsymbol{\gamma}\cdot\boldsymbol{p_1} + m_1)[S_\phi\Phi_1(\boldsymbol{p}) + C_\theta\Phi_2(\boldsymbol{p})\gamma_0 - C_\phi\Phi_1(\boldsymbol{p})\hat{\boldsymbol{p}}\boldsymbol{\gamma} - S_\theta\Phi_2(\boldsymbol{p})\hat{\boldsymbol{p}}\boldsymbol{\gamma}\gamma_0]\gamma_0\gamma_5\gamma_0\gamma_5 \\
&\quad - [S_\phi\Phi_1(\boldsymbol{p}) + C_\theta\Phi_2(\boldsymbol{p})\gamma_0 - C_\phi\Phi_1(\boldsymbol{p})\hat{\boldsymbol{p}}\boldsymbol{\gamma} - S_\theta\Phi_2(\boldsymbol{p})\hat{\boldsymbol{p}}\boldsymbol{\gamma}\gamma_0]\gamma_0\gamma_5\gamma_0\gamma_0(\boldsymbol{\gamma}\cdot\boldsymbol{p_2} + m_2)\gamma_5 \Big\} \\
&= -\mathrm{tr}\Big\{ (m_1 + m_2)C_\theta\Phi_2(\boldsymbol{p}) \Big\} \\
&= -4(m_1 + m_2)C_\theta\Phi_2(\boldsymbol{p}).
\end{aligned}
\tag{2.25}
$$

For the *potential part*:

$$
\begin{aligned}
&\mathrm{tr}\Big\{ [\Lambda_1^+(\boldsymbol{p_1})\Phi(\boldsymbol{p}')\gamma_0\Lambda_2^-(\boldsymbol{p_2})\gamma_5 - \Lambda_1^-(\boldsymbol{p_1})\Phi(\boldsymbol{p}')\gamma_0\Lambda_2^+(\boldsymbol{p_2})\gamma_5] \Big\} \\
&= \mathrm{tr}\Big\{ \frac{E_1(\boldsymbol{p_1}) + H_1(\boldsymbol{p_1})}{2E_1(\boldsymbol{p_1})}\Phi(\boldsymbol{p}')\gamma_0\frac{E_2(\boldsymbol{p_2}) - H_2(\boldsymbol{p_2})}{2E_2(\boldsymbol{p_2})}\gamma_5
\end{aligned}
$$

13

$$-\frac{E_1(\boldsymbol{p}_1) - H_1(\boldsymbol{p}_1)}{2E_1(\boldsymbol{p}_1)}\Phi(\boldsymbol{p}')\gamma_0\frac{E_2(\boldsymbol{p}_2) + H_2(\boldsymbol{p}_2)}{2E_2(\boldsymbol{p}_2)}\gamma_5\Big\}$$

$$= -4\left[S_\theta(\boldsymbol{p}')\Phi_2(\boldsymbol{p}')p\frac{E_2(\boldsymbol{p}_2) - E_1(\boldsymbol{p}_1)}{2E_1(\boldsymbol{p}_1)E_2(\boldsymbol{p}_2)} + C_\theta(\boldsymbol{p}')\Phi_2(\boldsymbol{p}')\frac{m_1E_2(\boldsymbol{p}_2) + m_2E_1(\boldsymbol{p}_1)}{2E_1(\boldsymbol{p}_1)E_2(\boldsymbol{p}_2)}\right]$$

$$= -4\left[S_\theta(\boldsymbol{p}')S_\theta(\boldsymbol{p}) + C_\theta(\boldsymbol{p}')C_\theta(\boldsymbol{p})\right]S_\phi(\boldsymbol{p})\Phi_2(\boldsymbol{p}'). \tag{2.26}$$

In the last step we have used the relation

$$S_\theta S_\phi = p\frac{E_2 - E_1}{2E_1E_2}, \qquad C_\theta S_\phi = \frac{m_1E_2 + m_2E_1}{2E_1E_2} \qquad \text{(see appendix C)}.$$

Combining the Eq. (2.23), (2.25) and (2.26), the Salpeter eigenvalue equation (2.16) with the kernel of time-component Lorentz-vector $\gamma_0 \otimes \gamma_0$ is finally reformed as

$$M\Phi_1(\boldsymbol{p}) = \left[E_1(\boldsymbol{p}_1) + E_2(\boldsymbol{p}_2)\right]\Phi_2(\boldsymbol{p})$$

$$+ \int \frac{\mathrm{d}^3p'}{(2\pi)^3}V(\boldsymbol{p}, \boldsymbol{p}')\left[S_\theta(\boldsymbol{p}')S_\theta(\boldsymbol{p}) + C_\theta(\boldsymbol{p}')C_\theta(\boldsymbol{p})\right]\Phi_2(\boldsymbol{p}'). \tag{2.27}$$

Since

$$\Phi_i(\boldsymbol{p}) = \Phi_i(p)Y_{l,m}(\hat{\boldsymbol{p}}) \tag{2.28}$$

and the integration of $Y_{l,m}(\hat{\boldsymbol{p}})$ satisfies

$$\int \mathrm{d}\Omega_p Y_{l,m}^*(\hat{\boldsymbol{p}})Y_{l',m'}(\hat{\boldsymbol{p}}) = \delta_{ll'}\delta_{mm'}, \tag{2.29}$$

by multiplying both sides of the Eq. (2.27) with $Y_{l',m'}^*(\hat{\boldsymbol{p}})$ and integrating over $\int \mathrm{d}\Omega_p$ one obtains

$$M\int \mathrm{d}\Omega_p \Phi_1(p)Y_{l',m'}^*(\hat{\boldsymbol{p}})Y_{l,m}(\hat{\boldsymbol{p}})$$

$$= \int \mathrm{d}\Omega_p(E_1(\boldsymbol{p}_1) + E_2(\boldsymbol{p}_2))\Phi_2(p)Y_{l',m'}^*(\hat{\boldsymbol{p}})Y_{l,m}(\hat{\boldsymbol{p}})$$

$$+ \int \frac{\mathrm{d}^3p'}{(2\pi)^3}\int \mathrm{d}\Omega_p V(\boldsymbol{p}, \boldsymbol{p}')\left[S_\theta(\boldsymbol{p}')S_\theta(\boldsymbol{p}) + C_\theta(\boldsymbol{p}')C_\theta(\boldsymbol{p})\right]\Phi_2(p)Y_{l',m'}^*(\hat{\boldsymbol{p}})Y_{l,m}(\hat{\boldsymbol{p}}). \tag{2.30}$$

With

$$\int \mathrm{d}^3p' \rightarrow \int_0^\infty \mathrm{d}p'p'^2\int \mathrm{d}\Omega_p' \tag{2.31}$$

14

and

$$\exp\{\mathtt{i}\boldsymbol{p}\cdot\boldsymbol{r}\} \;=\; 4\pi\sum_{l=0}^{\infty}\sum_{m=-l}^{l}\mathtt{i}^{l}j_{l}(pr)Y_{l,m}(\hat{\boldsymbol{p}})Y_{l,m}^{*}(\hat{\boldsymbol{r}})$$

$$\exp\{-\mathtt{i}\boldsymbol{p}'\cdot\boldsymbol{r}\} \;=\; 4\pi\sum_{l'=0}^{\infty}\sum_{m=-l'}^{l'}(-\mathtt{i})^{l'}j_{l'}(p'r)Y_{l',m'}^{*}(\hat{\boldsymbol{p}}')Y_{l',m'}(\hat{\boldsymbol{r}}), \qquad (2.32)$$

For the radial Salpeter function, $l=0$, the integration term

$$V(\boldsymbol{p}-\boldsymbol{p}') = \int \mathrm{d}^{3}rV(r)\exp\{\mathtt{i}(\boldsymbol{p}-\boldsymbol{p}')\cdot\boldsymbol{r}\} \qquad (2.33)$$

becomes

$$16\pi^{2}\int \mathrm{d}rr^{2}V(r)j_{0}(pr)j_{0}(p'r). \qquad (2.34)$$

Define (see [8])

$$V_{L}(p,p') = 8\pi\int_{0}^{\infty}\mathrm{d}rr^{2}V(r)j_{L}(pr)j_{L}(p'r), \qquad (2.35)$$

the term (2.34) becomes

$$16\pi^{2}\int \mathrm{d}r\ r^{2}V(r)j_{0}(pr)j_{0}(p'r) = 2\pi V_{0}(p,p'). \qquad (2.36)$$

Further analysis shows that [8]

$$\int \mathrm{d}\Omega_{p}\int \mathrm{d}\Omega_{p'}'V(\boldsymbol{p}-\boldsymbol{p}')\boldsymbol{p}\cdot\boldsymbol{p}'Y_{0,0}^{*}(\hat{\boldsymbol{p}})Y_{0,0}(\hat{\boldsymbol{p}}) = 2\pi pp'V_{1}(p,p')$$

$$\int \mathrm{d}\Omega_{p}\int \mathrm{d}\Omega_{p'}'V(\boldsymbol{p}-\boldsymbol{p}')Y_{0,0}^{*}(\hat{\boldsymbol{p}})Y_{0,0}(\hat{\boldsymbol{p}}) = 2\pi V_{0}(p,p'). \qquad (2.37)$$

Using the above results from (2.28) to (2.37), the eigenvalue equation (2.27) associated with the Salpeter component $\Phi_{1}(p)$ becomes

$$M\Phi_{1}(p) = [E_{1}+E_{2}]\Phi_{2}(p) + \int_{0}^{\infty}\frac{\mathrm{d}p'p'^{2}}{(2\pi)^{2}}[C_{\theta}V_{0}(p,p')C_{\theta}' + S_{\theta}V_{1}(p,p')S_{\theta}']\Phi_{2}(p'). (2.38)$$

With the substitutions

$$\Phi_{i}(p) \rightarrow \Phi_{i},\ \Phi_{i}(p') \rightarrow \Phi_{i}',\ \ i=0,1,$$
$$V_{L}(p,p') \rightarrow V_{L},\ L=0,1, \qquad (2.39)$$

equation (2.27) finally reads

$$M\Phi_{1} = [E_{1}+E_{2}]\Phi_{2} + \int_{0}^{\infty}\frac{\mathrm{d}p'p'^{2}}{(2\pi)^{2}}(C_{\theta}V_{0}C_{\theta}' + S_{\theta}V_{1}S_{\theta}')\Phi_{2}'. \qquad (2.40)$$

15

**The second step:** multiply with $\gamma_5\gamma_0$ from the right side for both sides of Eq. (2.16) and calculate the corresponding *trace*.

Using the same method stated in the first step, the eigenvalue Eq. (2.16) with kernels of time-component Lorentz-vector $\gamma_0 \otimes \gamma_0$ can be transformed to

$$
M\Phi_2(\boldsymbol{p}) = \Big[E_1(\boldsymbol{p}_1) + E_2(\boldsymbol{p}_2)\Big]\Phi_1(\boldsymbol{p})
$$

$$
+ \int \frac{\mathrm{d}^3 p'}{(2\pi)^3} V(\boldsymbol{p} - \boldsymbol{p}')\Big[S_\phi(\boldsymbol{p}')S_\phi(\boldsymbol{p}) + C_\phi(\boldsymbol{p}')C_\phi(\boldsymbol{p})\Big]\Phi_1(\boldsymbol{p}').\quad(2.41)
$$

Finally, with the results from (2.28) to (2.37) and substitutions (2.39) we obtain another eigenvalue equation associated with the Salpeter component $\Phi_2(p)$

$$
M\Phi_2(p) = [E_1 + E_2]\Phi_1(p) + \int_0^\infty \frac{\mathrm{d}p'p'^2}{(2\pi)^2}(S_\phi V_0 S'_\phi + C_\phi V_1 C'_\phi)\Phi_1(p').\quad(2.42)
$$

By using the same procedure, the Salpeter eigenvalue equation for other kernels of interaction Lorentz structures can also be obtained.

For Lorentz-scalar interaction kernel $1 \otimes 1$ [17],

$$
M\Phi_1 = [E_1 + E_2]\Phi_2 + \int_0^\infty \frac{\mathrm{d}p'p'^2}{(2\pi)^2}(-C_\theta V_0 C'_\theta + S_\theta V_1 S'_\theta)\Phi'_2,\quad(2.43)
$$

$$
M\Phi_2 = [E_1 + E_2]\Phi_1 + \int_0^\infty \frac{\mathrm{d}p'p'^2}{(2\pi)^2}(-S_\phi V_0 S'_\phi + C_\phi V_1 C'_\phi)\Phi'_1.\quad(2.44)
$$

For Lorentz-vector interaction kernel $\gamma_\mu \otimes \gamma^\mu$ [17],

$$
M\Phi_1 = [E_1 + E_2]\Phi_2 + \int_0^\infty \frac{\mathrm{d}p'p'^2}{(2\pi)^2}4C_\theta V_0 C'_\theta\Phi'_2,\quad(2.45)
$$

$$
M\Phi_2 = [E_1 + E_2]\Phi_1 + \int_0^\infty \frac{\mathrm{d}p'p'^2}{(2\pi)^2}(-2S_\phi V_0 S'_\phi)\Phi'_1.\quad(2.46)
$$

For Lorentz-pseudoscalar interaction kernel $\gamma_5 \otimes \gamma_5$,

$$
M\Phi_1 = [E_1 + E_2]\Phi_2 + \int_0^\infty \frac{\mathrm{d}p'p'^2}{(2\pi)^2}(-C_\theta V_0 C'_\theta)\Phi'_2,\quad(2.47)
$$

$$
M\Phi_2 = [E_1 + E_2]\Phi_1 + \int_0^\infty \frac{\mathrm{d}p'p'^2}{(2\pi)^2}(S_\phi V_0 S'_\phi + C_\phi V_1 C'_\phi)\Phi'_1.\quad(2.48)
$$

For Böhm-Joos-Krammer (BJK) structure [25, 26] $\frac{1}{2}(\gamma_\mu \otimes \gamma^\mu + \gamma_5 \otimes \gamma_5 - 1 \otimes 1)$,

$$
M\Phi_1 = [E_1 + E_2]\Phi_2 + \int_0^\infty \frac{\mathrm{d}p'p'^2}{(2\pi)^2}(2C_\theta V_0 C'_\theta)\Phi'_2,\quad(2.49)
$$

$$
M\Phi_2 = [E_1 + E_2]\Phi_1.\quad(2.50)
$$

16

Now we write all of the above Salpeter eigenvalue equations with different Lorentz structures as two coupled equations by introducing parameters $\varepsilon_i, i = 1, 2, 3, 4$,

$$M\Phi_1 = [E_1 + E_2]\Phi_2 + \int_0^\infty \frac{\mathrm{d}p' p'^2}{(2\pi)^2} (\varepsilon_1 C_\theta V_0 C'_\theta + \varepsilon_2 S_\theta V_1 S'_\theta)\Phi'_2, \qquad (2.51)$$

$$M\Phi_2 = [E_1 + E_2]\Phi_1 + \int_0^\infty \frac{\mathrm{d}p' p'^2}{(2\pi)^2} (\varepsilon_3 S_\phi V_0 S'_\phi + \varepsilon_4 C_\phi V_1 C'_\phi)\Phi'_1. \qquad (2.52)$$

In these two coupled equations we need to handle two functions. By inserting one to another, we obtain an equation for $M^2$ for just one unknown function.

The parameters $\varepsilon_i$ take the following values:

| $m_1 = m_2$ | $1 \otimes 1$ | $\gamma_0 \otimes \gamma_0$ | $\gamma_\mu \otimes \gamma^\mu$ | $\gamma_5 \otimes \gamma_5$ | $BJK$ |
|:---:|:---:|:---:|:---:|:---:|:---:|
| $\varepsilon_1$ | $-1$ | $1$ | $4$ | $-1$ | $2$ |
| $\varepsilon_2$ | $0$ | $1$ | $0$ | $0$ | $0$ |
| $\varepsilon_3$ | $-1$ | $1$ | $-2$ | $1$ | $0$ |
| $\varepsilon_4$ | $1$ | $1$ | $0$ | $1$ | $0$ |

**Table 2.1:** Parameter $\varepsilon_i$ in the Salpeter equations (2.51) and (2.52).

## 2.4 Reduced Salpeter Equation

Although the instantaneous Bethe-Salpeter equation has been widely used as the bound state equation for mesons for many years, numerical and analytical analysis point out it has negative energy solutions and includes solutions with zero norm [8]. However, both of these solutions do not exist in the so called reduced Salpeter equation. The reduced Salpeter equation has stable solutions for more kernel types than does the full Salpeter equation. For example, in the full Salpeter equation there are no stable solutions with pure Lorentz-scalar structure interaction kernel. But the reduced Salpeter equation has well-defined stable solutions with scalar confinement kernel. In addition, the reduced Salpeter equation can be transformed to a single eigenvalue equation with one Salpeter component amplitude which is easier to handle. From the practical and physical point of view, the reduced Salpeter equation is worthy to study.

### 2.4.1 Reduction Method

The reduced Salpeter equation has been studied for relativistic bound states in a number of papers [12, 16, 8, 9, 18, 81, 82, 95, 96]. A simplified version for the instantaneous Bethe-Salpeter equation known as the reduced Salpeter equation has been proposed by Lagaë [8]. This simplification process only involves radial wave functions. The final reduced Salpeter equation becomes identical to the full Salpeter equation if the constituent masses in the full Salpeter equation in the bound states is infinite. Compared with the full Salpeter equation, the reduced Salpeter equation is of a standard eigenvalue type equation whose solutions are algebraically simpler than those of the full Salpeter equation. In the following, we depict the main points of this simplification approach for the reduced Salpeter equation.

Remember the instantaneous Bethe-Salpeter equation, or the full Salpeter equation (2.1) mentioned in previous sections

$$
\Phi(\boldsymbol{p}) \;\; = \;\; \int \frac{\mathrm{d}^3 p'}{(2\pi)^3} \Bigg[ \frac{\Lambda_1^+(\boldsymbol{p}_1)\gamma_0[V(\boldsymbol{p},\boldsymbol{p}')\Phi(\boldsymbol{p}')]\gamma_0\Lambda_2^-(\boldsymbol{p}_2)}{M - E_1(\boldsymbol{p}_1) - E_2(\boldsymbol{p}_2)}
$$
$$
- \frac{\Lambda_1^-(\boldsymbol{p}_1)\gamma_0[V(\boldsymbol{p},\boldsymbol{p}')\Phi(\boldsymbol{p}')]\gamma_0\Lambda_2^+(\boldsymbol{p}_2)}{M + E_1(\boldsymbol{p}_1) + E_2(\boldsymbol{p}_2)} \Bigg]. \tag{2.53}
$$

For the heavy-quark systems

$$
\frac{M - E_1 - E_2}{M + E_1 + E_2} \ll 1, \tag{2.54}
$$

by dropping the second term of the above equation (2.53) and in the center-of-mass frame of the bound states using the relations $\boldsymbol{p} = \boldsymbol{p}_1 = -\boldsymbol{p}_2$, we obtain the so called reduced Salpeter equation:

$$
\Phi(\boldsymbol{p}) = \int \frac{\mathrm{d}^3 p'}{(2\pi)^3} \Bigg[ \frac{\Lambda_1^+(\boldsymbol{p})\gamma_0[V(\boldsymbol{p},\boldsymbol{p}')\Phi(\boldsymbol{p}')]\gamma_0\Lambda_2^-(-\boldsymbol{p})}{M - E_1(\boldsymbol{p}) - E_2(\boldsymbol{p})} \Bigg]. \tag{2.55}
$$

With the same handling procedure as for the full Salpeter equation, the corresponding eigenvalue equation of Eq. (2.55) is obtained

$$
M\Phi(\boldsymbol{p}) = (E_1 + E_2)\Phi(\boldsymbol{p}) + \int \frac{\mathrm{d}^3 p'}{(2\pi)^3}\Lambda_1^+(\boldsymbol{p})\gamma_0[V(\boldsymbol{p},\boldsymbol{p}')\Phi(\boldsymbol{p}')]\gamma_0\Lambda_2^-(-\boldsymbol{p}). \tag{2.56}
$$

According to Eq. (2.9), (2.16) and (2.55), the reduced Salpeter eigenvalue equation reads

$$
M\Phi(\boldsymbol{p})\gamma_0 = (E_1 + E_2)\Phi(\boldsymbol{p})\gamma_0 + \sum_i \int \frac{\mathrm{d}^3 p'}{(2\pi)^3} V_i(\boldsymbol{p},\boldsymbol{p}')\Lambda_1^+(\boldsymbol{p})\gamma_0\Gamma_i\Phi(\boldsymbol{p}')\Gamma_i\Lambda_2^-(-\boldsymbol{p}).
$$
$$
\tag{2.57}
$$

The reduced Salpeter equation has some advantages comparing with the full equation. As stated above, the full Salpeter equation has negative energy solutions and solutions with zero norm, but the reduced Salpeter equation does not have these types of solution. Olsson, et al. [17] have investigated the validity of the reduced Salpeter equation. The reduced Salpeter equation has stable solutions for more types of kernels than does the full equation.

For the fermion-antifermion bound states, with $|\boldsymbol{p}_1| = |\boldsymbol{p}_2| = p \equiv |\boldsymbol{p}|$ and $m_1(\boldsymbol{p}_1) = m_2(\boldsymbol{p}_2) = m$, $E_1(\boldsymbol{p}_1) = E_2(\boldsymbol{p}_2) \equiv E(\boldsymbol{p}) = \sqrt{p^2 + m^2}$, in the center-of-mass frame the full Salpeter equation satisfies the constraint (see Eq. (2.13))

$$\frac{H(\boldsymbol{p})}{E(\boldsymbol{p})}\Phi(\boldsymbol{p}) + \Phi(\boldsymbol{p})\frac{H(\boldsymbol{p})}{E(\boldsymbol{p})} = 0, \tag{2.58}$$

and the reduced Salpeter equation satisfies the contraints

$$H(\boldsymbol{p})\Phi(\boldsymbol{p}) = E(\boldsymbol{p})\Phi(\boldsymbol{p}), \tag{2.59}$$

$$\Phi(-\boldsymbol{p})H(\boldsymbol{p}) = -E(\boldsymbol{p})\Phi(\boldsymbol{p}). \tag{2.60}$$

Eq. (2.59) can be rewritten as

$$H(\boldsymbol{p})\Phi(\boldsymbol{p}) - E(\boldsymbol{p})\Phi(\boldsymbol{p})$$

$$= [\gamma_0(\boldsymbol{\gamma}\cdot\boldsymbol{p} + m) - E(\boldsymbol{p})]\Big(\frac{m}{E(\boldsymbol{p})}\Phi_1(\boldsymbol{p}) + \Phi_2(\boldsymbol{p})\gamma_0 - \frac{p}{E(\boldsymbol{p})}\Phi_1(\boldsymbol{p})\hat{\boldsymbol{p}}\boldsymbol{\gamma}\Big)\gamma_0\gamma_5$$

$$= \gamma_0\boldsymbol{\gamma}\cdot\boldsymbol{p}\gamma_5\Phi_2(\boldsymbol{p}) - \boldsymbol{\gamma}\cdot\boldsymbol{\gamma}\gamma_5\frac{\boldsymbol{p}^2}{E(\boldsymbol{p})}\Phi_1(\boldsymbol{p}) + \gamma_5\frac{m^2}{E(\boldsymbol{p})}\Phi_1(\boldsymbol{p}) + \gamma_0\gamma_5 m\Phi_2(\boldsymbol{p})$$

$$-\gamma_0\gamma_5 m\Phi_1(\boldsymbol{p}) - \gamma_5 E\Phi_2(\boldsymbol{p}) - \gamma_0\boldsymbol{\gamma}\cdot\boldsymbol{p}\gamma_5\Phi_1(\boldsymbol{p})$$

$$= [\gamma_0\boldsymbol{\gamma}\cdot\boldsymbol{p}\gamma_5 + \gamma_0\gamma_5 m - \gamma_5 E(\boldsymbol{p})][\Phi_2(\boldsymbol{p}) - \Phi_1(\boldsymbol{p})]$$

$$= 0. \tag{2.61}$$

This leads to
$$\Phi_1(\boldsymbol{p}) = \Phi_2(\boldsymbol{p}).$$

In the above calculation we have used the anticommutation relation $\{\gamma_i, \gamma_j\} = -2\delta_{ij}$.

Considering the constraints discussed above, the norm of the reduced Salpeter amplitude [15, 97, 98]

$$\| \Phi \|^2 = \int \frac{\mathrm{d}^3 p'}{(2\pi)^3} \mathrm{Tr}[\Phi^\dagger(\boldsymbol{p})\Phi(\boldsymbol{p})], \qquad (2.62)$$

can also be written as the normalization of bound states [18]

$$\| \Phi \|^2 = \frac{1}{(2\pi)^3} \langle B|B\rangle \qquad (2.63)$$

with $\langle B|B\rangle = 1$.

With the reduced Salpeter equation (2.57), one obtains

$$
\begin{aligned}
M \| \Phi \|^2 &= \int \frac{\mathrm{d}^3 p}{(2\pi)^3} [E_1 + E_2] \mathrm{Tr}[\Phi^\dagger(\boldsymbol{p})\Phi(\boldsymbol{p})] \\
&+ \sum_i \int \frac{\mathrm{d}^3 p}{(2\pi)^3} \int \frac{\mathrm{d}^3 p'}{(2\pi)^3} V_i(\boldsymbol{p}-\boldsymbol{p}') \mathrm{Tr}[\Phi^\dagger(\boldsymbol{p})\gamma_0\Gamma_i\Phi'(\boldsymbol{p})\Gamma_i\gamma_0]. (2.64)
\end{aligned}
$$

We will discuss the properties of the reduced Salpeter equation in the following sections.

## 2.4.2 Reduced Salpeter Eigenvalue Equations for Various Kernels

By using the same approach used to the full Salpeter equation, we can obtain the eigenvalue equations for the reduced Salpeter equation with various Lorentz structure interaction kernels.

For interactions of Lorentz-scalar Dirac structure, $\Gamma \otimes \Gamma = 1 \otimes 1$ [18],

$$M\Phi = [E_1 + E_2]\Phi + \frac{1}{2}\int_0^\infty \frac{\mathrm{d}p'p'^2}{(2\pi)^2}(-V_0 - S_\phi V_0 S'_\phi + C_\phi V_1 C'_\phi)\Phi', \qquad (2.65)$$

for interactions of time-component Lorentz-vector Dirac structure, $\Gamma \otimes \Gamma = \gamma_0 \otimes \gamma_0$ [18],

$$M\Phi = [E_1 + E_2]\Phi + \frac{1}{2}\int_0^\infty \frac{\mathrm{d}p'p'^2}{(2\pi)^2}(V_0 + S_\phi V_0 S'_\phi + C_\phi V_1 C'_\phi)\Phi', \qquad (2.66)$$

for interactions of Lorentz-vector Dirac structure, $\Gamma \otimes \Gamma = \gamma_\mu \otimes \gamma^\mu$ [18],

$$M\Phi = [E_1 + E_2]\Phi + \int_0^\infty \frac{\mathrm{d}p'p'^2}{(2\pi)^2}(2V_0 - S_\phi V_0 S'_\phi)\Phi', \qquad (2.67)$$

20

for interactions of Lorentz-pseudoscalar Dirac structure, $\Gamma \otimes \Gamma = \gamma_5 \otimes \gamma_5$,

$$M\Phi = [E_1 + E_2]\Phi + \frac{1}{2}\int_0^\infty \frac{\mathrm{d}p' p'^2}{(2\pi)^2}\Big[ -V_0 + S_\phi V_0 S'_\phi + C_\phi V_1 C'_\phi \Big]\Phi', \qquad (2.68)$$

and, for interactions of BJK Dirac structure [25, 26], $\Gamma \otimes \Gamma = \frac{1}{2}(\gamma_\mu \otimes \gamma^\mu + \gamma_5 \otimes \gamma_5 - 1 \otimes 1)$,

$$M\Phi = [E_1 + E_2]\Phi + \int_0^\infty \frac{\mathrm{d}p' p'^2}{(2\pi)^2}V_0\Phi'. \qquad (2.69)$$

We can write all of these equations with various Lorentz structures as one equation by introducing the parameters $\eta_i, i = 0, 1, 2$,

$$M\Phi = [E_1 + E_2]\Phi + \frac{1}{2}\int_0^\infty \frac{\mathrm{d}p' p'^2}{(2\pi)^2}(\eta_1 V_0 + \eta_2 S_\phi V_0 S'_\phi + \eta_3 C_\phi V_1 C'_\phi)\Phi', \qquad (2.70)$$

the parameters take values listed in the following table:

| $m_1 = m_2$ | $1 \otimes 1$ | $\gamma_0 \otimes \gamma_0$ | $\gamma_\mu \otimes \gamma^\mu$ | $\gamma_5 \otimes \gamma_5$ | $BJK$ |
|---|---|---|---|---|---|
| $\eta_1$ | $-1$ | $1$ | $4$ | $-1$ | $2$ |
| $\eta_2$ | $-1$ | $1$ | $-2$ | $1$ | $0$ |
| $\eta_3$ | $1$ | $1$ | $0$ | $1$ | $0$ |

**Table 2.2:** Parameters $\eta_i$ in the reduced Salpeter equation (2.70).

If the bound state includes two constituents with same masses, the reduced Salpeter equation will become much more simple.

## 2.5 Introducing the Exact Propagator for Salpeter Equation

### 2.5.1 Exact Propagator

The Salpeter equation is related to two assumptions, instantaneous interaction and free propagator. But the latter assumption gives rise to some conceptual problems as a light quark placed in a static chromoelectric field which polarizes the vacuum effectively can become a dressed constituent quark. Recently an exact-propagator instantaneous Bethe-Salpeter equation has been proposed by [14]. There

the fermion propagator $S_i(p)$ is defined by two (Lorentz-scalar) functions, the quark wave-function renormalization function $Z_i(p^2)$ and mass function $M_i(p)$,

$$S_i(p) = \frac{i\, Z_i(p^2)}{\not{p} - M_i(p^2) + i\,\varepsilon}\ , \qquad \not{p} \equiv p^\mu\, \gamma_\mu\ . \tag{2.71}$$

To generalize the Salpeter equation with exact propagator we have to assume the functions $M_i(p^2)$ and $Z_i(p^2)$ to depend only on the spatial components $\boldsymbol{p}$ of the momentum $p$. That allows to substitute $M_i(p^2)$ by $M_i(\boldsymbol{p^2})$ and $Z_i(p^2)$ by $Z_i(\boldsymbol{p^2})$. The energy $E(p) = \sqrt{M_i^2(p^2) + p^2}$.

## 2.5.2 Exact Propagator Instantaneous Bethe-Salpeter Formalism

In this section, we briefly review the exact-propagator instantaneous Bethe-Salpeter formalism.

With the constraints $\Lambda_i^+(\boldsymbol{p}) + \Lambda_i^-(\boldsymbol{p}) = 1$ and $\Lambda_i^\pm(\boldsymbol{p})\gamma_0 = \gamma_0\Lambda_i^\pm(-\boldsymbol{p})$ the exact propagator $S_i(p)$ can be rewritten as [14, 94]

$$S_i(p) = i\, Z_i(\boldsymbol{p^2})\Big(\frac{\Lambda_i^+(\boldsymbol{p})}{p_0 - E_i(\boldsymbol{p}) + i\,\varepsilon} + \frac{\Lambda_i^-(\boldsymbol{p})}{p_0 + E_i(\boldsymbol{p}) - i\,\varepsilon}\Big)\gamma_0. \tag{2.72}$$

By inserting the exact propagator $S_i(p)$ into the integral of the product of fermion propagators in the Bethe-Salpeter equation (2.53) and employing the residue theorem, we finally arrive at the exact propagator instantaneous Bethe-Salpeter formalism for fermion-antifermion bound states:

$$\Phi(\boldsymbol{p}) = Z_1(\boldsymbol{p}_1^2)\, Z_2(\boldsymbol{p}_2^2) \int \frac{d^3p'}{(2\pi)^3} \Big[\frac{\Lambda_1^+(\boldsymbol{p}_1)\gamma_0[V(\boldsymbol{p},\boldsymbol{p'})\Phi(\boldsymbol{p'})]\gamma_0\Lambda_2^-(\boldsymbol{p}_2)}{M - E_1(\boldsymbol{p}_1) - E_2(\boldsymbol{p}_2)}$$
$$-\frac{\Lambda_1^-(\boldsymbol{p}_1)\gamma_0[V(\boldsymbol{p},\boldsymbol{p'})\Phi(\boldsymbol{p'})]\gamma_0\Lambda_2^+(\boldsymbol{p}_2)}{M + E_1(\boldsymbol{p}_1) + E_2(\boldsymbol{p}_2)}\Big]. \tag{2.73}$$

### 2.5.3 Exact Propagator Reduced Salpeter Equation

Since the reduced Salpeter equation just has one Salpeter component, it is easier to extend the reduced Salpeter equation towards the exact-propagator case. Adopting the same fermion propagator $S_i(p)$ formula mentioned above, the reduced Salpeter equation with exact propagator simply reads

$$\Phi(\boldsymbol{p}) = Z^2(\boldsymbol{p^2}) \int \frac{d^3p'}{(2\pi)^3} \frac{\Lambda_1^+(\boldsymbol{p})\gamma_0[V(\boldsymbol{p},\boldsymbol{p'})\Phi(\boldsymbol{p'})]\gamma_0\Lambda_2^-(-\boldsymbol{p})}{M - E_1 - E_2}. \tag{2.74}$$

The corresponding eigenvalue equation is

$$M\Phi(\boldsymbol{p}) = \left[E_1(\boldsymbol{p}) + E_2(\boldsymbol{p})\right]\Phi(\boldsymbol{p})$$

$$+ Z^2(\boldsymbol{p}^2) \int \frac{\mathrm{d}^3 p'}{(2\pi)^3} \Lambda_1^+(\boldsymbol{p})\gamma_0[V(\boldsymbol{p},\boldsymbol{p}')\Phi(\boldsymbol{p}')]\gamma_0\Lambda_2^-(-\boldsymbol{p}). \quad (2.75)$$

### 2.5.4 Exact Propagator Reduced Salpeter Eigenvalue Equations for Various Kernels

Following the same way, we can deduce the exact-propagator reduced Salpeter eigenvalue equations for various interaction kernels acting on the reduced Salpeter amplitude. Here the two constituents of bound state have different mass value $m_1 \neq m_2$.

To simplify the description, we use the substitutions $Z^2 = Z^2(p^2)$, $E_i = E_i(p) = \sqrt{M_i^2(p^2) + p^2}$, $\Phi = \Phi(p)$, $\Phi' = \Phi(p')$.

For interactions of Lorentz-scalar Dirac structure $\Gamma \otimes \Gamma = 1 \otimes 1$,

$$M\Phi = [E_1 + E_2]\Phi + \frac{1}{2}Z^2 \int_0^\infty \frac{\mathrm{d}p'p'^2}{(2\pi)^2}(-V_0 - S_\phi V_0 S'_\phi + C_\phi V_1 C'_\phi)\Phi', \quad (2.76)$$

for interactions of time-component Lorentz-vector Dirac structure $\Gamma \otimes \Gamma = \gamma_0 \otimes \gamma_0$,

$$M\Phi = [E_1 + E_2]\Phi + \frac{1}{2}Z^2 \int_0^\infty \frac{\mathrm{d}p'p'^2}{(2\pi)^2}(V_0 + S_\phi V_0 S'_\phi - C_\phi V_1 C'_\phi)\Phi', \quad (2.77)$$

for interactions of Lorentz-vector Dirac structure $\Gamma \otimes \Gamma = \gamma_\mu \otimes \gamma^\mu$,

$$M\Phi = [E_1 + E_2]\Phi + Z^2 \int_0^\infty \frac{\mathrm{d}p'p'^2}{(2\pi)^2}(2V_0 - S_\phi V_0 S'_\phi)V_0\Phi', \quad (2.78)$$

for interactions of Lorentz-pseudoscalar Dirac structure $\Gamma \otimes \Gamma = \gamma_5 \otimes \gamma_5$,

$$M\Phi = [E_1 + E_2]\Phi + \frac{1}{2}Z^2 \int_0^\infty \frac{\mathrm{d}p'p'^2}{(2\pi)^2}\left[-V_0 + S_\phi V_0 S'_\phi + C_\phi V_1 C'_\phi\right]\Phi', \quad (2.79)$$

and, for interactions of BJK Dirac structure [25, 26] $\Gamma \otimes \Gamma = \frac{1}{2}(\gamma_\mu \otimes \gamma^\mu + \gamma_5 \otimes \gamma_5 - 1 \otimes 1)$,

$$M\Phi = [E_1 + E_2]\Phi + Z^2 \int_0^\infty \frac{\mathrm{d}p'p'^2}{(2\pi)^2}V_0\Phi'. \quad (2.80)$$

We can also write all of these equations with various kernels of Lorentz interaction structure using one equation by introducing the parameters $\eta_i, i = 0, 1, 2$

$$M\Phi = [E_1 + E_2]\Phi + \frac{1}{2}Z^2 \int_0^\infty \frac{\mathrm{d}p'p'^2}{(2\pi)^2}(\eta_1 V_0 + \eta_2 S_\phi V_0 S'_\phi + \eta_3 C_\phi V_1 C'_\phi)\Phi', \quad (2.81)$$

the parameters take that values listed in table 2.2.

## 2.6 Summary and Conclusion

In this chapter we have briefly reviewed the properties of Salpeter equation and discussed the interaction kernels with various Lorentz structures. Following Lagaë's method, by introducing a convenient set of basis and expanding the Salpeter amplitude on it, the Salpeter equation is transformed to a set of coupled eigenvalue equations. The form of Salpeter eigenvalue equation with time-component vector Lorentz structure interaction kernel $\gamma_0 \otimes \gamma_0$ is obtained and the eigenvalue equations for other Lorentz structures $1 \otimes 1$, $\gamma_\mu \otimes \gamma_\mu$, $\gamma_5 \otimes \gamma_5$, $\frac{1}{2}(\gamma_\mu \otimes \gamma^\mu + \gamma_5 \otimes \gamma_5 - 1 \otimes 1)$ have also been given in this chapter. Although the full Salpeter equation has been widely used and proved effective for some cases, the shortcomings are evident, for example it has negative energy solutions [17, 9]. In addition, the solutions are unstable in the case of some interaction kernels. That is partly the reason that the simplification schemes are developed to reduce the Salpeter equation. The reduced Salpeter equation evades some difficulties lying in the full one and can be handled more conveniently.

The exact quark propagator has been introduced to the Salpeter equation and reduced Salpeter equation for the quark-antiquark bound state. The eigenvalue equations for Salpeter equation and reduced Salpeter equation with exact quark propagator have also been obtained for the further discussion in next chapter.

# Chapter 3

# Salpeter Equation with Exact Propagator

Recently the instantaneous Bethe-Salpeter equation with exact quark propagator has been discussed in Refs. [14, 94]. In this chapter, we review the assumption of the exact quark propagator function for the instantaneous Bethe-Salpeter equation. By analyzing the properties of the exact quark propagator function and the corresponding exact-propagator instantaneous Bethe-Salpeter equation and exact-propagator reduced Salpeter equation, the influence induced by the exact quark propagator on pseudoscalar bound state will be discussed.

## 3.1   Introduction

As stated in the previous chapter, the instantaneous Bethe-Salpeter equation is related to the free propagator assumption. However, the assumption of free propagators for the bound-state constituents faces conceptual problem [27, 28, 31, 32, 33, 34, 38]. It is still questionable whether the free propagator can be applied to light quarks. In addition, as stated in Ref. [14], in quantum chromodynamics, the simultaneous free propagator assumptions for the bound-state constituents and confining interaction can not be consistent. This suggests us to investigate the problem with corresponding exact propagators [48, 51]. This chapter is mainly to study the influences of introducing exact quark propagators in the instantaneous Bethe-Salpeter equation.

This chapter is organized as follows. Sec. 3.2 presents the review of the quark propagator function from the Dyson-Schwinger equation and the analysis of the

behavior of quark propagator function. The exact-propagator instantaneous Bethe-Salpeter equation for pseudoscalar bound state is built up and transformed to a matrix problem in Sec. 3.3. Numerical solutions for the mass eigenvalue of the radial excited states are also obtained there. In Sec. 3.4, the exact-propagator instantaneous Bethe-Salpeter equation with various Lorentz structure interaction kernels is used to analyze the pseudoscalar bound state and the results of which are compared with those of the free-propagator Salpeter equation. Moreover, the plots of the radial wave functions of the pseudoscalar bound state obtained by solving both free-propagator Salpeter equation and exact-propagator instantaneous Bethe-Salpeter equation are presented. Sec. 3.5 is the summary of this chapter.

## 3.2  Quark Propagator from Dyson-Schwinger Equation

The Dyson-Schwinger equation (DSE) presents a nonperturbative method to study hadrons as bound states of quarks and the confinement of quarks and gluons within QCD. The simplest Dyson-Schwinger equation is the so called gap equation [50]

$$S^{-1}(p) = Z_2(\zeta^2, \Lambda^2)(i\gamma \cdot p + m_{bare}) + Z_1(\zeta^2, \Lambda^2) \int \frac{d^4q}{(2\pi)^4} g^2 D_{\mu\nu}(p-q)\frac{\lambda^a}{2}\gamma_\mu S(q)\Gamma_\nu^a(q;p)$$

(3.1)

where $D_{\mu\nu}(p-q)$ is the dressed propagator, $\Gamma_\nu^a(q;p)$ is the dressed quark-gluon vertex, $m_{bare}$ is the bare mass of current quark, $\Lambda$ is the regulation mass scale. $Z_{1,2}(\zeta^2, \Lambda^2)$ are the quark gluon vertex and quark wave function renormalization constants. The most general solution of the gap equation is the dressed quark propagator, or exact quark propagator [50]

$$S^{-1}(p) = i\gamma \cdot p A(p^2, \zeta^2) + B(p^2, \zeta^2) = \frac{1}{Z(p^2, \zeta^2)}[i\gamma \cdot p + m(p^2)].$$ (3.2)

The integration kernel in the DSE involves the exact gluon propagator $D_{\mu\nu}(p-q)$ which is a two-point Green function and the exact quark-gluon vertex $\Gamma_\nu^a(q;p)$ which is a three-point Green function. The gap equation is coupled to these two functions of Dyson-Schwinger equation to infinite hierarchy. So, it is necessary to make a truncation to these integral equations.

By using the so called "rainbow-ladder truncation" scheme [35, 48, 49, 51, 52, 53, 54, 56] to the Dyson-Schwinger equation and Bethe-Salpeter equation, the exact

gluon propagator and the exact quark-gluon vertex are replaced by their tree-level forms. In the literature [35], the exact quark propagators obtained from this truncation model are numerical solutions of quark Dyson-Schwinger equation by fitting the properties of pion and kaon. The Dyson-Schwinger equations are usually analyzed in Euclidean space, which implies that the exact quark propagators are also obtained as Euclidean-space functions. However, within QED and QCD, the analytical structure of the exact fermion propagators is still receiving intense interest and there is no definitive conclusion until now (see Refs. [55, 66, 72] and therein). So, in practical calculation, we have to assume that at least for light-quark propagators, it is necessary to make an analytical continuation from Euclidean to Minkowski space. In this case, the quark propagator functions $m(p^2)$ and $Z(p^2)$ for the $u$ and $d$ quark can be formalized in analytical form as

$$m(p^2) = \frac{a}{1 + \frac{p^4}{b}} + m_0, \quad Z(p^2) = 1 - \frac{c}{1 - \frac{p^2}{d}}, \quad (3.3)$$

where the values of the parameters for $u$ and $d$ quark are given by interpolation of the numerical results

$$a = 0.745 GeV, \quad b = (0.744 GeV)^4, \quad m_0 = 0.0055 GeV,$$

$$c = 0.545, \quad d = (1.85508 GeV)^2. \quad (3.4)$$

The parameters for $s$ quark reads

$$a = 0.8 GeV, \quad b = (1.2 GeV)^4, \quad m_0 = 0.09 GeV, \quad (3.5)$$

$$Z(p^2) = 1. \quad (3.6)$$

### 3.2.1 The Behavior of Quark Propagator Functions

For the instantaneous Bethe-Salpeter equation, in the "$p_0^2 = 0$" approximation [14], these functions can be written as

$$m(\boldsymbol{p}^2) = \frac{a}{1 + \frac{\boldsymbol{p}^4}{b}} + m_0, \quad Z(\boldsymbol{p}^2) = 1 - \frac{c}{1 + \frac{\boldsymbol{p}^2}{d}}. \quad (3.7)$$

Figure 3.1 and 3.2 show the behavior of mass function $m_n(\boldsymbol{p}^2)$ and $m_s(\boldsymbol{p}^2)$ with respect to $\boldsymbol{p}^2$ for the $u, d$ quark and $s$ quark respectively. Figure 3.3 shows the behavior of the wave function renormalization function $Z(\boldsymbol{p}^2)$ with respect to $\boldsymbol{p}^2$.
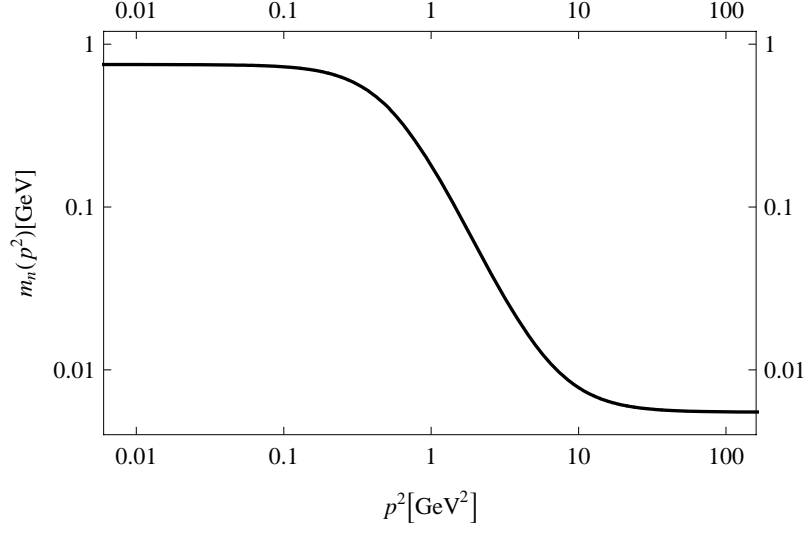
27

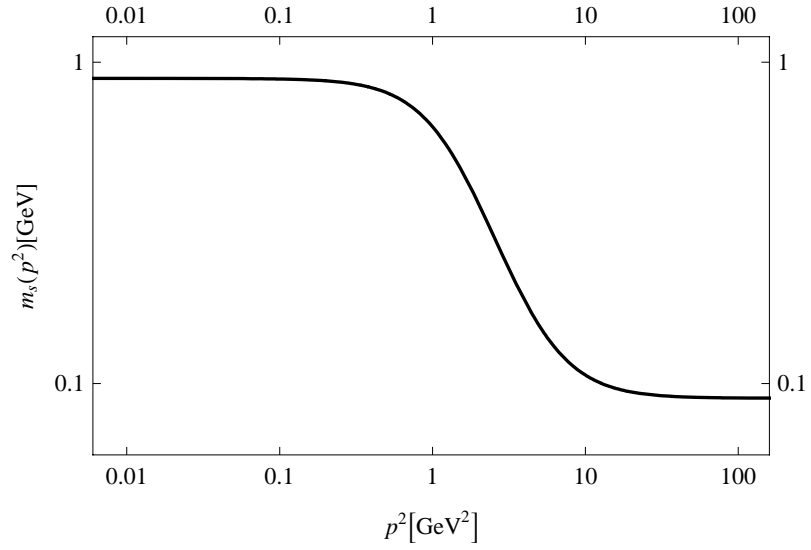Figure 3.1: Mass function $m_n(\boldsymbol{p^2})$ for $u$ and $d$ quark, $n = u, d$.



Figure 3.2: Mass function $m_s(\boldsymbol{p^2})$ for $s$ quark.
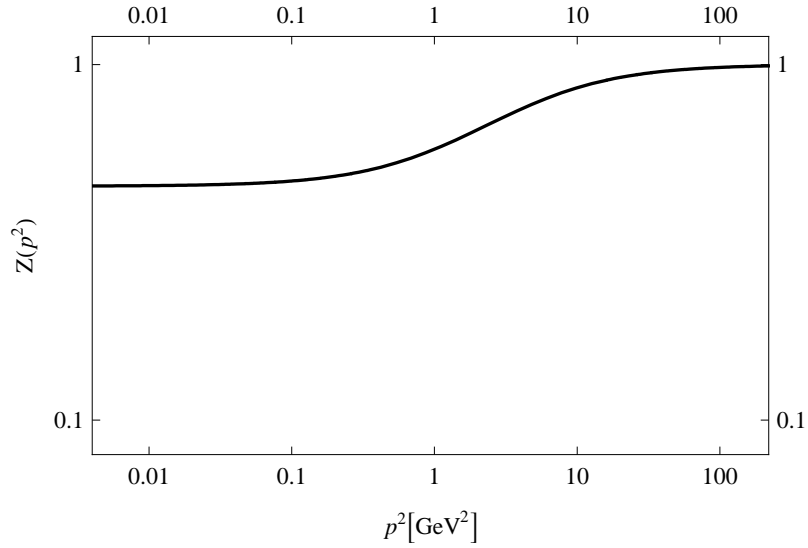
Figure 3.3: Wave-function renormalization function $Z(\boldsymbol{p}^2)$ for $u$ and $d$ quark.

For light quarks, such as $u$ and $d$ quark, the mass function $m_n(\boldsymbol{p}^2)$ is dominated by the nonperturbative mechanism responsible for dynamical chiral-symmetry breaking.

From Fig. 3.1 we can see the value of $m_n(\boldsymbol{p}^2)$ drops at $\boldsymbol{p}^2 \approx (0.57 GeV)^2$ by more than two orders from the starting position $m_n(\boldsymbol{0}) = 0.7505 GeV$. It will approach the current light-quark mass $m_0 = 0.0055 GeV$ in the limit $\boldsymbol{p}^2 \to \infty$. From Fig. 3.2, for the strange quark, we can find the value of mass $m_s(p^2)$ drops by approximately one order from the starting position $m_s(\boldsymbol{0}) = 0.89 GeV$. In contrast, the wave function renormalization function $Z(\boldsymbol{p}^2)$ changes very mildly. With increasing of $\boldsymbol{p}^2$, $Z(\boldsymbol{p}^2)$ rises slowly from $Z(\boldsymbol{0}) = 0.455$ to the value 1 as $\boldsymbol{p} \to \infty$, as shown in Fig. 3.3. The two functions of the exact propagator of light $u$ and $d$ quarks are obtained by numerically solving the quark Dyson–Schwinger equation in the "renormalization-group-improved rainbow–ladder truncation" model.

## 3.3 Exact Propagator Instantaneous Bethe-Salpeter Equation for Pseudoscalar Bound States

In the present work we focus on fermion-antifermion bound states. The general form of instantaneous Bethe-Salpeter equation with exact propagator has been stated in Chapter 2. Now we discuss the practical computation process for the pseudoscalar

fermion-antifermion bound state. The analysis of reduced Salpeter equation with exact propagator is also given in the following.

The pseudoscalar states are denoted with $J^{PC} = 0^{-+}$. The kernel $\hat{K}(\boldsymbol{p}, \boldsymbol{p}')$ in the Bethe-Salpeter integrals with time-component Lorentz-vector structure reads $V(\boldsymbol{p} - \boldsymbol{p}')\gamma_0 \otimes \gamma_0$ where $V(\boldsymbol{p} - \boldsymbol{p}')$ is any potential. In the following we will see the exact-propagator instantaneous Bethe-Salpeter equation (2.73) can be reduced to a set of coupled equations for the radial Salpeter amplitude [8, 17].

### 3.3.1 The Formalism

Generally, in the case of the Salpeter equation (2.73), the expansion of the Salpeter amplitude $\Phi(\boldsymbol{p})$ over a complete set of Dirac matrices involves the full 16 independent Salpeter components. However, because of the constraints $\Lambda_1^{\pm}(\boldsymbol{p})_1 \Phi(\boldsymbol{p}) \Lambda_2^{\pm}(\boldsymbol{p})_2 = 0$, the Salpeter amplitude $\Phi(\boldsymbol{p})$ just has eight independent components. For the pseudoscalar states, only two of them, $\Phi_1(\boldsymbol{p})$ and $\Phi_2(\boldsymbol{p})$ are relevant. Therefore, in the center-of-momentum frame of the fermion-antifermion bound state, the corresponding Salpeter amplitude reads

$$\Phi(\boldsymbol{p}) = \left[ \Phi_1(\boldsymbol{p}) \frac{H(\boldsymbol{p})}{E(\boldsymbol{p})} + \Phi_2(\boldsymbol{p}) \right] \gamma_5, \qquad (3.8)$$

where the $E(\boldsymbol{p})$ is the one-particle energy and $H(\boldsymbol{p})$ is the corresponding Hamiltonian introduced in the last chapter.

For the equal mass case $m_1 = m_2$, since $p \equiv |\boldsymbol{p}|$, we have $Z_1(\boldsymbol{p}^2) = Z_2(\boldsymbol{p}^2) \equiv Z(p^2)$, $m_1(\boldsymbol{p}^2) = m_2(\boldsymbol{p}^2) \equiv m(p^2)$ and of course $E_1(\boldsymbol{p}) = E_2(\boldsymbol{p}) = E(p) \equiv \sqrt{p^2 + m^2(p^2)}$. By inserting the wave function renormalization function $Z(p^2)$ in all interaction terms and replacing all constant constituent masses $m$ by the mass function $m(p^2)$, for the time component Lorentz-vector structure we obtain two coupled equations.

$$M\Phi_1(p) = 2E(p)\Phi_2(p) + Z^2(p^2) \int_0^\infty \frac{\mathrm{d}p' p'^2}{(2\pi)^2} V_0(p, p') \Phi_2(p'), \qquad (3.9)$$

$$M\Phi_2(p) = 2E(p)\Phi_1(p)$$

$$+ \; Z^2(p^2) \int_0^\infty \frac{\mathrm{d}p' p'^2}{(2\pi)^2} \left[ \frac{m(p^2)}{E(p)} V_0(p, p') \frac{m(p'^2)}{E(p')} \right.$$

$$+ \; \left. \frac{p}{E(p)} V_1(p, p') \frac{p'}{E(p')} \right] \Phi_1(p'). \qquad (3.10)$$

The configuration and momentum space representations of radial function are related by Fourier-Bessel transformations (see appendix B) which involve spherical

Bessel functions of the first kind $j_n(z)(n = 0, \pm 1, \pm 2, ...)$ [74]. To solve this set of coupled equations, we insert Eq. (3.9) into (3.10) to obtain an eigenvalue equation for $M^2$:

$$
\begin{aligned}
M^2\, \Phi_2(p) \;=\;& 4\,E^2(p)\,\Phi_2(p) + 2\,Z^2(p^2)\,E(p) \int_0^\infty \frac{\mathrm{d}p'\,p'^2}{(2\pi)^2}\, V_0(p,p')\,\Phi_2(p') \\[2mm]
&+\; 2\frac{Z^2(p^2)}{E(p)} \int_0^\infty \frac{\mathrm{d}p'\,p'^2}{(2\pi)^2} \left[ m(p^2)\,M(p'^2)\,V_0(p,p') + pp'V_1(p,p') \right] \Phi_2(p') \\[2mm]
&+\; Z^2(p^2) \int_0^\infty \frac{\mathrm{d}p'\,p'^2}{(2\pi)^2} \left[ \frac{m(p^2)}{E(p)}\,V_0(p,p')\,\frac{M(p'^2)}{E(p')} + \frac{p}{E(p)}\,V_1(p,p')\,\frac{p'}{E(p')} \right] \\[2mm]
&\times\; Z^2(p'^2) \int_0^\infty \frac{\mathrm{d}p''\,p''^2}{(2\pi)^2}\, V_0(p',p'')\,\Phi_2(p'') \;. \qquad\qquad (3.11)
\end{aligned}
$$

with

$$
V_L(p,p') \equiv 8\pi \int_0^\infty \mathrm{d}r\, r^2 V(r) j_L(pr) j_L(p'r), \qquad L = 0, 1, 2, .... \qquad (3.12)
$$

As stated in the last section, by taking the approximation $m(p^2) \simeq m$ and $Z(p^2) \simeq 1$ for the propagator, we obtain the Salpeter equation for the free propagator.

### 3.3.2 Matrix Method for Solving the Salpeter Equation

Several techniques have been developed to numerically solve the reduced Salpeter equation [57, 61] and even the full Salpeter equation [8]. In our computation we use a generalization of the method of Refs. [8, 59, 64, 65]; that is, in order to numerically calculate the full Salpeter equation, we transform the corresponding eigenvalue equation to a matrix equation by expanding the components of the Bethe-Salpeter amplitue on a set of orthonormal basis. The orthonormal basis functions are summarized in appendix B. For the numerical calculation, this matrix has to be truncated with a suitable number of basis functions. The approximate solutions depend on the size of the basis.

By multiplying with $\int_0^\infty \mathrm{d}p\,p^2 \phi_i^{(0)}(p)$ from the left side for both sides of Eq. (3.11), and expanding $\Phi_2(p)$ in terms of the radial basis functions $\phi_i^{(0)}(p)$, the instantaneous Bethe-Salpeter equation can be transformed to a set of matrix equations and solved by diagonalizing the corresponding matrix:

$$
M_{ij} = \mathrm{I}_{ij} + \mathrm{II}_{ij} + \mathrm{III}_{ij} + \mathrm{IV}_{ij} + \mathrm{V}_{ij} + \mathrm{VI}_{ij} \qquad (3.13)
$$

31

where the $\mathrm{I}_{ij}, \mathrm{II}_{ij}, \mathrm{III}_{ij}, \mathrm{IV}_{ij}, \mathrm{V}_{ij}, \mathrm{VI}_{ij}$ represents:

$$\mathrm{I}_{ij} = 4 \int_0^\infty \mathrm{d}p p^2 E^2(p) \phi_i^{(0)}(p) \phi_j^{(0)}(p),$$

$$\mathrm{II}_{ij} = 2 \int_0^\infty \frac{\mathrm{d}p p^2}{(2\pi)^2} Z^2(p^2) E(p) \phi_i^{(0)}(p) \int_0^\infty \mathrm{d}p' p'^2 V_0(p, p') \phi_j^{(0)}(p'),$$

$$\mathrm{III}_{ij} = 2 \int_0^\infty \frac{\mathrm{d}p p^2}{(2\pi)^2} \frac{Z^2(p^2) m(p^2)}{E(p)} \phi_i^{(0)}(p) \int_0^\infty \mathrm{d}p' p'^2 M(p'^2) V_0(p, p') \phi_j^{(0)}(p'),$$

$$\mathrm{IV}_{ij} = 2 \int_0^\infty \frac{\mathrm{d}p p^2}{(2\pi)^2} \frac{p Z^2(p^2)}{E(p)} \phi_i^{(0)}(p) \int_0^\infty \mathrm{d}p' p'^2 \; p' V_1(p, p') \phi_j^{(0)}(p'),$$

$$\mathrm{V}_{ij} = \int_0^\infty \frac{\mathrm{d}p p^2}{(2\pi)^2} \frac{Z^2(p^2) m(p^2)}{E(p)} \phi_i^{(0)}(p) \int_0^\infty \mathrm{d}p' p'^2 \frac{Z^2(p'^2) M(p'^2)}{E(p')} V_0(p, p')$$

$$\times \int_0^\infty \frac{\mathrm{d}p'' p''^2}{(2\pi)^2} V_0(p', p'') \phi_j^{(0)}(p''),$$

$$\mathrm{VI}_{ij} = \int_0^\infty \frac{\mathrm{d}p p^2}{(2\pi)^2} \frac{p Z^2(p^2)}{E(p)} \phi_i^{(0)}(p) \int_0^\infty \mathrm{d}p' p'^2 \frac{p' Z^2(p'^2)}{E(p')} V_1(p, p')$$

$$\times \int_0^\infty \frac{\mathrm{d}p'' p''^2}{(2\pi)^2} V_0(p', p'') \phi_j^{(0)}(p'').$$

The first term $\mathrm{I}_{ij}$ is the matrix element of the square $E^2$. We define $a_{ij}$ as the integral part

$$a_{ij} = \int_0^\infty \mathrm{d}p p^2 E^2(p) \phi_i^{(0)}(p) \phi_j^{(0)}(p). \tag{3.14}$$

In order to calculate the other terms $\mathrm{II}_{ij}, \mathrm{III}_{ij}, ..., \mathrm{VI}_{ij}$, we expand relevant expressions in these integrals in terms of a set of basis functions $\phi_i^{(l)}(p), l = 0, 1$ in momentum space:

$$Z^2(p^2) E(p) \phi_i^{(0)}(p) = \sum_{j=0}^N b_{ji} \phi_j^{(0)}(p),$$

$$\frac{Z^2(p^2) m(p^2)}{E(p)} \phi_i^{(0)}(p) = \sum_{j=0}^N c_{ji} \phi_j^{(0)}(p),$$

32

$$\frac{p\ Z^2(p^2)}{E(p)}\phi_i^{(0)}(p) = \sum_{j=0}^{N} d_{ji}\phi_j^{(1)}(p),$$

$$p\phi_i^{(0)}(p) = \sum_{j=0}^{N} e_{ji}\phi_j^{(1)}(p),$$

$$M(p^2)\phi_i^{(0)}(p) = \sum_{j=0}^{N} f_{ji}\phi_j^{(0)}(p). \tag{3.15}$$

Fourier-Bessel transformations are used in the above calculations.

By using the orthonormality of the basis functions $\phi_i^{(l)}(p)$, the expansion coefficients $b_{ij}, d_{ij}, e_{ij}, f_{ij}$ can be expressed as:

$$b_{ij} = \int_0^\infty \mathrm{d}pp^2 Z^2(p^2)E(p)\phi_i^{*(0)}(p)\phi_j^{(0)}(p),$$

$$c_{ij} = \int_0^\infty \mathrm{d}pp^2 \frac{Z^2(p^2)m(p^2)}{E(p)}\phi_i^{*(0)}(p)\phi_j^{(0)}(p),$$

$$d_{ij} = \int_0^\infty \mathrm{d}pp^2 \frac{pZ^2(p^2)}{E(p)}\phi_i^{*(1)}(p)\phi_j^{(0)}(p),$$

$$e_{ij} = \int_0^\infty \mathrm{d}pp^2 p\phi_i^{*(1)}(p)\phi_j^{(0)}(p),$$

$$f_{ij} = \int_0^\infty \mathrm{d}pp^2 M(p^2)\phi_i^{*(0)}(p)\phi_j^{(0)}(p). \tag{3.16}$$

Then we expand $V(r)\phi_i^{(l)}(p)$ in terms of $\phi_i^{(l)}(p)$:

$$V(r)\phi_i^{(l)}(p) = \sum_{j=0}^{N} V_{ji}^{(l)}\phi_j^{(l)}(p), \quad l = 0, 1. \tag{3.17}$$

Here $V_{ji}^{(l)}$ is the real and symmetric matrix of expectation values of the potential $V(\boldsymbol{r})$. With respect to the basis functions $\phi_i^{(l)}(p)$, it can be written as:

$$V_{ij}^{(l)} = \int_0^\infty \mathrm{d}rr^2 V(r)\phi_i^{*(l)}(p)\phi_j^{(l)}(p). \tag{3.18}$$

In the present calculation, we use the potential: $V(r) = \lambda r^b, \ \lambda > 0$. The general expression for $V_{ij}^{(l)}$ can be simplified to [23]

$$V_{ij}^{(l)} = \langle \Phi_i | V(r) | \Phi_j \rangle$$

$$= \lambda \int \mathrm{d}^3 r \Phi_{i,lm}^*(r)\boldsymbol{r}^b \Phi_{j,lm}(r)$$

33

$$= \sqrt{\frac{i!\, j!}{\Gamma(2l+i+3)\Gamma(2l+j+3)}} \frac{\lambda}{(2\mu)^b} \sum_{r=0}^{i}\sum_{s=0}^{j} \frac{(-1)^{r+s}}{r!s!}$$

$$\times \begin{pmatrix} i+2l+2 \\ i-r \end{pmatrix} \begin{pmatrix} j+2l+2 \\ j-s \end{pmatrix} \Gamma(2l+b+r+s+3). \qquad (3.19)$$

Collecting the matrix expressions of all the above terms, for the linear potential $V(r) = \lambda r$, we can rewrite the matrix $M_{ij}$,

$$M_{ij} = 4a_{ij} + 2\sum_{r=0}^{N} b_{ri}V_{rj}^{(0)} + 2\sum_{r=0}^{N}\sum_{s=0}^{N} c_{ri}V_{rs}^{(0)}f_{sj}$$

$$+2\sum_{r=0}^{N}\sum_{s=0}^{N} d_{ri}^{*}V_{rs}^{(1)}e_{sj} + \sum_{r=0}^{N}\sum_{s=0}^{N}\sum_{t=0}^{N} c_{ri}V_{rs}^{(0)}c_{st}V_{tj}^{(0)}$$

$$+\sum_{r=0}^{N}\sum_{s=0}^{N}\sum_{t=0}^{N} d_{ri}^{*}V_{sr}^{(1)}d_{st}V_{tj}^{(0)}. \qquad (3.20)$$

Numerical calculation of Eq. (3.20) with a suitable matrix size $N$ gives the matrix elements. Diagonalization the matrix $M_{ij}$ leads to the eigenvalues of the Salpeter equation.

### 3.3.3 Numerical Results

Now we apply the method developed in the above sections to a linear shape confining potential, $V(r) = \lambda r$, with slope $\lambda = 0.2 GeV^2$. For confining interactions the solutions of time-component Lorentz-vector structure have no stability problems which exist for the solutions of kernel of Lorentz-scalar structure [17, 24, 62].

One of our goals is to analyze the stability of solutions of the instantaneous Bethe-Salpeter equation with exact quark propagator. Therefore, for a $J^{PC} = 0^{-+}$ bound state, we compare the mass eigenvalues $M$ of Eq. (2.73) for exact-propagator with $m_0 = 0$ (corresponding to the chiral limit of QCD) with that of the (free-propagator) Salpeter equation [23, 63].

As stated above, to solve the eigenvalue equation, we need to expand the Salpeter amplitude on a set of basis functions in the Hilbert space. These basis functions involve a variational parameter $\mu > 0$. These basis vectors construct a complete orthonormal system for any value of $\mu$. Therefore, if the Salpeter amplitude can be expanded over the full set of basis vectors, the results may be independent of the parameter $\mu$. In practical computation, we have to make a truncation of expansions to a finite number of basis vectors which will induce some $\mu$-dependence to the

results. However, if we take into account a large enough number of basis vectors, the solutions of Eq. (2.73) will have less dependence on $\mu$ and exhibit some stability. Such a region of stability shows us that the numerical value predicted for mass eigenvalue $M$ is constant over some range of $\mu$. In our computation we adopt a $50 \otimes 50$ matrix to perform numerical calculations. From Fig. 3.4, we can see that using the exact propagator, the mass eigenvalue of ground state of Eq. (2.73) would be higher whereas its values of radial excitations would be lower and all the level spacings are obviously smaller than that of the free-propagator Salpeter equation.

For time-component Lorentz-vector structure $\Gamma \otimes \Gamma = \gamma_0 \otimes \gamma_0$, the first ten eigenvalues of the free-propagator full Salpeter equation with masses $m_1 = m_2 = 0.336 GeV$ and linear potential $V(r) = 0.2r$ are

$$\{5.106,\ 4.853,\ 4.584,\ 4.299,\ 3.994,\ 3.663,\ 3.299,\ 2.889,\ 2.410,\ 1.813\ \}.$$

In the above data group, the last number denotes the eigenvalue of the ground state, the next to the last one denotes the first excited state and the others are in analogy to this order:

$$\{\ \underbrace{\ldots\ldots}_{higher\ excited\ states};\ \underbrace{2.889}_{2nd\ excited\ state};\ \underbrace{2.410}_{1st\ excited\ state};\ \underbrace{1.813}_{ground\ state}\ \} \tag{3.21}$$

In the following, we use the same expression order for the group of eigenvalues as shown above. The first ten eigenvalues of the exact-propagator full Salpeter equation with parameters defined by Eq. (3.3) and (3.4) are

$$\{2.980,\ 2.860,\ 2.738,\ 2.611,\ 2.481,\ 2.345,\ 2.204,\ 2.056,\ 1.895,\ 1.750\}.$$

Table 3.1 lists the mass eigenvalues $M$ of the three lowest-lying states calculated from the free-propagator Salpeter equation and exact-propagator instantaneous Bethe-Salpeter equation Eq. (2.73). For the latter one the full parameters of exact light-quark propagators noted in Eq. (3.4) and (3.7) are used in the calculation.

We use the current mass $m_0 = 0.0055 GeV$ which is different from the value used in previous calculation shown in Fig. 3.4 where $m_0 = 0$ corresponds to the chiral limit of QCD. However, since the current mass $m_0 = 0.0055 GeV$ is small, these mass

eigenvalues are less than 0.5% larger than the corresponding chiral-limit values. So, it is impossible to distinguish these two sets of values in Fig. 3.4 (full lines).

| State | Exact-propagator bound-state equation | Free-propagator Salpeter equation |
|---|---|---|
| $1^1S_0$ | 1.750 | 1.813 |
| $2^1S_0$ | 1.895 | 2.410 |
| $3^1S_0$ | 2.056 | 2.889 |

**Table 3.1** The bound states masses $M$ (in units of GeV) for the three lowest $J^{PC} = 0^{-+}$ eigenstates (denoted by $1^1S_0, 2^1S_0, 3^1S_0$) of exact-propagator instantaneous Bethe-Salpeter equation and of the general free-propagator Salpeter equation for the time-component Lorentz-vector kernels. For the exact-propagator case the mass values adopt light-quark propagator parameters described in Eq. (3.4) and (3.7), For free-propagator equation the mass values take constituent light-quark mass $m = 0.336 GeV$. The linear confining potential $V(r) = \lambda r$ is used with slope $\lambda = 0.2 GeV^2$. All of the mass eigenvalues are obtained by converting both Salpeter equations to $50 \times 50$ matrices.

These mass values are listed with the mass eigenvalues $M$ of the free-propagator Salpeter equation where the masses of the light $u$ and $d$ quarks take the "constituent quark mass" value $m = 0.336 GeV$ which is frequently adopted by nonrelativistic and relativistic constituent quark models to describe hadrons [38, 39]. In our calculation, we find when the constituent quark mass $m$ raise from $m = 0 GeV$ to $m = 0.336 GeV$, the corresponding mass eigenvalues $M$ of the three lowest bound state in Salpeter equation increase by $0.1 GeV$. It suggests that, at least for the light $u$ and $d$ quark, any neglect of the proper behavior of the momentum-dependent quark mass $m(p^2)$ is questionable.

Fig. 3.5 shows the behavior of the components of the radial Salpeter amplitude $\Phi_2(r)$ in configuration space and $\Phi_2(p)$ in momentum space for the $J^{PC} = 0^{-+}$ ground state of the exact-propagator instantaneous Bethe-Salpeter equation. The norm $\parallel \Phi \parallel$ of the Salpeter amplitude $\Phi(\boldsymbol{p})$ for $J^{PC} = 0^{-+}$ bound states [8, 17, 23] is given by

$$\parallel \Phi \parallel^2 = 4 \int \frac{\mathrm{d}^3 p}{(2\pi)^3} [\Phi_1^*(\boldsymbol{p})\Phi_2(\boldsymbol{p}) + \Phi_2^*(\boldsymbol{p})\Phi_1(\boldsymbol{p})]. \tag{3.22}$$

Since

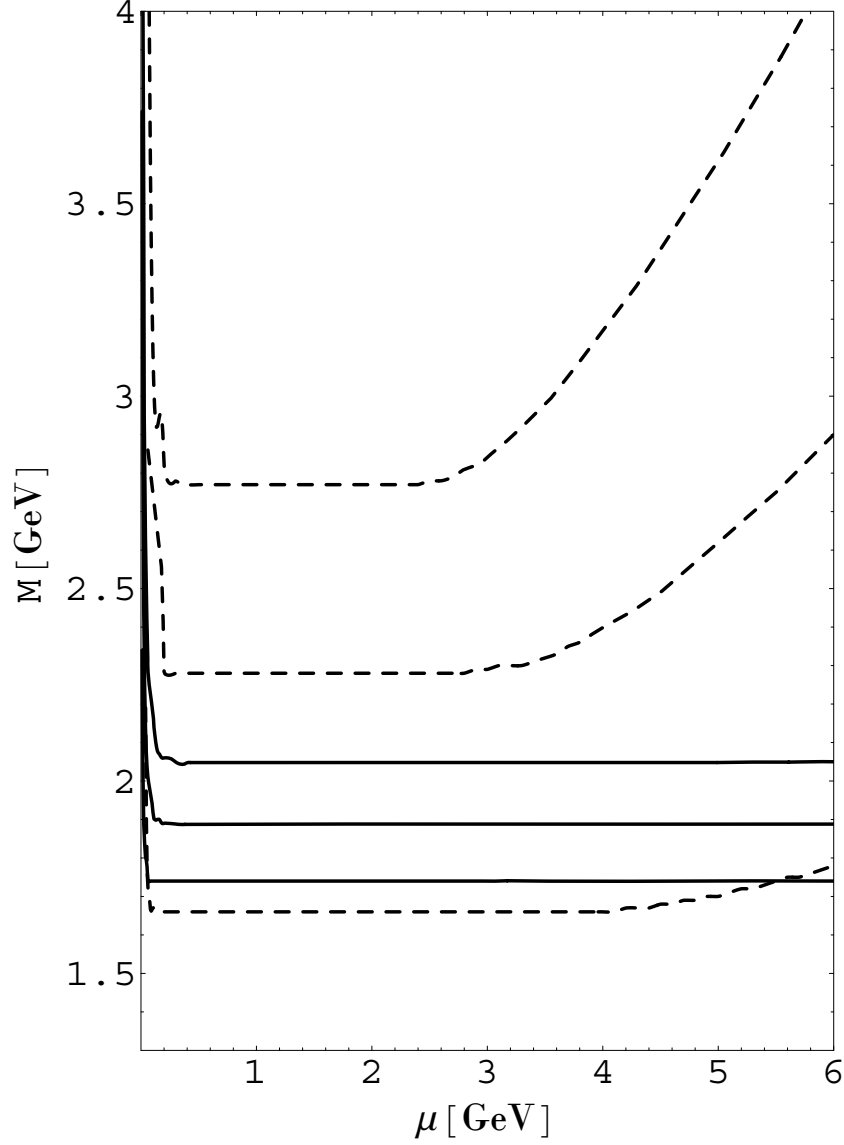$$\Phi(\boldsymbol{p}) = \Phi(p) Y_{l,m}(\hat{p}), \tag{3.23}$$

36

Figure 3.4: Bound-state masses $M$ of the three lowest $J^{PC} = 0^{-+}$ eigenstates of the exact-propagator instantaneous Bethe-Salpeter equation(full lines) and of the general free-Salpeter equation (dashed lines) for a time-component vector kernel $\gamma_0 \otimes \gamma_0$. The potential used here is a linear potential $V(r) = \lambda r$ with slope $\lambda = 0.2 GeV^2$.
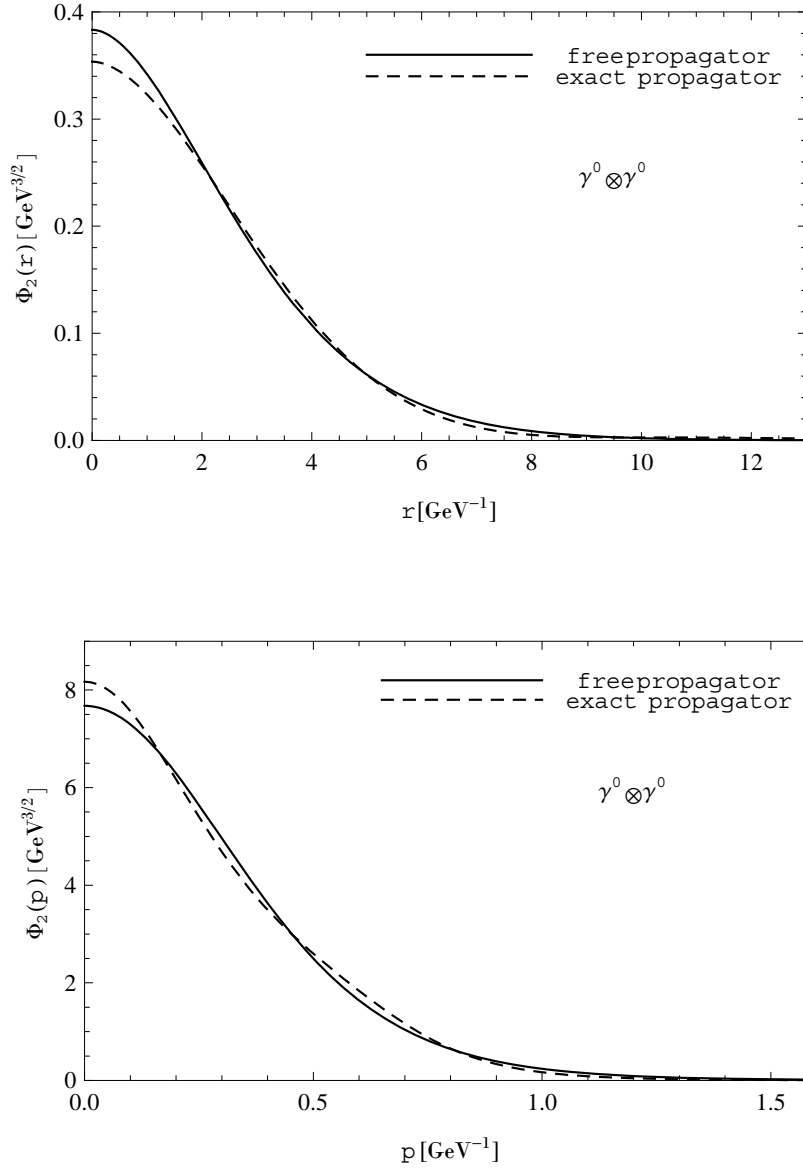
Figure 3.5: Radial Salpeter functions $\Phi_2(r)$ and $\Phi_2(p)$ in configuration space and momentum space for the lowest $J^{PC} = 0^{-+}$ state of exact propagator instantaneous Bethe-Salpeter equation with parameters listed in Eq. (3.4) and (3.7)(dashed lines) and of the free propagator Salpeter equation with light quark constituent mass $m = 0.336 GeV$ (full lines). The interaction kernel takes the time-component Lorentz-vector structure with linear confining potential $V(r) = \lambda r$, $\lambda = 0.2 GeV^2$.

and the integration of $Y_{l,m}(\hat{p})$ over $\int d\Omega$ satisfies

$$\int d\Omega Y_{l,m}^*(\hat{p})Y_{l,m}(\hat{p}) = \delta_{ll'}\delta_{mm'}, \tag{3.24}$$

the norm of the Salpter amplitude $\parallel \Phi \parallel$ is translated to

$$\parallel \Phi \parallel^2 = 4\int_0^\infty \frac{dpp^2}{(2\pi)^3}[\Phi_1^*(p)\Phi_2(p) + \Phi_2^*(p)\Phi_1(p)]. \tag{3.25}$$

In Fig 3.5, we have chosen the normalization such that $\Phi_2$ satisfies

$$\int_0^\infty dr\ r^2|\Phi_2(r)|^2 = \int_0^\infty dpp^2|\Phi_2(p)|^2 = 1\ . \tag{3.26}$$

From Fig. 3.5 one can find that the exact- and free-propagator Salpeter components $\Phi_2(r)$ and $\Phi_2(p)$ show evident difference for $r < 2.2 GeV^{-1}$ for $\Phi_2(r)$ and $r < 0.8 GeV^{-1}$ for $\Phi_2(p)$. It is hard to distinguish from each other when $r > 9 GeV^{-1}$ for $\Phi_2(r)$ and when $r > 0.8 GeV^{-1}$ for $\Phi_2(p)$.

## 3.4 Eigenfunctions of Full Salpeter Equation for Various Kernels

Apart from mass eigenvalues, we also obtain the eigenfunctions of the full free-propagator Salpeter equation and of the exact-propagator instantaneous Bethe-Salpeter equation for the three lowest pseudoscalar bound states $J^{PC} = 0^{-+}$ with the following Lorentz structure interaction kernels:

Time-component Lorentz-vector structure $\quad\Gamma \otimes \Gamma = \gamma_0 \otimes \gamma_0,$

Lorentz-vector structure $\quad\quad\quad\quad\quad\quad\quad\Gamma \otimes \Gamma = \gamma_\mu \otimes \gamma^\mu,$

Böhm-Joos-Krammer (BJK) structure [25, 26] $\Gamma \otimes \Gamma = \frac{1}{2}(\gamma_\mu \otimes \gamma^\mu + \gamma_5 \otimes \gamma_5 - 1 \otimes 1).$

The corresponding analysis shows that there is no bound state for the full Salpeter equation with Lorentz-pseudoscalar structure $\Gamma \otimes \Gamma = \gamma_5 \otimes \gamma_5$ interaction kernels [95]. In the following analysis, we assume the two constituents of the bound state take equal masses and then adopt the parameters defined in Eq. (3.4) and (3.7) for the exact-propagator instantaneous Bethe-Salpeter equation and massless constituent quark masses for free-propagator Salpeter equation. The harmonic oscillator potential $V(r) = r^2$ is used here. The solutions of mass eigenvalues also exhibit stability for the reduced and full Salpeter equation with respect to the parameter $\mu$. In the following calculations we employ $\mu = 1$.

Using the procedure developed in appendix D, the eigenvalues of the reduced Salpeter equation of the ground state and the excited states, as well as the corresponding eigenfunctions are obtained numerically. The corresponding eigenvalues and Salpeter component functions $\Phi_2(r)$ of the full free-propagator Salpeter equation for the three lowest bound states for various Lorentz structures are listed in the following.
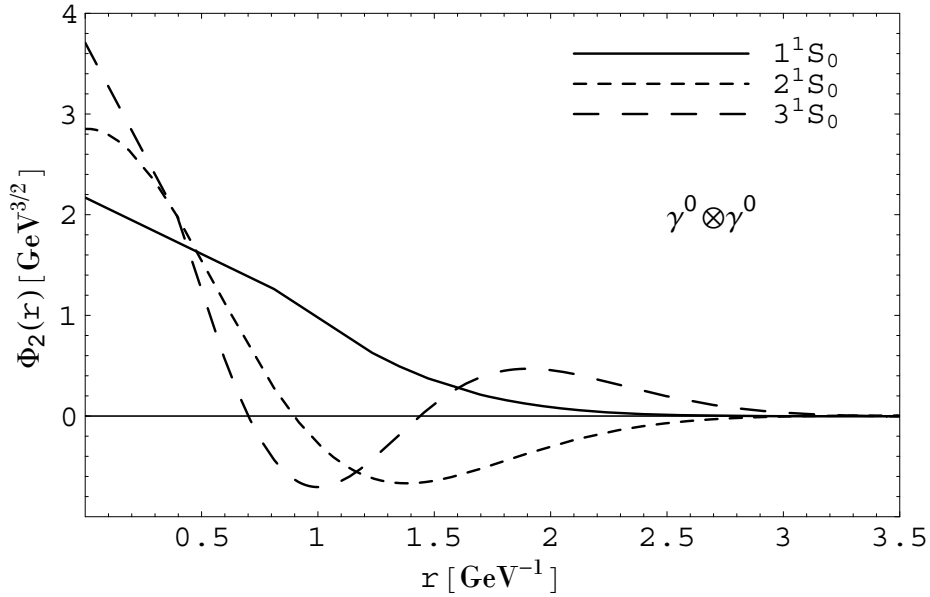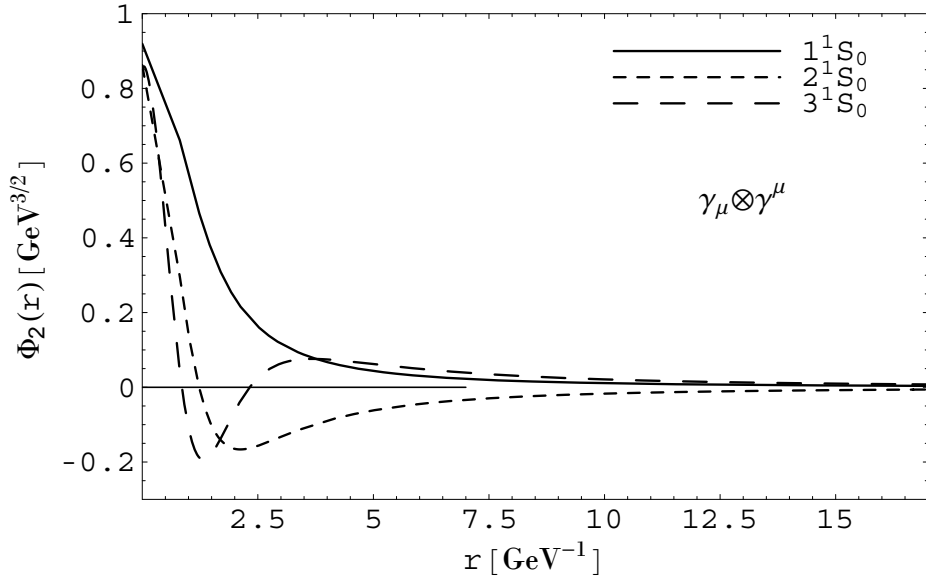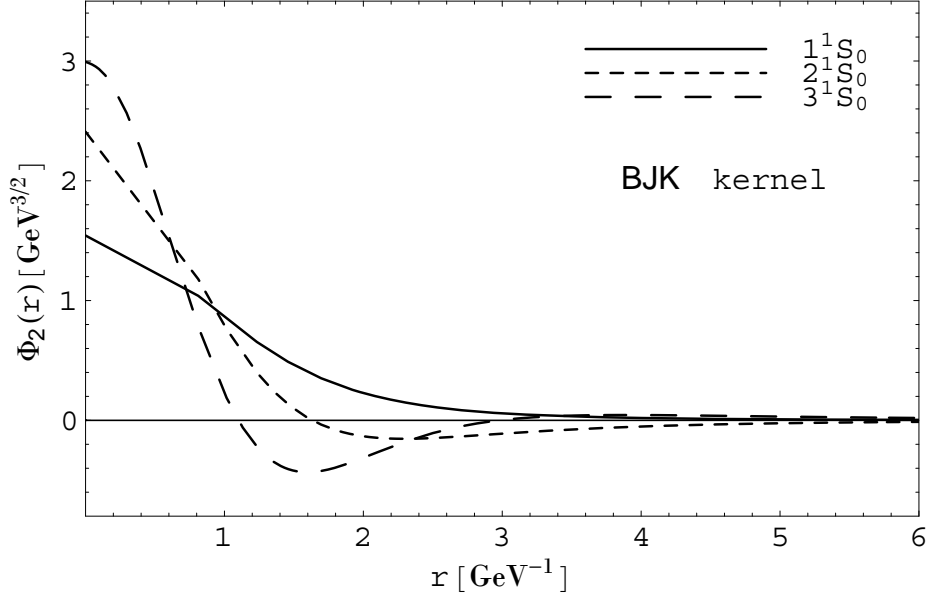


Figure 3.6: Salpeter component functions $\Phi_2(r)$ of the full free-propagator Salpeter equation for the three lowest bound states with vanishing constituent mass $m_1 = m_2 = 0 GeV$ for time-component Lorentz-vector structure $\gamma_0 \otimes \gamma_0$ with harmonic oscillator potential $V(r) = r^2$.

For the time-component Lorentz vector structure $\Gamma \otimes \Gamma = \gamma_0 \otimes \gamma_0$, the first ten eigenvalues of the full free-propagator Salpeter equation with vanishing constituent masses $m_1 = m_2 = 0 GeV$ are

$\{23.691, 20.912, 18.561, 16.517, 14.804, 13.076, 11.277, 9.326, 7.151, 4.595\}$.

Figure 3.7: Salpeter component functions $\Phi_2(r)$ of the full free-propagator Salpeter equation for the three lowest bound states with vanishing constituent mass $m_1 = m_2 = 0\,GeV$ for Lorentz-vector structure $\gamma_\mu \otimes \gamma^\mu$ with harmonic oscillator potential $V(r) = r^2$.

For the Lorentz vector structure $\Gamma \otimes \Gamma = \gamma_\mu \otimes \gamma^\mu$, the first ten eigenvalues of the full free-propagator Salpeter equation with vanishing constituent masses $m_1 = m_2 = 0\,GeV$ are

$\{17.388, 16.173, 14.937, 13.656, 12.316, 10.901, 9.389, 7.745, 5.901, 3.687\}$.

Figure 3.8: Salpeter component functions $\Phi_2(r)$ of the full free-propagator Salpeter equation for the three lowest bound states with vanishing constituent mass $m_1 = m_2 = 0 GeV$ for Böhm-Joos-Krammer (BJK) structure [25, 26] $\frac{1}{2}(\gamma_\mu \otimes \gamma^\mu + \gamma_5 \otimes \gamma_5 - 1 \otimes 1)$ with harmonic oscillator potential $V(r) = r^2$.

For Böhm-Joos-Krammer (BJK) structure [25, 26] $\Gamma \otimes \Gamma = \frac{1}{2}(\gamma_\mu \otimes \gamma^\mu + \gamma_5 \otimes \gamma_5 - 1 \otimes 1)$, the first ten eigenvalues of the full free-propagator Salpeter equation with vanishing constituent masses $m_1 = m_2 = 0 GeV$ are

$\{13.790, 12.843, 11.866, 10.849, 9.783, 8.658, 7.456, 6.149, 4.684, 2.927\}$.

In the following, we give the eigenvalues of both the free-propagator full Salpeter equation and exact-propagator instantaneous Bethe-Salpeter equation with different Lorentz structure and plot the corresponding eigenfunctions in configuration space. It is helpful to see the influence of exact propagator on the eigenfunction of Salpeter equation compared with the free propagator case.
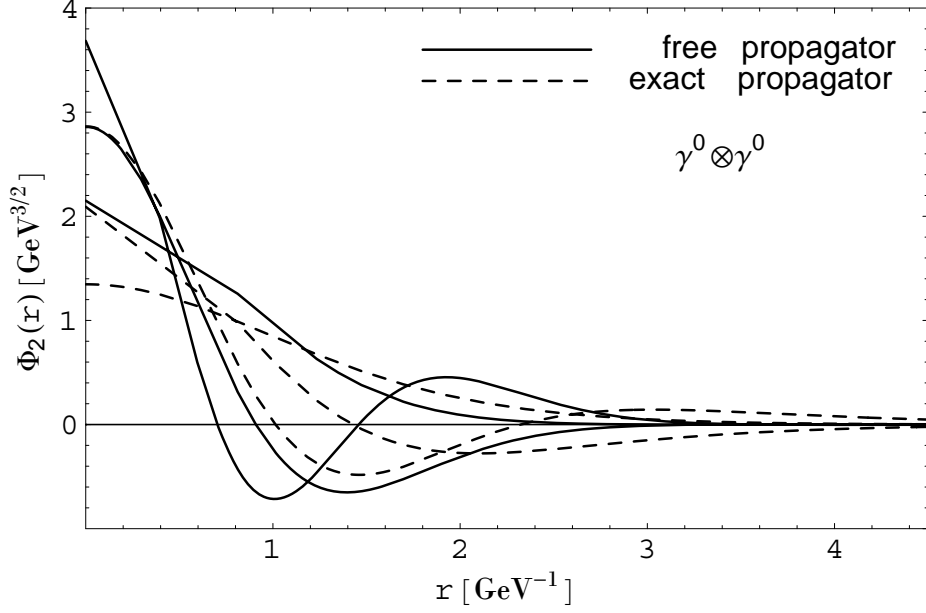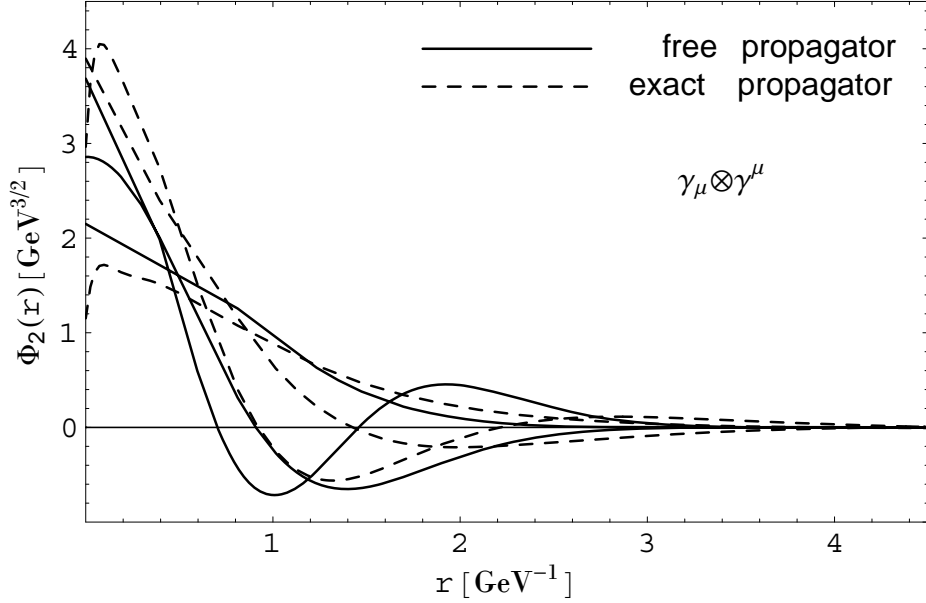
Figure 3.9: Salpeter component functions $\Phi_2(r)$ of the full free-propagator Salpeter equation (full lines) and the exact-propagator instantaneous Bethe-Salpeter equation (dashed lines) for the three lowest bound states with light-quark constituent mass $m_1 = m_2 = 0.336 GeV$ (for free-propagator case) and renormalization mass function and wave-function renormalization function (3.3), (3.4) (for exact-propagator case), with harmonic oscillator potential $V(r) = r^2$, for time-component Lorentz-vector structure interaction kernel $\gamma_0 \otimes \gamma_0$.

For time-component Lorentz-vector structure $\Gamma \otimes \Gamma = \gamma_0 \otimes \gamma_0$, the first ten eigenvalues of the full free-propagator Salpeter equation with constituent masses $m_1 = m_2 = 0.336 GeV$ are

$\{23.528, 20.885, 18.430, 16.459, 14.735, 13.018, 11.227, 9.288, 7.132, 4.612\}$,

the first ten eigenvalues of the exact-propagator instantaneous Bethe-Salpeter equation with constituent mass functions and wave-function renormalization function defined by Eq. (3.3) and (3.4) are

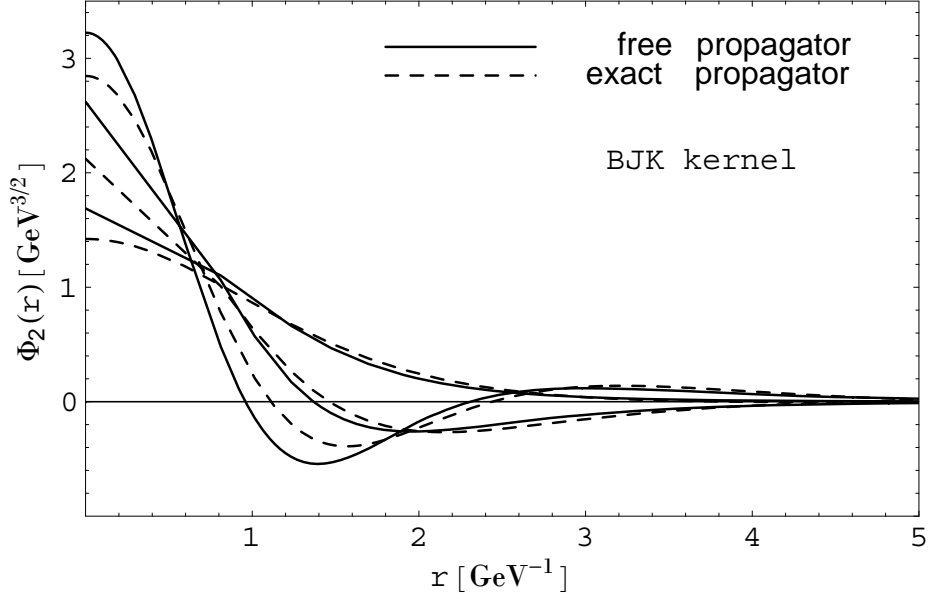$\{17.284, 15.749, 14.289, 12.849, 11.378, 9.852, 8.260, 6.599, 4.884, 3.118\}$.

Figure 3.10: Salpeter component functions $\Phi_2(r)$ of the full free-propagator Salpeter equation (full lines) and the exact-propagator instantaneous Bethe-Salpeter equation (dashed lines) for the three lowest bound states with light-quark constituent mass $m_1 = m_2 = 0.336 GeV$ (for free-propagator case) and renormalization mass function and wave-function renormalization function (3.3), (3.4) (for exact-propagator), with harmonic oscillator potential $V(r) = r^2$, for Lorentz-vector structure $\gamma_\mu \otimes \gamma^\mu$.

For Lorentz-vector structure $\Gamma \otimes \Gamma = \gamma_\mu \otimes \gamma^\mu$, the first ten eigenvalues of the full Salpeter equation with free-propagator and constituent masses $m_1 = m_2 = 0.336 GeV$ are

{21.845, 20.473, 20.246i, 18.579, 16.730, 15.186, 13.431, 11.570, 9.539, 7.230, 6.277i, 4.409}

where the eigenvalue of the ground state is 4.409, the eigenvalue of the first excited state is 7.230. Imaginary value do not correspond to any bound state since it leads to zero norm of the Bethe-Salpeter amplitude. We will discuss this in Sec. 4.7.

The first ten eigenvalues of the exact-propagator full Salpeter equation with constituent mass functions and wave-function renormalization function defined by Eq. (3.3) and (3.4) are

{18.418, 16.883, 15.549, 14.077, 12.559, 10.947, 9.203, 7.946i, 7.286, 5.111, 2.683}.

44

Figure 3.11: Salpeter component functions $\Phi_2(r)$ of the full free-propagator Salpeter equation (full lines) and of the exact-propagator instantaneous Bethe-Salpeter equation (dashed lines) for the three lowest bound states with light-quark constituent mass $m_1 = m_2 = 0.38 GeV$ (for free-propagator case) and renormalization mass function and wave-function renormalization function (3.3), (3.4) (for exact-propagator case), with harmonic oscillator potential $V(r) = r^2$, for Böhm-Joos-Krammer (BJK) structure [25, 26] $\frac{1}{2}(\gamma_\mu \otimes \gamma^\mu + \gamma_5 \otimes \gamma_5 - 1 \otimes 1)$.

For Böhm-Joos-Krammer (BJK) Lorentz structure [25, 26] $\Gamma \otimes \Gamma = \frac{1}{2}(\gamma_\mu \otimes \gamma^\mu + \gamma_5 \otimes \gamma_5 - 1 \otimes 1)$, the first ten eigenvalues of the full Salpeter equation with free-propagator and constituent masses $m_1 = m_2 = 0.38 GeV$ are

$\{18.218, 16.689, 15.378, 14.071, 12.736, 11.321, 9.792, 8.099, 6.154, 3.728\}$,

the first ten eigenvalues of the full Salpeter equation with exact-propagator and constituent mass functions and wave-function renormalization function defined by Eq. (3.3) and (3.4) are

$\{14.156, 13.136, 12.088, 10.998, 9.858, 8.658, 7.387, 6.027, 4.540, 2.771\}$.

## 3.5 Eigenfunctions of Reduced Salpeter Equation for Different Kernels

In this section, in a similar way as stated above, we plot the eigenfunctions of the reduced Salpeter equation with free- and exact-propagator together in the one figure.
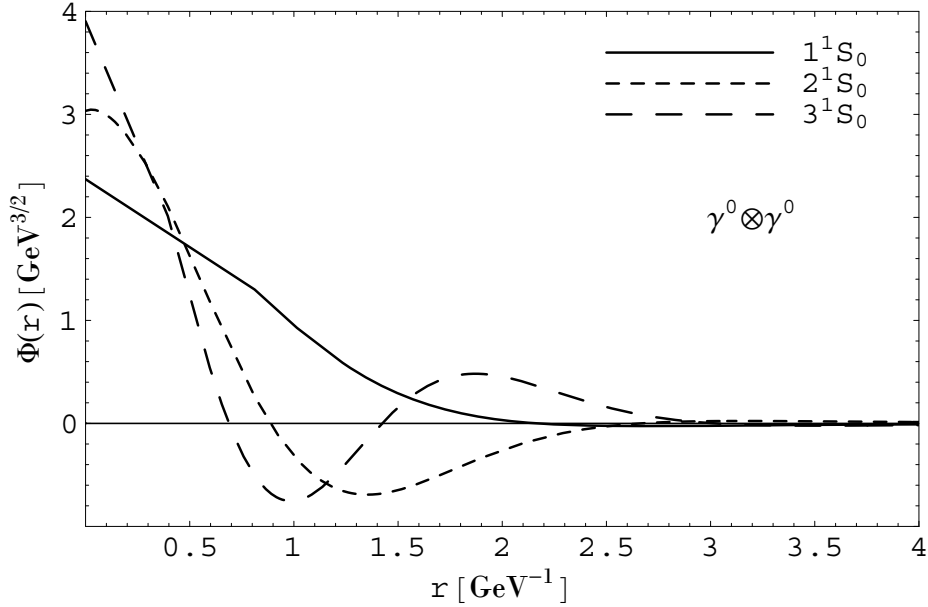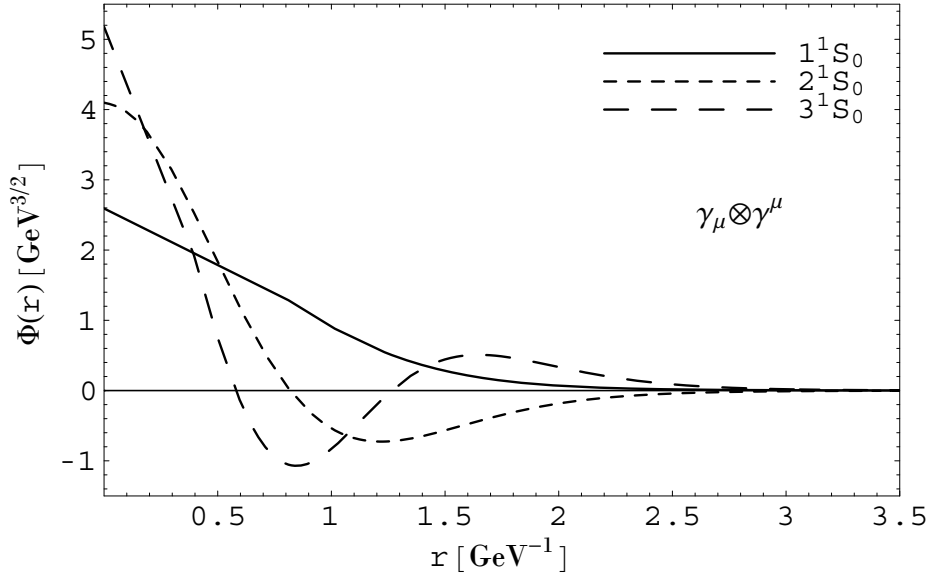


Figure 3.12: Eigenfunctions of the free-propagator reduced Salpeter equation for the three lowest states with vanishing constituent mass $m_1 = m_2 = 0 GeV$ for time-component Lorentz vector structure $\gamma_0 \otimes \gamma_0$ with harmonic oscillator potential $V(r) = r^2$.

Comparing Fig. 3.12 with Fig. 3.6, we find that, with free-propagator, the eigenfunctions of the full Salpeter equation are not distinguished different from that of reduced Salpeter equation in configuration space, for time-component Lorentz vector structure $\gamma_0 \otimes \gamma_0$ with harmonic oscillator potential $V(r) = r^2$.

For time-component Lorentz-vector structure $\Gamma \otimes \Gamma = \gamma_0 \otimes \gamma_0$, the first ten eigenvalues of the free-propagator reduced Salpeter equation with vanishing constituent masses $m_1 = m_2 = 0 GeV$ are

{24.070, 21.138, 18.672, 16.652, 14.898, 13.177, 11.383, 9.442, 7.281, 4.748}.
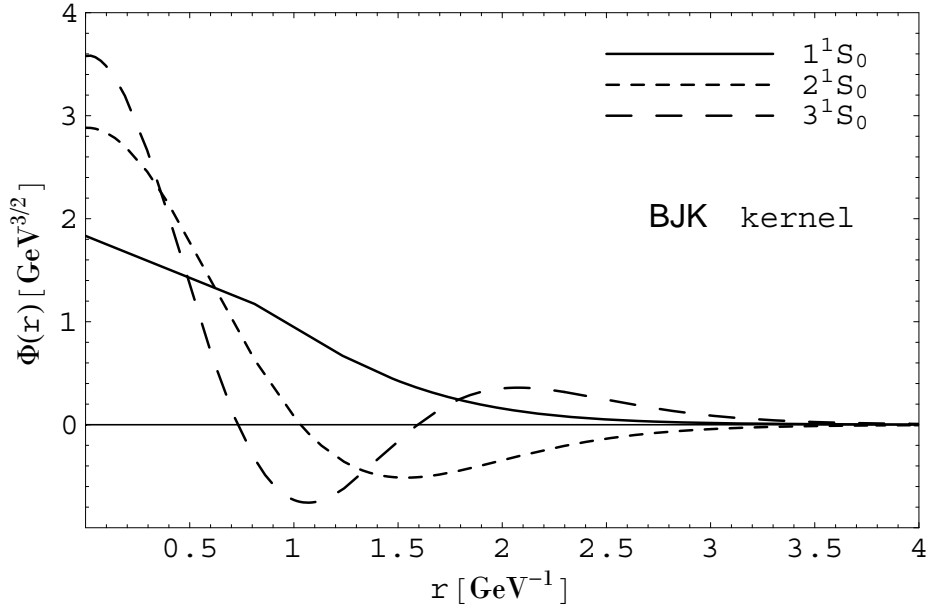
Figure 3.13: Eigenfunctions of the free-propagator reduced Salpeter equation for the three lowest states with vanishing constituent mass $m_1 = m_2 = 0 GeV$ for Lorentz-vector structure $\gamma_\mu \otimes \gamma^\mu$ with harmonic oscillator potential $V(r) = r^2$.

For Lorentz-vector structure interaction kernel $\Gamma \otimes \Gamma = \gamma_\mu \otimes \gamma^\mu$, the first ten eigenvalues of the reduced Salpeter equation with free-propagator and vanishing constituent masses $m_1 = m_2 = 0 GeV$ are

$\{31.709,\ 28.160,\ 23.636,\ 20.686,\ 18.232,\ 15.906,\ 13.576,\ 11.041,\ 8.176,\ 4.676\}.$

Figure 3.14: Eigenfunctions of the free-propagator reduced Salpeter equation for the three lowest states with vanishing constituent mass $m_1 = m_2 = 0\,GeV$ for Böhm-Joos-Krammer (BJK) structure $\frac{1}{2}(\gamma_\mu \otimes \gamma^\mu + \gamma_5 \otimes \gamma_5 - 1 \otimes 1)$ with harmonic oscillator potential $V(r) = r^2$.

For Böhm-Joos-Krammer (BJK) Lorentz structure $\Gamma \otimes \Gamma = \frac{1}{2}(\gamma_\mu \otimes \gamma^\mu + \gamma_5 \otimes \gamma_5 - 1 \otimes 1)$, the first ten eigenvalues of the reduced free-propagator Salpeter equation with vanishing constituent masses $m_1 = m_2 = 0\,GeV$ are

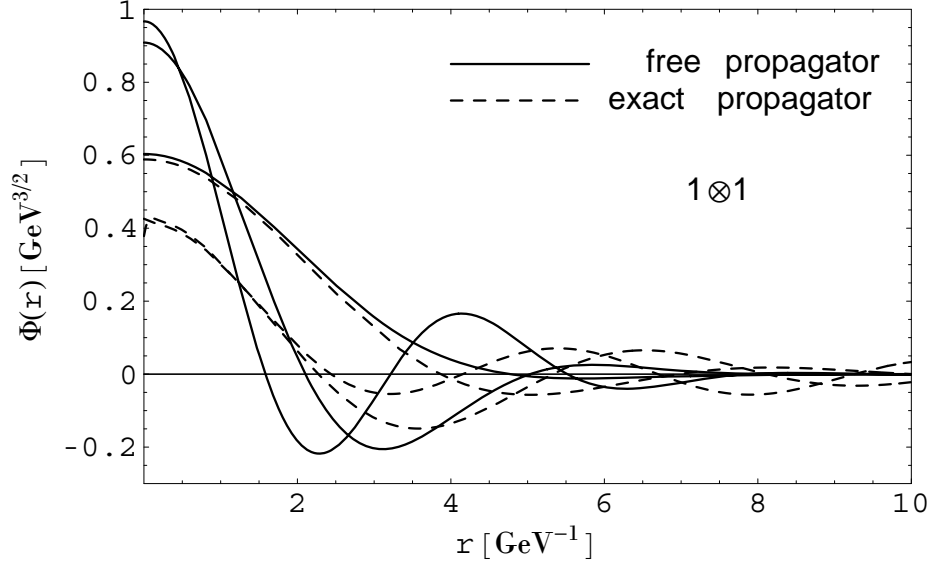$\{22.576,\ 20.223,\ 17.935,\ 16.045,\ 14.350,\ 12.612,\ 10.773,\ 8.763,\ 6.489,\ 3.712\}$.

Figure 3.15: Eigenfunctions of the reduced Salpeter equation for the three lowest states with light-quark constituent mass $m_1 = m_2 = 0.336 GeV$ (for free-propagator case) and renormalization mass function and wave-function renormalization function (3.3), (3.4) (for exact-propagator case), with harmonic oscillator potential $V(r) = r^2$, for Lorentz-scalar structure $1 \otimes 1$.

For Lorentz-scalar structure $\Gamma \otimes \Gamma = 1 \otimes 1$, the first ten eigenvalues of the reduced free-propagator Salpeter equation with constituent masses $m_1 = m_2 = 0.336 GeV$ are

$\{7.319, 6.882, 6.467, 6.054, 5.606, 5.099, 4.505, 3.766, 2.731, 0.578\}$,

the first ten eigenvalues of the exact-propagator reduced Salpeter equation with constituent mass functions and renormalization of wave functions defined by Eq. (3.3) and (3.4) are

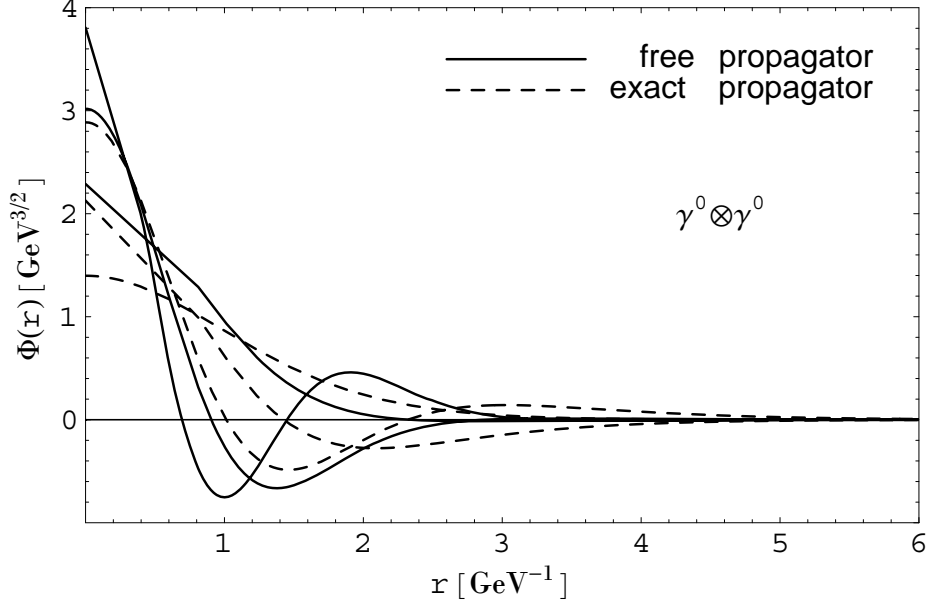$\{3.690, 3.471, 3.294, 3.133, 2.974, 2.799, 2.575, 2.245, 1.587\}$.

Figure 3.16: Eigenfunctions of the reduced Salpeter equation for the three lowest states with light-quark constituent mass $m_1 = m_2 = 0.336 GeV$ (for free-propagator) and renormalization mass function and wave-function renormalization function (3.3), (3.4) (for exact-propagator case), with harmonic oscillator potential $V(r) = r^2$, for time-component Lorentz-vector structure $\gamma_0 \otimes \gamma_0$.

For time-component Lorentz-vector structure $\Gamma \otimes \Gamma = \gamma_0 \otimes \gamma_0$, the first ten eigenvalues of the reduced Salpeter equation with free-propagator and constituent masses $m_1 = m_2 = 0.336 GeV$ are

$\{23.710, 20.899, 18.464, 16.509, 14.772, 13.065, 11.281, 9.353, 7.213, 4.720\}$,

the first ten eigenvalues of the exact-propagator reduced Salpeter equation with constituent mass functions and wave-function renormalization function defined by Eq. (3.3) and (3.4) are

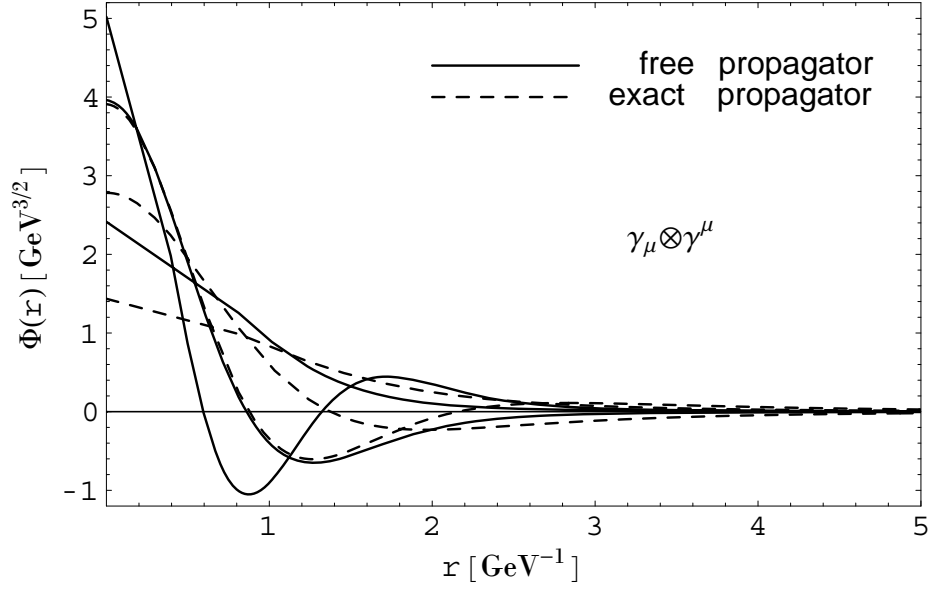$\{17.312, 15.755, 14.290, 12.852, 11.382, 9.856, 8.265, 6.606, 4.901, 3.165\}$.

Figure 3.17: Eigenfunctions of the reduced Salpeter equation for the three lowest states with light-quark constituent mass $m_1 = m_2 = 0.336 GeV$ (for free-propagator case) and renormalization mass function and wave function renormalization function (3.3), (3.4) (for exact-propagator case), with harmonic oscillator potential $V(r) = r^2$, for Lorentz-vector structure $\gamma_\mu \otimes \gamma^\mu$.

For Lorentz-vector structure $\Gamma \otimes \Gamma = \gamma_\mu \otimes \gamma^\mu$, the first ten eigenvalues of the reduced Salpeter equation with free-propagator and constituent masses $m_1 = m_2 = 0.336 GeV$ are

$\{30.891, 27.332, 22.986, 20.322, 17.879, 15.612, 13.294, 10.774, 7.934, 4.494\}$,

the first ten eigenvalues of the reduced Salpeter equation with exact-propagator and constituent mass functions and wave-function renormalization function defined by Eq. (3.3) and (3.4) are

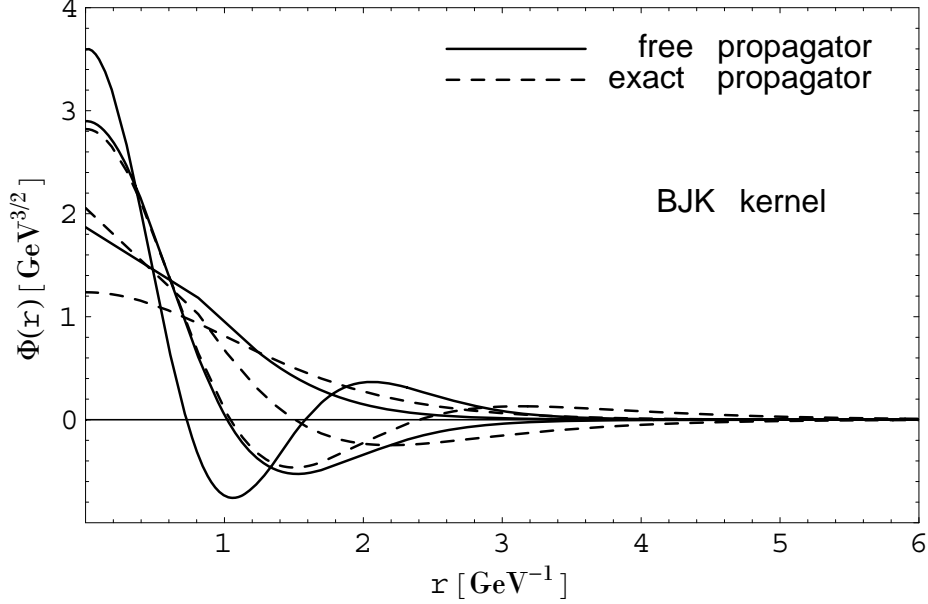$\{22.069, 19.936, 17.813, 15.874, 13.957, 11.967, 9.886, 7.687, 5.330, 2.697\}$.

Figure 3.18: Eigenfunctions of the reduced Salpeter equation for the three lowest states with light-quark constituent mass $m_1 = m_2 = 0.38 GeV$ (for free-propagator case) and renormalization mass function and wave function renormalization function (3.3), (3.4) (for exact-propagator case), with harmonic oscillator potential $V(r) = r^2$, for Böhm-Joos-Krammer (BJK) structure $\frac{1}{2}(\gamma_\mu \otimes \gamma^\mu + \gamma_5 \otimes \gamma_5 - 1 \otimes 1)$.

For Böhm-Joos-Krammer (BJK) Lorentz structure [25, 26] $\Gamma \otimes \Gamma = \frac{1}{2}(\gamma_\mu \otimes \gamma^\mu + \gamma_5 \otimes \gamma_5 - 1 \otimes 1)$, the first ten eigenvalues of the reduced Salpeter equation with free-propagator and constituent masses $m_1 = m_2 = 0.38 GeV$ are

$\{22.644, 20.272, 17.994, 16.095, 14.404, 12.671, 10.840, 8.8406, 6.585, 3.849\}$,

and the first ten eigenvalues of the reduced Salpeter equation with exact-propagator and constituent mass functions and wave-function renormalization function defined by Eq. (3.3) and (3.4) are

$\{17.095, 15.605, 14.151, 12.702, 11.217, 9.672, 8.058, 6.365, 4.578, 2.635\}$.

From the above plots of eigenfunctions, we find that the influence of introducing the exact propagator on the eigenfunction of both full and reduced Salpeter equation are rather large and therefore can not be ignored.

52

## 3.6  Summary and Conclusion

In this chapter, we extended the general instantaneous Bethe-Salpeter equation to the exact propagator instantaneous Bethe-Salpeter equation by introducing the exact quark propagator deduced from the Dyson-Schwinger equation. For the pseudoscalar bound states, we gave the approach of transferring the Bethe-Salpeter equation to an eigenvalue equation and matrix problem. The stability of the solution is rather good for a considerable scale. The influence of the exact propagator on the mass eigenvalues and on eigenfunctions of bound states can not be neglected.

We investigated both the full instantaneous Bethe-Salpeter equation and reduced Salpeter equation with exact propagator and compared the eigenfunctions for three different Lorentz structures: time-component Lorentz-vector structure $\gamma_0 \otimes \gamma_0$, Lorentz-vector structure $\gamma_\mu \otimes \gamma^\mu$ and $BJK$ Dirac structure [25, 26]. Within the numerical calculation, for the kernel of Lorentz-vector structure, there exist imaginary numbers in the solutions of the bound state of the full Salpeter equation. These imaginary values are not corresponding to bound states, because the imaginary values lead to zero norm of the eigenfunction (see section 4.7) which is not consistent with the physical reality.

# Chapter 4

# Salpeter Model for Meson with Instanton Interaction

In the previous chapters we analyzed the Bethe-Salpeter equation for fermion-antifermion bound states with instantaneous interaction kernels. We also introduced the exact quark propagator for both the instantaneous Bethe-Salpeter equation and reduced Salpeter equation. In this chapter we would like to apply it to the study of a meson model [20] based on the quark-antiquark Bethe-Salpeter equation with two-body Lorentz structure interaction kernels. The interaction kernel includes a linearly rising confinement potential with a suitable spin structure which was combined with the effective residual interaction presented by 't Hooft from instanton effects in QCD [84]. This relativistic approach employing 't Hooft's interaction provides significant improvements comparing to other approaches.

## 4.1  Introduction

Despite many years of research on the problem of bound states in QCD, there are still a lot of questions far from being well understood. The nonrelativistic potential model of quarks is reasonable to describe the mass spectra of hadrons [19], but it fails in describing the decay properties of bound states like the pion. It is not valid for the interactions if the bound state constituents involved are light or massless dynamical quarks. Therefore, one has to consider a relativistic formalism for the bound states when the interaction involves $u$ and $d$ quarks. In addition, the perturbative treatment which obtains great success in QED is not suitable to QCD in the low-energy region. Therefore, some effective theoretical descriptions for hadrons have

been developed. One of the important and widely accepted approaches was made by 't Hooft, who introduced the instanton concept and derived an effective interaction within the low energy scale for light quarks by computing the QCD partition function. Based on the Salpeter equation that includes an instanton interaction, the relativistic quark models for the light pseudoscalar and vector mesons [20, 70], for the light scalar mesons [69] have been investigated. This instanton induced interaction is also adopted to the calculation of mass spectrum and decay properties of heavy mesons including heavy quarkonia in Refs. [22, 68, 70]. The instantaneous Bethe-Salpeter equation with 't Hooft's instanton induced interaction gives good results for both the light and heavy mesons.

In this chapter, by adopting 't Hooft's interaction which is based on QCD-instanton effects, the mesons spectra and eigenfunctions are given with details. This chapter is organized as follows. In Sec. 4.2, we introduce the 't Hooft instanton interaction for the quark confining potential. The parameters of potential and relevant 't Hooft coupling factor are presented in Sec. 4.3. Sec. 4.4 is devoted to describing the free-propagator Salpeter equation and exact-quark propagator instantaneous Bethe-Salpeter equation with instanton interaction. In Sec. 4.5, both the free-propagator Salpeter equation and exact-quark propagator instantaneous Bethe-Salpeter equation with instanton interaction are solved to obtain the mass spectra of the pseudoscalar mesons. The results are compared with that of Koll's model [20] and the latest experiments from Particle Data Group (PDG) [37]. Furthermore, the eigenfunctions of both the free-propagator Salpeter equation and exact-quark propagator instantaneous Bethe-Salpeter equation with instanton-induced interaction in momentum space are plotted in Sec. 4.6. Finally, the decay constants for the pseudoscalar meson such as pion and kaon are investigated in Sec. 4.7. Sec. 4.8 is the summary of this chapter.

## 4.2  't Hooft Interaction

It is not enough to describe the scalar and pseudoscalar mesons $\pi, K, \eta, \eta'$ from nonrelativistic potential quark models with only a confining potential. Usually an additional contribution to the interaction kernel which comes from a one-gluon-exchange (OGE) should be considered. This extension works quite well for heavy quarkonia [81, 82, 83], but not for light mesons where perturbation theory is not valid. In order to circumvent this problem, higher order diagrams should be taken into account. But it makes the problem more complicated when the higher order

calculations are introduced. 't Hooft proposed a QCD based approach to compute the residual quark-antiquark interaction from instanton effects [84, 85, 86] which can produce rather good results for meson and baryon mass spectra [19].

As that adopted in the literature [20], we consider the linear confinement potential $V(r)$ in coordinate space and a suitable spin structure $\Gamma \otimes \Gamma$ in Dirac space, say $V(r) = (a_c + b_c r)\Gamma \otimes \Gamma$, to describe the underlying quark model. Here the free parameters $a_c, b_c$ are the confinement offset and slope of potential respectively.

The 't Hooft force is a flavor dependent instanton-induced interaction. Following the idea of 't Hooft [84, 87] and Shifman [85], the integral of the instanton induced interaction kernel is

$$\int \frac{\mathrm{d}^3 p'}{(2\pi)^3} V(\boldsymbol{p}, \boldsymbol{p}')\Phi(\boldsymbol{p}') = 4g_{f_1 f_2} \int \frac{\mathrm{d}^3 p'}{(2\pi)^3} R_\Lambda(\boldsymbol{p}, \boldsymbol{p}')\Big(\mathrm{tr}[\mathrm{I}\ \Phi(\boldsymbol{p}')]\mathrm{I} + \mathrm{tr}[\gamma^5\Phi(\boldsymbol{p}')]\gamma^5\Big) \quad (4.1)$$

where $R_\Lambda = \frac{1}{(\Lambda\sqrt{\pi})^3}\mathrm{e}^{-r^2/\Lambda^2}$ is a regularizing function. The coupling strength $g_{f_1 f_2}$ with the flavor $f_i$ and the finite effective range $\Lambda$ are free parameters in this model. $g_{f_1 f_2}$ takes the value listed in Table 4.1.

## 4.3   Parameters

In this chapter we first obtain consistent results for the masses and decay properties of the low lying pseudoscalar mesons with the literature [20, 21, 22, 80] and experiments [37]. After confirming the validity of the approach, we apply it to calculate the exact-propagator instantaneous Bethe-Salpeter equation for pseudoscalar mesons such as $\pi, K, B, B_s$, and so on. For this purpose we investigate the model of confinement kernel with BJK spin structure [25, 26] which was also adopted in Ref. [21].

The relativistic quark model discussed above contains some free parameters: the confinement potential parameters $a_c$ and $b_c$, the coupling strength $g_{f_1 f_2}$ for 't Hooft's instanton-induced force with an effective range $\Lambda$, and the effective constituent quark masses $m_n, m_s, m_c, m_b$. The spin structure used in this chapter is Böhm-Joos-Krammer (BJK) structure [25, 26] $\Gamma \otimes \Gamma = \frac{1}{2}(\gamma_\mu \otimes \gamma^\mu + \gamma_5 \otimes \gamma_5 - 1 \otimes 1)$ which is also investigated by Böhm [34], Koll [20] and Münz [101].

In the previous chapter the instantaneous Bethe-Salpeter equation with free-propagator was extended to the exact-propagator case. Now we solve both the corresponding free-propagator and exact-propagator instantaneous equations to obtain the mass spectra of pseudoscalar mesons. For the exact-propagator instantaneous

Bethe-Salpeter equation, the constituent quark masses should be replaced by the corresponding mass function and meanwhile a wave function renormalization function should be considered. The mass function is only used for light quarks $u, d, s$. The effective constituent quark masses and mass functions of light quarks are listed in Table 4.1 and 4.2.

| | Parameter | Value |
|---|---|---|
| | $g_{nn}$ $[GeV^{-2}]$ | 1.62 |
| | $g_{ns}$ $[GeV^{-2}]$ | 1.35 |
| 't Hooft | $g_{nc}$ $[GeV^{-2}]$ | 1.58 |
| interaction | $g_{nb}$ $[GeV^{-2}]$ | 1.07 |
| $n = u, d$ | $g_{sc}$ $[GeV^{-2}]$ | 1.27 |
| | $g_{sb}$ $[GeV^{-2}]$ | 0.76 |
| | $\Lambda$ $[GeV^{-1}]$ | 2.13 |
| Confinement | $a_c$ $[GeV]$ | $-1.135$ |
| parameters | $b_c$ $[GeV^2]$ | 0.256 |

**Table 4.1:** The parameters of the confinement potential and the 't Hooft interaction [22].

| | Parameter | free propagator model | exact propagator model |
|---|---|---|---|
| | $m_n(\boldsymbol{p}^2)$ $[GeV]$ | 0.38 | $\frac{0.745}{1+\frac{\boldsymbol{p}^4}{0.744^4}} + 0.0055$[94] |
| Mass | $m_s(\boldsymbol{p}^2)$ $[GeV]$ | 0.55 | $\frac{0.8}{1+\frac{\boldsymbol{p}^4}{1.2^4}} + 0.09$ |
| function | $m_c(\boldsymbol{p}^2)$ $[GeV]$ | 1.78 | 1.78 |
| | $m_b(\boldsymbol{p}^2)$ $[GeV]$ | 5.09 | 5.09 |
| Wave-function | $Z_{n,s}(\boldsymbol{p}^2)$ | 1 | $1 - \frac{0.545}{1+\frac{\boldsymbol{p}^2}{1.85508^2}}$[94] |
| renormalization function | $Z_{b,c}(\boldsymbol{p}^2)$ | 1 | 1 |

**Table 4.2:** The constituent quark masses, mass functions and wave function renormalization function of quarks in free- and exact-propagator Salpater model.

## 4.4 Salpeter Eigenvalue Equation with Instanton Interaction

In this section, following the same way stated in the last chapter, we transform the instantaneous Bethe-Salpeter equation with instanton interaction to the corresponding eigenvalue equation for both free-propagator and exact-propagator cases.

### 4.4.1 Free Propagator Salpeter Equation with Instanton Interaction

By using the eigenvalue equation of the Salpeter equation with Böhm-Joos-Krammer (BJK) structure [25, 26] and calculating the corresponding trace appearing in the instanton interaction kernel as shown in Eq. (4.1), we can easily transform the instanton-induced Salpeter equation to the form of eigenvalue equation.

In Eq. (4.1), the traces are evaluated as

$$\mathrm{tr}[\mathrm{I}\ \Phi(\boldsymbol{p}')]\mathrm{I} \ = \ 0, \tag{4.2}$$

$$\mathrm{tr}[\gamma^5\Phi(\boldsymbol{p}')]\gamma^5 \ = \ -4C'_\theta\Phi'_2\gamma^5, \tag{4.3}$$

therefore Eq. (4.1) becomes

$$\int \frac{\mathrm{d}^3p'}{(2\pi)^3}V(\boldsymbol{p},\boldsymbol{p}')\Phi(\boldsymbol{p}') = -16g_{f_1f_2}\int \frac{\mathrm{d}^3p'}{(2\pi)^3}R_\Lambda(\boldsymbol{p},\boldsymbol{p}')C'_\theta\Phi'_2\gamma^5. \tag{4.4}$$

By adding the integral of the instanton induced interaction kernel (4.4) into the full Salpeter eigenvalue equation (2.49) and (2.50), we obtain

$$M\Phi_1 \ = \ (E_1+E_2)\Phi_2 + \int \frac{\mathrm{d}p'p'^2}{(2\pi)^2}(2C_\theta V_0 C'_\theta - 16g_{f_1f_2}R_\Lambda C_\theta C'_\theta)\Phi'_2 \tag{4.5}$$

$$M\Phi_2 \ = \ (E_1+E_2)\Phi_1. \tag{4.6}$$

These two coupled equations are the instanton-induced Salpeter eigenvalue equations. They can be evaluated numerically by using the matrix method developed in the last chapter. The corresponding results are listed in Table 4.3.

### 4.4.2 Exact Propagator Instantaneous Bethe-Salpeter Equation with Instanton Interaction

Using the same approach we derive the exact-propagator instantaneous Bethe-Salpeter eigenvalue equation with instanton induced interaction for the BJK kernel:

$$M\Phi_1 = (E_1 + E_2)\Phi_2 + Z^2(p^2)\int \frac{\mathrm{d}p'p'^2}{(2\pi)^2}(2C_\theta V_0 C'_\theta - 16g_{f_1 f_2}R_\Lambda C_\theta C'_\theta)\Phi'_2 \quad (4.7)$$

$$M\Phi_2 = (E_1 + E_2)\Phi_1, \quad (4.8)$$

where the function $Z(p^2)$ is the wave function renormalization function and the constituent masses take the mass function $m(p^2)$ as shown in chapter 3.

## 4.5 Mass Spectra of the Pseudoscalar Mesons

Following the same way stated in chapter 3, we calculate the mass eigenvalue of the free-propagator Salpeter equation and exact-propagator instantaneous Bethe-Salpeter equation with instanton-induced interaction in this section. The exact-propagator assumption is only applied for the light quarks. A heavy quark with mass $m_q$ much larger than the QCD scale $\Lambda_{QCD}$ can be considered as free quark since correction of the static approximation is of the order of $m_q/\Lambda_{QCD}$. So, the calculations of mass spectra of heavy quarks are just performed under the free propagator approximation.

In the free-propagator Salpeter model with constituent quark masses, parameters of confinement offset $a_c$ and slope $b_c$, rather good results of the masses of pseudoscalar mesons are obtained in [20, 21, 22], especially for the light ones. The masses of pseudoscalar meson $\pi(0^-)$, $K(0^-)$, $D(0^-)$, $D_s(0^-)$, $B(0^-)$, $B_s(0^-)$ obtained from our free-propagator Salpeter model are exactly consistent with that of Koll's model [20, 21] and agree nicely with the newest experimental values listed in PDG2007 [37]. The masses of pseudoscalar meson $\eta_c(0^-)$ and $\eta_b(0^-)$ obtained from our free- and exact-propagator Salpeter model are closer to the newest experimental values [37] than that from Koll's model [20, 21].

From the results we can see that the masses calculated in exact-propagator instantaneous Bethe-Salpeter equation are different from the results of other models. The influence from the exact quark propagator leads to higher masses for light mesons.

Table 4.3 shows the mass spectra of the ground state and first excited state of pseudoscalar mesons calculated in the two different models.

| Meson($J^P$) | $n$ | Koll model | free-propagator | exact-propagator | PDG 2007[37] |
|---|---|---|---|---|---|
| $\pi(0^-)$ | 0 | 140 | 140 | 1465 | $139.57108 \pm 0.00035$ |
| | 1 | 1331 | 1331 | 1676 | $1300 \pm 100$ |
| $K(0^-)$ | 0 | 506 | 506 | 1484 | $493.667 \pm 0.016$ |
| | 1 | 1470 | 1470 | 1877 | — |
| $D(0^-)$ | 0 | 1869 | 1869 | 2380 | $1869.62 \pm 0.2$ |
| | 1 | 2578 | 2578 | 2763 | — |
| $D_s(0^-)$ | 0 | 1969 | 1969 | 2143 | $1968.5 \pm 0.6$ |
| | 1 | 2683 | 2683 | 2838 | — |
| $B(0^-)$ | 0 | 5279 | 5279 | 5685 | $5279.0 \pm 0.5$ |
| | 1 | 5869 | 5869 | 6021 | — |
| $B_s(0^-)$ | 0 | 5369 | 5369 | 5539 | $5366.1 \pm 0.6$ |
| | 1 | 5960 | 5960 | 6097 | — |
| $B_c(0^-)$ | 0 | — | 6381 | 6381 | $6286 \pm 5$ |
| | 1 | — | 6890 | 6890 | — |
| $\eta_c(0^-)$ | 0 | 3114 | 2983 | 2983 | $2979.8 \pm 1.2$ |
| | 1 | 3708 | 3653 | 3653 | — |
| $\eta_b(0^-)$ | 0 | 9565 | 9479 | 9479 | $9300 \pm 20$ |
| | 1 | 9985 | 9939 | 9939 | — |

**Table 4.3** Masses of pseudoscalar mesons in [MeV] with instanton interaction, calculated with the parameters of Koll's model [20, 21], free-propagator and exact-propagator model. Here $n$ denotes the radial excitation.

## 4.6 Eigenfunctions of the Full Salpeter Equation with Instanton Interaction

In this section, the eigenfunctions of the three lowest states of pseudoscalar mesons in configuration space are plotted. Using the same procedure stated in the last chapter, we transfer the eigenvalue equation to a matrix problem which can be solved by diagonalizing the corresponding matrix. Then, by calculating the eigenvector of the matrix and multiplying it with the generalized Laguerre basis, the wave function of

the pseudoscalar bound states will be obtained. The relevant details and computation codes are given in the appendix D. In appendix E we present the plots of the corresponding eigenfunction in momentum space. For $c\bar{c}$ and $b\bar{b}$ bound state, the exact-propagator has no influence on the $c$ and $b$ quark due to their heavy masses (see Table 4.2).
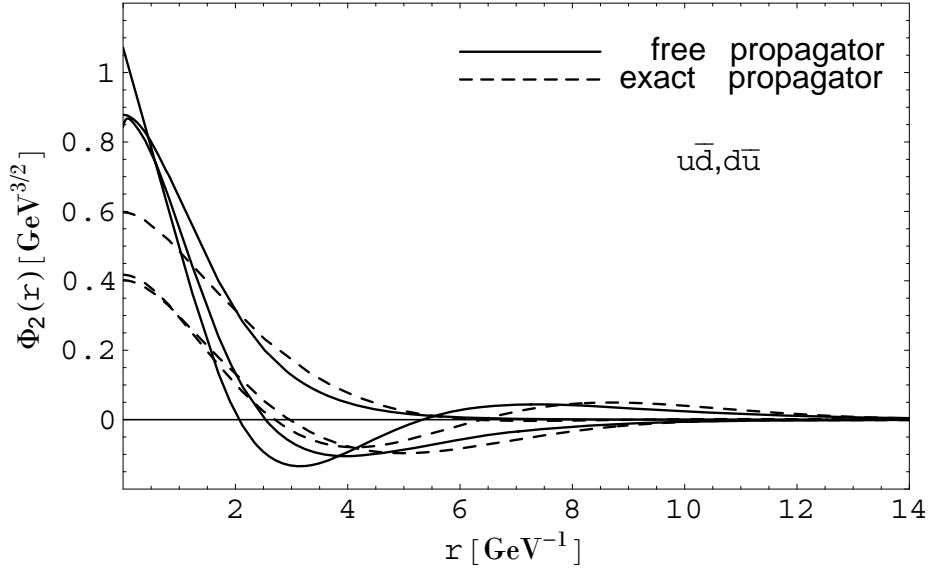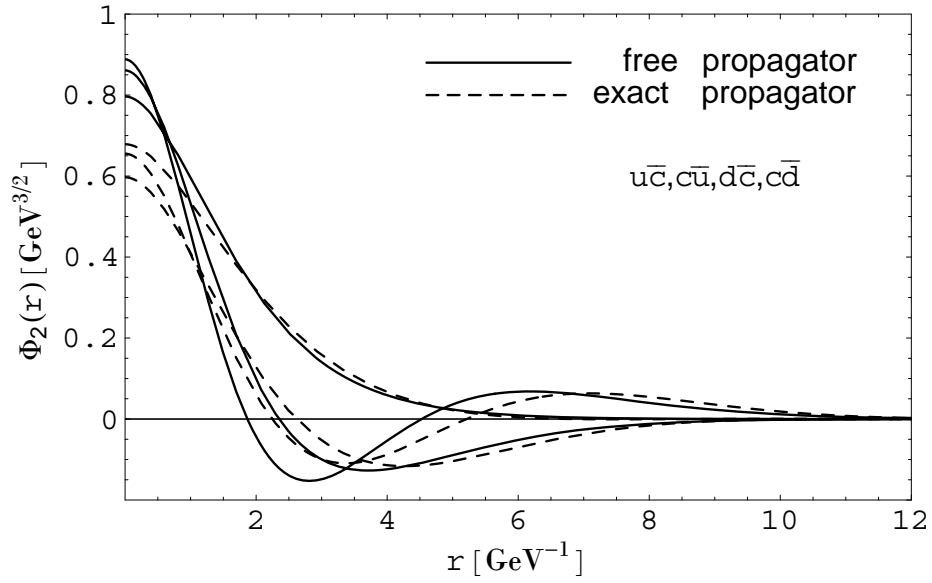


Figure 4.1: Salpeter component functions $\Phi_2(r)$ of the free-propagator Salpeter equation (full lines) and of the exact-propagator instantaneous Bethe-Salpeter equation (dashed lines) with instanton interaction for the three lowest states of $u\bar{d}/d\bar{u}$.
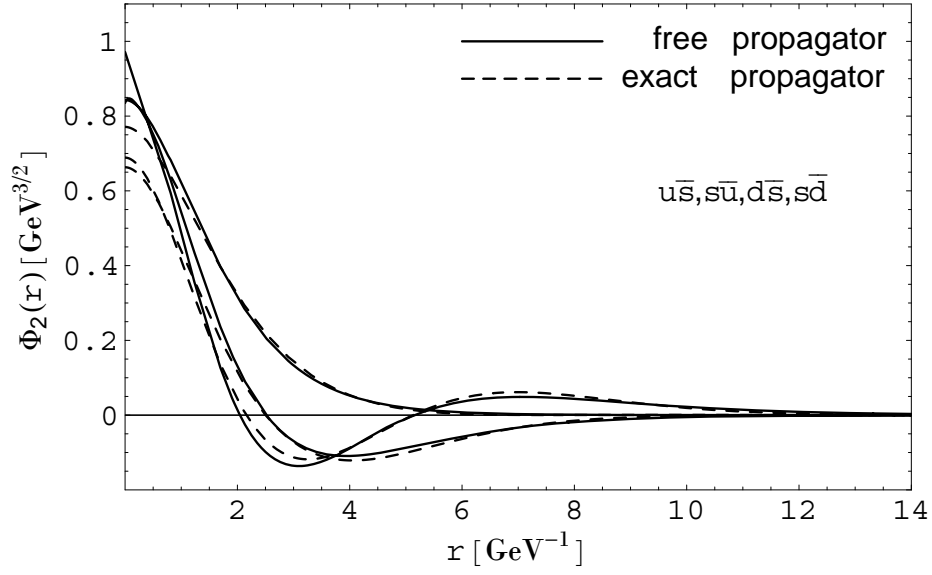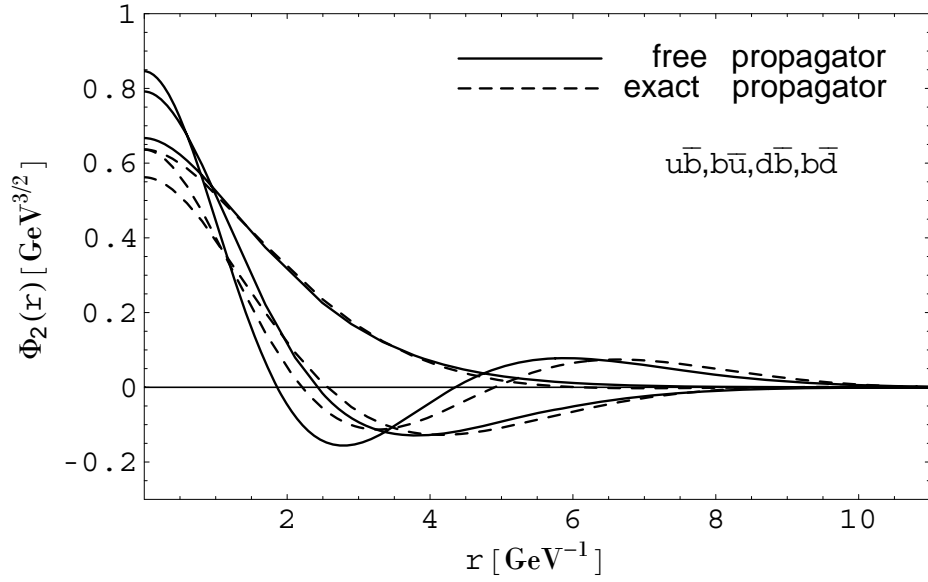
Figure 4.2: Salpeter component functions $\Phi_2(r)$ of the free-propagator Salpeter equation (full lines) and of the exact-propagator instantaneous Bethe-Salpeter equation (dashed lines) with instanton interaction for the three lowest states of $u\bar{s}/s\bar{u}$; $d\bar{s}/s\bar{d}$.



Figure 4.3: Salpeter component functions $\Phi_2(r)$ of the free-propagator Salpeter equation (full lines) and of the exact-propagator instantaneous Bethe-Salpeter equation (dashed lines) with instanton interaction for the three lowest states of $u\bar{c}/c\bar{u}$; $d\bar{c}/c\bar{d}$.
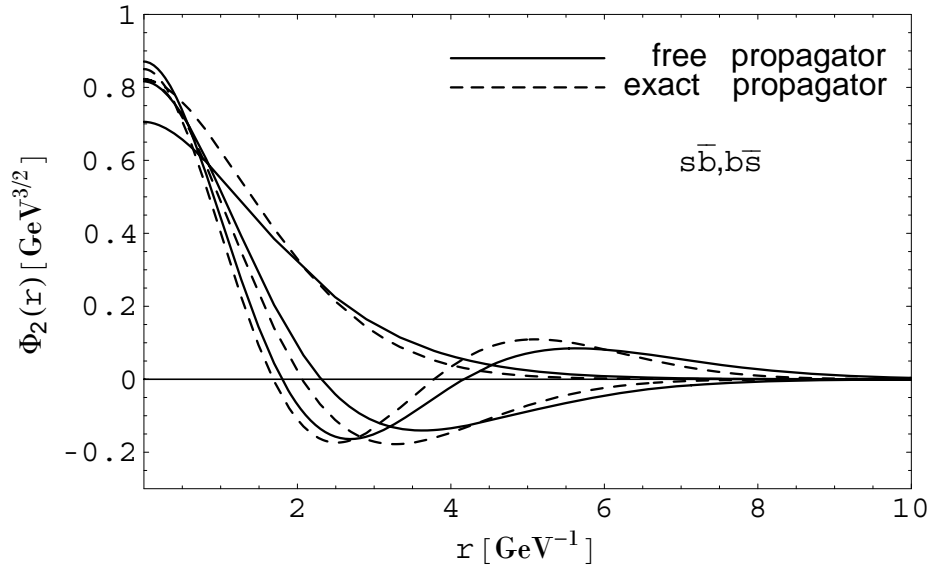
Figure 4.4: Salpeter component functions $\Phi_2(r)$ of the free-propagator Salpeter equation (full lines) and of the exact-propagator instantaneous Bethe-Salpeter equation (dashed lines) with instanton interaction for the three lowest states of $u\bar{b}/b\bar{u}$; $d\bar{b}/b\bar{d}$.



Figure 4.5: Salpeter component functions $\Phi_2(r)$ of the free-propagator Salpeter equation (full lines) and of the exact-propagator instantaneous Bethe-Salpeter equation (dashed lines) with instanton interaction for the three lowest states of $s\bar{b}/b\bar{s}$.
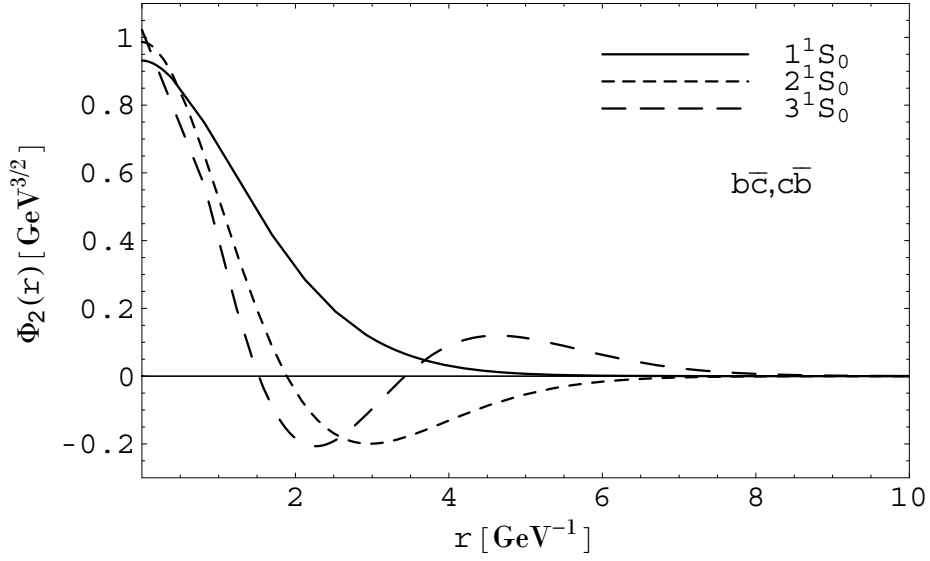
64

Figure 4.6: Salpeter component functions $\Phi_2(r)$ of the free-propagator Salpeter equation (full lines) and of the exact-propagator instantaneous Bethe-Salpeter equation (dashed lines) with instanton interaction for the three lowest states of $b\bar{c}/c\bar{b}$.
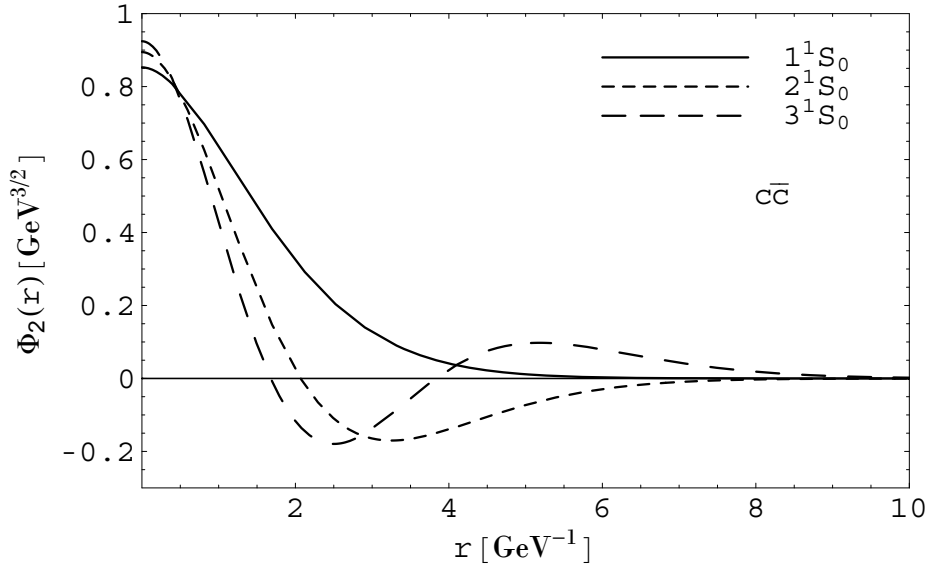


Figure 4.7: Salpeter component functions $\Phi_2(r)$ of the free-propagator Salpeter equation (full lines) and of the exact-propagator instantaneous Bethe-Salpeter equation (dashed lines) with instanton interaction for the three lowest states of $c\bar{c}$.
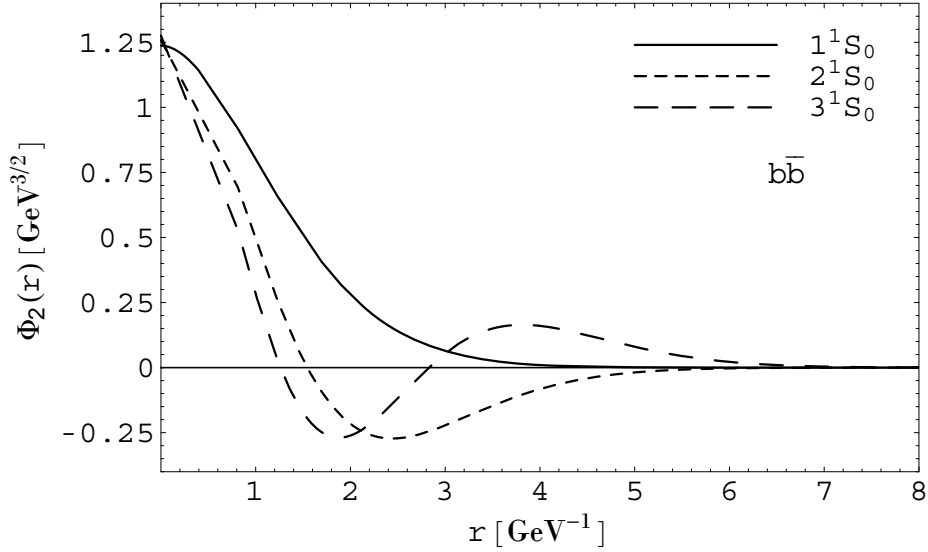
65

Figure 4.8: Salpeter component functions $\Phi_2(r)$ of the free-propagator Salpeter equation (full lines) and of the exact-propagator instantaneous Bethe-Salpeter equation (dashed lines) with instanton interaction for the three lowest states of $b\bar{b}$.

## 4.7 Meson Decay Constants

Besides the description of mass spectra of mesons, a realistic model should also be able to describe the decay properties. In recent years, the question of pseudoscalar meson decay constants of $\pi, K, D, D_s$ mesons received great interest in the literature (see e.g. [102, 20, 21, 22] and references therein). In this section we discuss the influence of the exact-propagator model on the decay constants of the pseudoscalar bound states.

We start the discussion with the decay constant of the pseudoscalar bound state $f_{0^-}$. According to the definition of the norm of the Bethe-Salpeter amplitude [98, 93], we have

$$\| \Phi \|^2 = \int \frac{\mathrm{d}^3 p}{(2\pi)^3} \frac{1}{2} \mathrm{Tr}\left[ (\gamma_0 \Phi^\dagger) \left[ \frac{H_1}{E_1}(\Phi\gamma_0) - (\Phi\gamma_0)\frac{H_2}{E_2} \right] \right], \tag{4.9}$$

which is related to the normalization of bound states (see Eq. (2.63))

$$\| \Phi \|^2 = \frac{1}{(2\pi)^3}. \tag{4.10}$$

66

Because the Salpeter amplitude satisfies the constraint condition (2.58), the norm (4.9) can be rewritten as [17]

$$\parallel \Phi \parallel^2 = \int \frac{\mathrm{d}^3 p}{(2\pi)^3} \mathrm{Tr}\left[(\gamma_0 \Phi^\dagger) \frac{H_1}{E_1}(\Phi \gamma_0)\right]. \tag{4.11}$$

By inserting the Salpeter amplitude (2.8) into the norm (4.11) and using (4.6)

$$\Phi_1 = \frac{M}{E_1 + E_2}\Phi_2, \tag{4.12}$$

we obtain

$$
\begin{aligned}
\parallel \Phi \parallel^2 &= 4N^2 \int \frac{\mathrm{d}^3 p}{(2\pi)^3}\left[\Phi_2{}^* \Phi_1 + \Phi_1{}^* \Phi_2\right] \\
&= 4N^2 \int \frac{\mathrm{d}^3 p}{(2\pi)^3}\left[\frac{M + M^*}{E_1 + E_2}\Phi_2{}^* \Phi_2\right] \\
&= 4N^2 \int \frac{\mathrm{d}^3 p}{(2\pi)^3}\left[\frac{2\mathrm{Re}[M]}{E_1 + E_2}\Phi_2{}^* \Phi_2\right].
\end{aligned}
\tag{4.13}
$$

In the practical numerical calculation, the result of mass eigenvalue $M$ may become an imaginary number. However, from the above formula and especially the numerator $M + M^*$, the pure imaginary number should be ignored otherwise the norm would be zero. That is also the reason why we neglect the pure imaginary values appearing in the mass eigenvalue spectra in Sec. 3.4 since they are no physical values. Therefore we have $M + M^* = 2\mathrm{Re}[M] = 2M$. Using the definition of the pseudoscalar decay constant with the axial current $j_5^\mu =: \bar{\psi}(x)\gamma^\mu \gamma_5 \psi(x) :$, we have [92]

$$\langle 0|j_5^\mu(x)|P\rangle = \frac{1}{(2\pi)^{3/2}} \frac{\mathrm{i}}{\sqrt{2p_0}} f_{0^-} p^\mu \mathrm{e}^{-\mathrm{i}px}, \tag{4.14}$$

in the rest frame $p = (M, \mathbf{0})$.

For the pseudoscalar bound state

$$
\begin{aligned}
\langle 0|j_5^0(0)|P\rangle &= \langle 0|T\bar{\psi}_\alpha(\gamma_0\gamma_5)_{\alpha\beta}\psi_\beta|P\rangle \\
&= -(\gamma_0\gamma_5)_{\alpha\beta}\langle 0|T\psi_\beta\bar{\psi}_\alpha|P\rangle \\
&= -\mathrm{Tr}\{\gamma_0\gamma_5\Phi_{(M,0)}(x = 0)\} \\
&= -\int \frac{\mathrm{d}^4 p}{(2\pi)^4}\mathrm{Tr}\{\gamma_0\gamma_5\Phi(p)\} \\
&= -4N\int \frac{\mathrm{d}^3 p}{(2\pi)^3}S_\phi\Phi_1(\mathbf{p}).
\end{aligned}
\tag{4.15}
$$

67

In the above calculation we have transformed to the momentum space. From Eq. (4.14) and (4.15) we obtain the decay constant of the pion

$$|f_{0^-}| = \frac{4\sqrt{3M}}{\sqrt{\pi}} N \int \mathrm{d}p p^2 S_\phi \frac{\Phi_2(p)}{E_1 + E_2} \tag{4.16}$$

with the color factor $3 \cdot \dfrac{1}{\sqrt{3}}$.

Now we can calculate weak decay constants of pseudoscalar pions with free- and exact-propagator Salpeter amplitude respectively. The decay constant of other mesons such as $K, D, D_s$ can also be obtained in the same way stated above. In Table 4.4 the results of $f_\pi, f_K, f_D$ and $f_{D_s}$ for free- and exact-propagator Salpeter model are listed. The exact-propagator model brings some improvement for the $f_\pi$ and $f_K$ comparing with the free-propagator case.

| Decay Constant | Koll model | free-propagator | exact-propagator | PDG 2007[37] |
|---|---|---|---|---|
| $f_\pi[MeV]$ | 219 | 219 | 181 | $130.7 \pm 0.46$ |
| $f_K[MeV]$ | 238 | 238 | 219 | $159.8 \pm 1.88$ |
| $f_D[MeV]$ | — | 263 | 237 | $222.6 \pm 16.7$ |
| $f_{D_s}[MeV]$ | — | 284 | 309 | $294 \pm 27$ |

**Table 4.4:** The pseudoscalar decay constants of the $\pi, K, D$ and $D_s$ mesons.

## 4.8 Summary and Conclusion

By introducing the 't Hooft instanton interaction, we investigated the properties of the free-propagator Salpeter equation and exact-propagator instantaneous Bethe-Salpeter equation with instanton interaction in this chapter. The mass eigenvalues of mesons $\pi$, $K$, $D$, $D_s$, $B$, $B_s$, $B_c$, $\eta_c$ and $\eta_b$ and the corresponding eigenfunctions of free-propagator full Salpeter equation and exact-propagator instantaneous Bethe-Salpeter equation have been presented in this chapter. The decay constant $f$ of $\pi$, $K$, $D$, $D_s$ mensons was also calculated within the instanton-induced model by using the same parameters of confinement potential used by previous literature [20, 21].

# Chapter 5

# Analytical Treatment

Up to now, all of our analysis for the mass eigenvalue and eigenfunction of the pseudoscalar bound states are based on numerical calculations which depend on the matrix size. For some Lorentz structure interaction kernels, this numerical calculation may produce unphysical values such as imaginary number for the mass eigenvalue of the bound state. Therefore, it is necessary to perform an analytical or semianalytical research. In this chapter we present an analytical discussion for the relevant Salpeter eigenvalue equations. The basic idea is to transform the relevant Salpeter eigenvalue equation to the corresponding differential equation which can be discussed from an analytical point of view.

## 5.1   Introduction

In the previous chapters we have evaluated the Salpeter eigenvalue equation by expanding the Salpeter amplitude on a complete set of orthonormal basis and then transforming it to a matrix problem. In the practical computation, we have to choose an appropriate size of matrix. Therefore the numerical results are dependent on the matrix size and it can be imaginary in some cases depending on the structure of the kernel. Analytical study would be better to confirm the validity of our numerical method. In this chapter we adopt an analytical approach, i.e., the method of ordinary differential equation, to study the full Salpeter eigenvalue equation and the reduced Salpeter eigenvalue equation derived from the full Salpeter equation by neglecting some interaction terms.

   This chapter is organized as follows. In Sec. 5.2, we review the eigenvalue

equations of the full and reduced Salpeter equation. In Sec. 5.3, we employ the harmonic-oscillator confining interactions to discuss the reduced Salpeter eigenvalue equations by using the differential equation method. Then we apply this method to the case of exact-propagator in Sec. 5.4. Sec. 5.5 is the summary of this chapter.

## 5.2 Eigenvalue Treatment of Reduced Salpeter Equation for Various Kernels

With the harmonic-oscillator interaction in configuration space

$$V(r) = ar^2, \quad a = a^* \neq 0, \quad r \equiv |\boldsymbol{x}|,$$

the reduced Salpeter equation from the previous chapter can be investigated to a large extent analytically. For harmonic-oscillator type of potential, with the help of a differential equation [74] which is satisfied by spherical Bessel functions of all kinds $w_n(z)(n = 0, \pm 1, \pm 2, ...)$,

$$z^2 \frac{\mathrm{d}^2}{\mathrm{d}z^2} w_n(z) + 2z \frac{\mathrm{d}}{\mathrm{d}z} w_n(z) + [z^2 - n(n+1)] w_n(z) = 0, \tag{5.1}$$

we can analytically determine all potential functions $V_L(p, p')$ in the radial Salpeter eigenvalue equations.

### 5.2.1 Differential Operator

With the aid of second-order differential operators

$$\triangle_p^{(L)} \equiv \frac{\mathrm{d}^2}{\mathrm{d}p^2} + \frac{2}{p} \frac{\mathrm{d}}{\mathrm{d}p} - \frac{L(L+1)}{p^2}, \quad L = 0, 1, 2, ..., \tag{5.2}$$

the spherical Bessel functions of the first kind, $j_L(pr)$, satisfy

$$\triangle_p^{(L)} j_L(pr) = -r^2 j_L(pr), \quad L = 0, 1, 2, ... \ . \tag{5.3}$$

Using this relation and the "orthogonality relations"

$$\int_0^\infty \mathrm{d}r r^2 j_L(pr) j_L(p'r) = \frac{\pi}{2p^2} \delta(p - p'), \quad L = 0, 1, 2, ..., \tag{5.4}$$

we replace the expression $r^2$ in the potential function $V_L(p, p')$ (see Eq. (2.35)) by the differential operator $\triangle_p^{(L)}$. The equivalent potential functions for harmonic oscillators can be evaluated as

$$
\begin{aligned}
V_L(p, p') &= 8\pi \int_0^\infty \mathrm{d}r\, r^2 V(r) j_L(pr) j_L(p'r) \\
&= -8\pi a \int_0^\infty \mathrm{d}r\, r^2 \triangle_p^{(L)} j_L(pr) j_L(p'r) \\
&= -8\pi a \triangle_p^{(L)} \frac{\pi}{2p^2} \delta(p - p') \\
&= -\frac{(2\pi)^2 a}{p^2} \triangle_p^{(L)} \delta(p - p'), \quad L = 0, 1, 2, \dots ,
\end{aligned}
\tag{5.5}
$$

where the harmonic oscillator potential $V(r) = ar^2$.

## 5.2.2  Harmonic Oscillator Reduced Salpeter Equation as Differential Equation

By employing the potential function (5.5), all radial integral eigenvalue equations derived in chapter 3 can be simplified to second-order homogeneous linear differential equations.

The general form of the reduced Salpeter eigenvalue equation for $m_1 = m_2 = m$ can be expressed as

$$
M\Phi(p) = 2E(p)\Phi(p) + \frac{1}{2}\int_0^\infty \frac{\mathrm{d}p'\, p'^2}{(2\pi)^2}(\underbrace{\eta_1 V_0}_{I} + \underbrace{\eta_2 \frac{m}{E(p)} V_0 \frac{m}{E(p')}}_{II} + \underbrace{\eta_3 \frac{p}{E(p)} V_1 \frac{p'}{E(p')}}_{III})\Phi(p').
$$

$$\tag{5.6}$$

Now we evaluate the first term

$$
\begin{aligned}
I &= \frac{\eta_1}{2}\int_0^\infty \frac{\mathrm{d}p'\, p'^2}{(2\pi)^2} V_0 \Phi(p') \\
&= \frac{\eta_1}{8\pi^2}\int_0^\infty \mathrm{d}p'\, p'^2 \cdot 8\pi a \int_0^\infty \mathrm{d}r\, r^2 r^2 j_0(pr) j_0(p'r)\Phi(p') \\
&= \frac{\eta_1 a}{\pi}\int_0^\infty \mathrm{d}p'\, p'^2 \int_0^\infty \mathrm{d}r\, r^2 (-\triangle_p^{(0)}) j_0(pr) j_0(p'r)\Phi(p') \\
&= -\frac{\eta_1 a}{2}\triangle_p^{(0)}\int_0^\infty \mathrm{d}p'\, p'^2 \frac{1}{p^2}\delta(p - p')\Phi(p') \\
&= -\frac{\eta_1 a}{2}\triangle_p^{(0)}\Phi(p).
\end{aligned}
\tag{5.7}
$$

71

The evaluation of the second term is

$$
\begin{aligned}
II &= \frac{\eta_2}{2} \int_0^\infty \frac{dp'p'^2}{(2\pi)^2} \frac{m}{E} V_0 \frac{m}{E'} \Phi(p') \\
&= \frac{\eta_2}{8\pi^2} \int_0^\infty dp'p'^2 \frac{m^2}{E(p)} \cdot 8\pi a \int_0^\infty dr r^2 r^2 j_0(pr) j_0(p'r) \frac{1}{E(p')} \Phi(p') \\
&= \frac{\eta_2 a}{\pi} \int_0^\infty dp'p'^2 \int_0^\infty dr r^2 \frac{m^2}{E(p)} (-\triangle_p^{(0)}) j_0(pr) j_0(p'r) \frac{1}{E(p')} \Phi(p') \\
&= -\frac{\eta_2 a}{2} \frac{m^2}{E(p)} \triangle_p^{(0)} \int_0^\infty dp'p'^2 \frac{1}{p^2} \delta(p-p') \frac{1}{E(p')} \Phi(p') \\
&= -\frac{\eta_2 a}{2} \frac{m^2}{E(p)} \triangle_p^{(0)} \frac{\Phi(p)}{E(p)}.
\end{aligned}
$$

$$(5.8)$$

The integration of the third term is

$$
\begin{aligned}
III &= \frac{\eta_3}{2} \int_0^\infty \frac{dp'p'^2}{(2\pi)^2} \frac{p}{E(p)} V_1 \frac{p'}{E(p')} \Phi(p') \\
&= \frac{\eta_3}{8\pi^2} \int_0^\infty dp'p'^2 \frac{p}{E(p)} \cdot 8\pi a \int_0^\infty dr r^2 r^2 j_1(pr) j_1(p'r) \frac{p'}{E(p')} \Phi(p') \\
&= \frac{\eta_3 a}{\pi} \int_0^\infty dp'p'^2 \int_0^\infty dr r^2 \frac{p}{E(p)} (-\triangle_p^{(1)}) j_1(pr) j_1(p'r) \frac{p'}{E(p')} \Phi(p') \\
&= -\frac{\eta_3 a}{2} \frac{p}{E(p)} \triangle_p^{(1)} \int_0^\infty dp'p'^2 \frac{1}{p^2} \delta(p-p') \frac{p'}{E(p')} \Phi(p') \\
&= -\frac{\eta_3 a}{2} \frac{p}{E(p)} \triangle_p^{(1)} \frac{p}{E(p)} \Phi(p).
\end{aligned}
$$

$$(5.9)$$

By using

$$
\triangle_p^{(0)} \frac{\Phi(p)}{E(p)} = \left( \triangle_p^{(0)} \frac{1}{E(p)} \right) \Phi(p) + 2 \left( \frac{d}{dp} \frac{1}{E(p)} \right) \left( \frac{d}{dp} \Phi(p) \right) + \frac{1}{E(p)} (\triangle_p^{(0)} \Phi(p)), \quad (5.10)
$$

$$
\triangle_p^{(0)} \frac{p\Phi(p)}{E(p)} = \left( \triangle_p^{(0)} \frac{p}{E(p)} \right) \Phi(p) + 2 \left( \frac{d}{dp} \frac{p}{E(p)} \right) \left( \frac{d}{dp} \Phi(p) \right) + \frac{p}{E(p)} (\triangle_p^{(0)} \Phi(p)) \quad (5.11)
$$

and

$$
\begin{aligned}
\triangle_p^{(1)} &= \frac{d^2}{dp^2} + \frac{2}{p} \frac{d}{dp} - \frac{2}{p^2} \\
&= \triangle_p^{(0)} - \frac{2}{p^2},
\end{aligned}
$$

$$(5.12)$$

72

we finally obtain

$$M\Phi(p) = 2E(p)\Phi(p)$$

$$-\frac{a}{2}\left[\eta_1\triangle_p^{(0)}\Phi(p) + \eta_2\frac{m^2}{E(p)}\triangle_p^{(0)}\left(\frac{\Phi(p)}{E(p)}\right) + \eta_3\frac{p}{E(p)}\left(\triangle_p^{(0)} - \frac{2}{p^2}\right)\left(\frac{p}{E(p)}\Phi(p)\right)\right]$$

$$= \left[2E(p) - \frac{a}{2}\left(\eta_1 + \frac{\eta_2 m^2 + \eta_3 p^2}{E^2(p)}\right)\triangle_p^{(0)} - a(\eta_3 - \eta_2)\frac{m^2 p}{E^4(p)}\frac{\mathrm{d}}{\mathrm{d}p}\right.$$

$$\left.+\frac{a}{2E^6(p)}\left(3\eta_2 m^4 + \eta_3 p^2(5m^2 + 2p^2)\right)\right]\Phi(p) \qquad (5.13)$$

where the parameters $\eta_i$ take the values shown in the following table.

| $m_1 = m_2$ | $1\otimes 1$ | $\gamma_0\otimes\gamma_0$ | $\gamma_\mu\otimes\gamma^\mu$ | $\gamma_5\otimes\gamma_5$ | $BJK$ |
|---|---|---|---|---|---|
| $\eta_1$ | $-1$ | $1$ | $4$ | $-1$ | $2$ |
| $\eta_2$ | $-1$ | $1$ | $-2$ | $1$ | $0$ |
| $\eta_3$ | $1$ | $1$ | $0$ | $1$ | $0$ |

**Table 5.1:** Values of parameter $\eta_i$.

These parameter $\eta_i$ are connected with the parameters $\varepsilon_i$ listed in Table 2.1

$$\eta_1 = \varepsilon_1, \quad \eta_2 = \varepsilon_3, \quad \eta_3 = \varepsilon_4.$$

Now we write the reduced Salpeter eigenvalue equation for each Lorentz structure kernel respectively. For Lorentz-scalar structure kernel, $\Gamma\otimes\Gamma = 1\otimes 1$,

$$M\Phi(p) = \left[2E(p) + a\left(\frac{1}{E^2(p)} + \frac{m^2(p^2 - 5m^2)}{2E^6(p)} - \frac{2m^2 p}{E^4(p)}\frac{\mathrm{d}}{\mathrm{d}p} + \frac{m^2}{E^2(p)}\triangle_p^{(0)}\right)\right]\Phi(p),$$

$$(5.14)$$

for time-component Lorentz-vector structure kernel, $\Gamma\otimes\Gamma = \gamma^0\otimes\gamma^0$,

$$M\Phi(p) = \left[2E(p) + a\left(\frac{2p^2 + 3m^2}{2E^4(p)} - \triangle_p^{(0)}\right)\right]\Phi(p), \qquad (5.15)$$

for Lorentz-vector structure kernel, $\Gamma\otimes\Gamma = \gamma_\mu\otimes\gamma^\mu$,

$$M\Phi(p) = \left[2E(p) - \frac{3am^4}{E^6(p)} - \frac{2am^2 p}{E^4(p)}\frac{\mathrm{d}}{\mathrm{d}p} - a\left(2 - \frac{m^2}{E^2(p)}\right)\triangle_p^{(0)}\right]\Phi(p), \qquad (5.16)$$

73

for Lorentz-pseudoscalar structure kernel, $\Gamma \otimes \Gamma = \gamma_5 \otimes \gamma_5$,

$$M\Phi(p) = \left[2E(p) + a\frac{2p^2 + 3m^2}{2E^4(p)}\right]\Phi(p), \tag{5.17}$$

and, for Böhm-Joos-Krammer (BJK) kernel [25, 26], $\Gamma \otimes \Gamma = \frac{1}{2}(\gamma_\mu \otimes \gamma^\mu + \gamma_5 \otimes \gamma_5 - 1 \otimes 1)$,

$$M\Phi(p) = \left[2E(p) - a\triangle_p^{(0)}\right]\Phi(p). \tag{5.18}$$

Evidently, for the Lorentz-pseudoscalar structure $\gamma_5 \otimes \gamma_5$, the harmonic-oscillator reduced Salpeter equation is represented by a pure multiplication operator. This leads to the continuous eigenvalue spectrum for the Hamiltonian. In other words, there are no bound states.

## 5.3 Transformation to Schrödinger Equation

For nonvanishing mass of bound-state constituents, i.e., $m \neq 0$, the ordinary differential equations corresponding to the harmonic-oscillator reduced Salpeter equation with Lorentz-scalar and Lorentz-vector structure are not the standard form of Schrödinger eigenvalue equations. In order to investigate this analytically, we try to transform both of them to the form of the second-order ordinary differential equation

$$\left[-\frac{d^2}{dp^2} - 2g(p)\frac{d}{dp} + h(p)\right]\Phi(p) = 0. \tag{5.19}$$

This equation involves two functions, $g(p)$ and $h(p)$. The mass eigenvalue of bound state, $M$, appearing in the function $h(p)$ only, is a parameter. By replacing the amplitude $\Phi(p)$ with $\Phi(p) = f(p)\psi(p)$ we obtain the eigenvalue equation for $\psi(p)$

$$\left\{-\frac{d^2}{dp^2} - 2\left[\frac{1}{f(p)}\frac{d}{dp}f(p) + g(p)\right]\frac{d}{dp} + \left[h(p) - 2\frac{g(p)}{f(p)}\frac{d}{dp}f(p) - \frac{1}{f(p)}\frac{d^2}{dp^2}f(p)\right]\right\}\psi(p)$$
$$= 0 . \tag{5.20}$$

In order to transform it to the Schrödinger type operator

$$-\triangle_p^{(0)} + U(p) = -\frac{d^2}{dp^2} - \frac{2}{p}\frac{d}{dp} + U(p), \tag{5.21}$$

we choose function $f(p)$ and $g(p)$ satisfying

$$\frac{1}{f(p)}\frac{\mathrm{d}}{\mathrm{d}p}f(p) + g(p) = \frac{1}{p} \quad , \tag{5.22}$$

it follows

$$f(p) = p\,\exp\left[-\int \mathrm{d}pg(p)\right] \tag{5.23}$$

and leads to

$$\frac{1}{f(p)}\frac{\mathrm{d}^2}{\mathrm{d}p^2}f(p) = g(p)^2 - \frac{\mathrm{d}}{\mathrm{d}p}g(p) - \frac{2g(p)}{p} \ . \tag{5.24}$$

With the aid of Eq. (5.22) and (5.24), the eigenvalue equation (5.20) finally becomes

$$\left\{-\frac{\mathrm{d}^2}{\mathrm{d}p^2} - \frac{2}{p}\frac{\mathrm{d}}{\mathrm{d}p} + \left[h(p) + \frac{\mathrm{d}}{\mathrm{d}p}g(p) + g^2(p)\right]\right\}\psi(p) = 0 \ . \tag{5.25}$$

Corresponding to eigenvalue 0, with the Schrödinger type operator $-\triangle_p^{(0)} + U(p)$, the potential $U(p)$ becomes

$$U(p) = h(p) + \frac{\mathrm{d}}{\mathrm{d}p}g(p) + g^2(p) \ . \tag{5.26}$$

Now we apply this transformation approach to the two Lorentz structure interaction kernels.

- For the kernels of Lorentz-scalar structure $\Gamma \otimes \Gamma = 1 \otimes 1$, recalling the eigenvalue equation (5.14), with simply steps we obtain

$$\left\{-\frac{\mathrm{d}^2}{\mathrm{d}p^2} - 2\left[\frac{1}{p} - \frac{p}{E^2(p)}\right]\frac{\mathrm{d}}{\mathrm{d}p} + \frac{E^2(p)}{am^2}[M - 2E(p)] - \frac{2E^4(p) + m^2p^2 - 5m^4}{2m^2E^4(p)}\right\}\Phi(p)$$

$$= 0. \tag{5.27}$$

Comparing this equation with Eq. (5.19), one easily finds

$$g(p) = \frac{1}{p} - \frac{p}{E^2(p)}, \tag{5.28}$$

$$h(p) = \frac{E^2(p)}{am^2}[M - 2E(p)] - \frac{2E^4(p) + m^2p^2 - 5m^4}{2m^2E^4(p)} \ . \tag{5.29}$$

The integration of $g(p)$ gives $f(p) = E(p)$. By inserting Eq. (5.28) and (5.29) into Eq. (5.26), we obtain the potential

$$U(p) = \frac{E^2(p)}{am^2}[M - 2E(p)] - \frac{1}{m^2} - \frac{1}{2E^2(p)} \ . \tag{5.30}$$

75

Finally the eigenvalue equation (5.20) becomes the standard Schrödinger type equation

$$[-\triangle_p^{(0)} + U(p)]\psi(p) = 0. \tag{5.31}$$

● For the kernels of Lorentz-vector structure $\Gamma \otimes \Gamma = \gamma_\mu \otimes \gamma^\mu$, using the same approach we obtain

$$g(p) = \frac{1}{p} + \frac{m^2 p}{E^2(p)[E^2(p) + p^2]}, \tag{5.32}$$

$$h(p) = \frac{E^2(p)[2E(p) - M]}{a[E^2(p) + p^2]} - \frac{3m^4}{E^4(p)[E^2(p) + p^2]}. \tag{5.33}$$

The integration of $g(p)$ gives

$$f(p) = \frac{E(p)}{\sqrt{E^2(p) + p^2}}. \tag{5.34}$$

Inserting the above equations (5.32) and (5.33) into the potential function (5.26) yields

$$U(p) = \frac{E^2(p)[2E(p) - M]}{a[E^2(p) + p^2]} - \frac{2m^2 p^2}{E^2(p)[E^2(p) + p^2]}. \tag{5.35}$$

In the following, using the path paved above we discuss the harmonic-oscillator reduced Salpeter equation for the exact-propagator case in the frame of Schrödinger type equation.

## 5.4 Exact Propagator Harmonic Oscillator Reduced Salpeter Equation as Differential Equation

In the last section, the harmonic-oscillator reduced Salpeter equation was discussed with free-propagator. In this section we extend it to the exact-propagator case.

With the mass function $m(p^2)$ and wave-function renormalization function $Z(p^2)$ (see Eq. (3.3)), the reduced Salpeter eigenvalue equation for various Lorentz-structure kernel becomes

$$
\begin{aligned}
M\Phi(p) =\ & 2E(p)\Phi(p) \\
& + \frac{1}{2}Z^2(p^2) \int_0^\infty \frac{\mathrm{d}p' p'^2}{(2\pi)^2} \left( \eta_1 V_0 + \eta_2 \frac{m}{E(p)} V_0 \frac{m}{E(p')} + \eta_3 \frac{p}{E(p)} V_1 \frac{p'}{E(p')} \right) \Phi(p'),
\end{aligned}
\tag{5.36}
$$

where the energy $E(p) = \sqrt{p^2 + m^2(p^2)}$.

The corresponding ordinary differential equations for harmonic-oscillator reduced Salpeter equations with exact propagator read:

$$M\Phi(p) = \left[2E(p) - \frac{a}{2}\left(\eta_1 + \frac{\eta_2 m^2 + \eta_3 p^2}{E^2(p)}\right)Z^2(p^2)\triangle_p^{(0)} - a(\eta_3 - \eta_2)\frac{m^2 p}{E^4(p)}Z^2(p^2)\frac{\mathrm{d}}{\mathrm{d}p}\right.$$

$$\left. + \frac{a}{2E^6(p)}\left(3\eta_2 m^4 + \eta_3 p^2(5m^2 + 2p^2)\right)Z^2(p^2)\right]\Phi(p), \tag{5.37}$$

where $m = m(p^2)$ is the mass function of the exact propagator.

## 5.5   Summary and Conclusion

In this chapter we transformed the reduced Salpeter equations with harmonic-oscillator interaction into differential equations. For both free-propagator Salpeter equation and exact-propagator instantaneous Bethe-Salpeter equation with the harmonic-oscillator potential we derived their corresponding eigenvalue equations for various Lorentz structure interaction kernels. For some special kernels such as Lorentz-scalar structure and Lorentz-vector structure, the reduced Salpeter eigenvalue equation can be transformed to the standard Schrödinger type equation which can be computed analytically.

# Appendix A

# Properties of $\gamma$ matrices

In the present work, we use the metric tensor

$$g_{\mu\nu} = g^{\mu\nu} = \begin{pmatrix} 1 & 0 & 0 & 0 \\ 0 & -1 & 0 & 0 \\ 0 & 0 & -1 & 0 \\ 0 & 0 & 0 & -1 \end{pmatrix}. \tag{A.1}$$

The four-vectors are denoted by light italic type and the three-vectors are denoted by bold-face type:

$$x^\mu = (x^0, \boldsymbol{x}), \qquad x_\mu = g_{\mu\nu}x^\nu = (x^0, -\boldsymbol{x}), \tag{A.2}$$

$$p \cdot x = g_{\mu\nu}p^\mu x^\nu = p^0 x^0 - \boldsymbol{p} \cdot \boldsymbol{x}, \tag{A.3}$$

where $\mu, \nu = 0, 1, 2, 3$.

The Dirac $\gamma$ matrices used in this work are

$$\gamma_0 = \begin{pmatrix} I & 0 \\ 0 & -I \end{pmatrix}, \qquad \gamma^i = \begin{pmatrix} 0 & \sigma^i \\ -\sigma^i & 0 \end{pmatrix}, \tag{A.4}$$

$$\gamma^5 \equiv -\mathrm{i}\gamma^0\gamma^1\gamma^2\gamma^3 = -\begin{pmatrix} 0 & I \\ I & 0 \end{pmatrix}, \tag{A.5}$$

where the Pauli matrices are

$$\sigma^1 = \begin{pmatrix} 0 & 1 \\ 1 & 0 \end{pmatrix}, \quad \sigma^2 = \begin{pmatrix} 0 & -\mathrm{i} \\ \mathrm{i} & 0 \end{pmatrix}, \quad \sigma^3 = \begin{pmatrix} 1 & 0 \\ 0 & -1 \end{pmatrix}. \tag{A.6}$$

Trace identities of $\gamma$ matrices

$$\mathrm{tr}(\text{odd number of } \gamma) \;=\; 0 \tag{A.7}$$

$$\mathrm{tr}(\gamma^\mu \gamma^\nu) \;=\; 4g^{\mu\nu} \tag{A.8}$$

$$\mathrm{tr}(\gamma^5) \;=\; 0. \tag{A.9}$$

Hermitian properties of $\gamma$ matrices

$$(\gamma^5)^\dagger \;=\; \gamma^5 \tag{A.10}$$

$$(\gamma^\mu)^\dagger \;=\; \gamma^0 \gamma^\mu \gamma^0. \tag{A.11}$$

Commutation and anti-commutation relations

$$[\gamma^i, \gamma^j] \;=\; -2\mathrm{i}\epsilon_{ijk}\sigma^k I, \tag{A.12}$$

where $\epsilon_{ijk}$ is the antisymmetric symbol with $\epsilon_{123} = 1$,

$$\{\gamma^\mu, \gamma^\nu\} \;=\; 2g^{\mu\nu} \tag{A.13}$$

$$\{\gamma^5, \gamma^\mu\} \;=\; 0. \tag{A.14}$$

# Appendix B

# The Generalized Laguerre Basis for Radial Functions

In the present work we use the generalized Laguerre basis to transform the Salpeter eigenvalue equations to a set of matrix equations as stated in Refs. [88, 89]. In Hilbert space $L_2(R^3)$ all square-integrable functions can be expanded on a complete set of basis functions. Each of which can be expressed as the product of a radial function and an angular function. The latter is represented by a spherical harmonic function $\mathcal{Y}_{lm}(\Omega)$ for angular momentum $l = 0, 1, 2, ...$ and its projection $m = -l, -l+1, ..., +l$. $\mathcal{Y}_{lm}(\Omega)$ depends on the solid angle $\Omega \equiv (\theta, \phi)$ and satisfies the orthonormalization condition

$$\int d\Omega \mathcal{Y}_{lm}^*(\Omega)\mathcal{Y}_{l'm'}(\Omega) = \delta_{ll'}\delta_{mm'}. \tag{B.1}$$

By using Fourier-Bessel transformation, the configuration-space representation $\Phi_i^{(l)}(r)$ and the momentum-space representation $\phi_i^{(l)}(p)$ of the radial functions are related to each other.

$$\phi_i^{(l)}(r) = i^l \sqrt{\frac{2}{\pi}} \int_0^\infty dp \ p^2 j_l(pr)\phi_i^{(l)}(p), \quad i = 0, 1, 2, ... \ , \quad l = 0, 1, 2, ... \ , \tag{B.2}$$

$$\phi_i^{(l)}(p) = (-i)^l \sqrt{\frac{2}{\pi}} \int_0^\infty dr \ r^2 j_l(pr)\phi_i^{(l)}(r), \quad i = 0, 1, 2, ... \ , \quad l = 0, 1, 2, ... \ . \tag{B.3}$$

The spherical Bessel functions of the first kind, $j_n(z)(n = 0, \pm 1, \pm 2, ...)$ [74], are remnants of the angular integration. They can be easily deduced from the expansion

of the plane wave functions over spherical harmonics $\mathcal{Y}_{lm}(\Omega)$ in configuration $(\Omega_r)$ and momentum $(\Omega_p)$ space

$$\exp(i\boldsymbol{p}\cdot\boldsymbol{x}) = 4\pi\sum_{l=0}^{\infty}\sum_{m=-l}^{+l} i^l j_l(pr)\mathcal{Y}_{lm}^*(\Omega_p)\mathcal{Y}_{l'm'}(\Omega_r). \tag{B.4}$$

We choose the radial basis in configuration-space representation

$$\phi_i^{(l)} = \sqrt{\frac{(2\mu)^{2l+3}i!}{\Gamma(2l+i+3)}}\, r^l\exp(-\mu r)L_i^{(2l+2)}(2\mu r), \quad i = 0, 1, 2, \dots, \tag{B.5}$$

where the orthogonal polynomials of generalized-Laguerre type $L_i^{(l)}(x)$ are

$$L_i^{(\gamma)}(x) = \sum_{t=0}^{i}(-1)^t \begin{pmatrix} i+\gamma \\ i-t \end{pmatrix}\frac{x^t}{t!}, \quad i = 0, 1, 2, \dots, \tag{B.6}$$

which satisfy the orthonormal-relation

$$\int_0^{\infty} dx\, x^{\gamma}\exp(-x)L_i^{(\gamma)}(x)L_j^{(\gamma)}(x) = \frac{\Gamma(\gamma+i+1)}{i!}\delta_{ij}, \quad i, j = 0, 1, 2, \dots. \tag{B.7}$$

These basis functions involve one positive real parameter $\mu$ which has the dimension of mass. The normalization condition requires $\mu > 0$. And these radial basis functions satisfy the orthonormalization condition

$$\int_0^{\infty} dr\, r^2\phi_i^{(l)}(r)\phi_j^{(l)}(r) = \delta_{ij}, \quad i, j = 0, 1, 2, \dots. \tag{B.8}$$

The corresponding momentum-space representation $\phi_i^{(l)}(p)$ of the basis function is

$$\phi_i^{(l)}(p) = \sqrt{\frac{(2\mu)^{(2l+3)}i!}{\Gamma(2l+i+3)}}\, \frac{(-i)^l p^l}{2^{l+\frac{1}{2}}\Gamma\left(l+\frac{3}{2}\right)}\sum_{t=0}^{i}\frac{(-1)^t}{t!}\begin{pmatrix} i+2l+2 \\ i-t \end{pmatrix}\frac{\Gamma(2l+t+3)(2\mu)^t}{(p^2+\mu^2)^{(2l+t+3)/2}}$$

$$\times F\left(\frac{2l+t+3}{2}, -\frac{1+t}{2}; l+\frac{3}{2}; \frac{p^2}{p^2+\mu^2}\right), \quad i = 0, 1, 2, \dots. \tag{B.9}$$

The hypergeometric $F(u, v; \omega; z)$ function is given in terms of the gamma function $\Gamma$ by

$$F(u, v; \omega; z) = \frac{\Gamma(\omega)}{\Gamma(u)\Gamma(v)}\sum_{n=0}^{\infty}\frac{\Gamma(u+n)\Gamma(v+n)}{\Gamma(\omega+n)}\frac{z^n}{n!}. \tag{B.10}$$

In the momentum space the radial basis function $\Phi_i^{(l)}(p)$ satisfies the orthonormalization condition

$$\int_0^{\infty} dp\, p^2\phi_i^{*(l)}(p)\phi_j^{(l)}(p) = \delta_{ij}, \quad i, j = 0, 1, 2, \dots. \tag{B.11}$$

82

For all even values of $l$, the basis functions are real

$$\phi_i^{*(l)}(p) = \phi_i^{(l)}(p), \quad l = 0, 2, 4, \dots, \quad i = 0, 1, 2, \dots . \tag{B.12}$$

In this thesis, we mainly use the radial functions for two values $l = 0$ and $l = 1$ of the angular momentum. In momentum space we are just employing the expressions:

$$
\begin{aligned}
\phi_i^{(0)}(p) &= \sqrt{\frac{i!}{\mu\pi\Gamma(i+3)}} \frac{4}{p} \sum_{t=0}^{i} (-2)^t (t+1) \binom{i+2}{i-t} \left(1 + \frac{p^2}{\mu^2}\right)^{-(t+2)/2} \\
&\quad \times \sin\left((t+2)\arctan\frac{p}{\mu}\right) \\
&= \frac{\mathrm{Im}\{(p+i\mu)^{2i+3}[p - i(3+2i)\mu]\}}{\sqrt{\mu\pi(i+1)(i+2)}\, p(p^2+\mu^2)^{2+i}}, \tag{B.13}
\end{aligned}
$$

$$
\begin{aligned}
\phi_i^{(1)}(p) &= -i\sqrt{\frac{\mu^5}{\pi(i+1)(i+2)(i+3)(i+4)}} \frac{8}{p^2} \sum_{t=0}^{i} \frac{(-2)^t}{t!} \binom{i+4}{i-t} \frac{(t+3)!\mu^t}{(p^2+\mu^2)^{(t+3)/2}} \\
&\quad \times \left[\frac{\sqrt{p^2+\mu^2}}{t+2}\sin\left((t+2)\arctan\frac{p}{\mu}\right) - \frac{\mu}{t+3}\sin\left((t+3)\arctan\frac{p}{\mu}\right)\right] \\
&= \frac{i}{2\sqrt{\mu^3\pi(i+1)(i+2)(i+3)(i+4)}\, p^2(p^2+\mu^2)^3} \\
&\quad \times \mathrm{Im}\left\{\frac{(p-i\mu)^{i+5}}{(p+i\mu)^i}[3p^3 + 3i(5+2i)p^2\mu - (5+2i)^2 p\mu^2 - i(5+2i)\mu^3]\right\}. \tag{B.14}
\end{aligned}
$$

# Appendix C

# Formula of $S_\theta(p), C_\theta(p), S_\phi(p), C_\phi(p)$

For convenience of expression, we have made the substitutions:

$$S_\theta(p) \to S_\theta, \ C_\theta(p) \to C_\theta; \ m_i(p) \to m_i, \ E_i(p) \to E_i, \ i = 1, 2. \tag{C.1}$$

In the thesis $S_\theta, C_\theta, S_\phi, C_\phi$ are

$$S_\theta = \sqrt{\frac{E_1 E_2 - p^2 - m_1 m_2}{2 E_1 E_2}}, \ C_\theta = \sqrt{\frac{E_1 E_2 + p^2 + m_1 m_2}{2 E_1 E_2}},$$

$$S_\phi = \sqrt{\frac{E_1 E_2 - p^2 + m_1 m_2}{2 E_1 E_2}}, \ C_\phi = \sqrt{\frac{E_1 E_2 + p^2 - m_1 m_2}{2 E_1 E_2}}.$$

The products of $S_\theta, C_\theta, S_\phi, C_\phi$ can be written as

$$S_\theta S_\phi = p \frac{E_2 - E_1}{2 E_1 E_2}, \qquad S_\theta C_\phi = \frac{|m_1 E_1 - m_2 E_2|}{2 E_1 E_2}, \tag{C.2}$$

$$S_\theta C_\theta = p \frac{|m_1 - m_2|}{2 E_1 E_2}, \qquad C_\theta S_\phi = \frac{m_1 E_2 + m_2 E_1}{2 E_1 E_2},$$

$$C_\theta C_\phi = p \frac{E_2 + E_1}{2 E_1 E_2}, \qquad S_\phi C_\phi = p \frac{m_1 + m_2}{2 E_1 E_2}.$$

If the constituents of bound state have the same masses, i.e., $m_1 = m_2 = m$ and $E_1 = E_2 = E$ we have

$$S_\theta = 0, \ C_\theta = 1,$$

$$S_\phi = \frac{m}{E}, \ C_\phi = \frac{p}{E}. \tag{C.3}$$

# Appendix D

# Codes of the Numerical Calculation

Here we present as an example the computation codes for the numerical calculations of Salpeter eigenvalue equation with time-component Lorentz-vector interaction structure $\Gamma \otimes \Gamma = \gamma^0 \otimes \gamma^0$, and for the relevant computations of the pseudoscalar $u\bar{d}/d\bar{u}$ bound state. These codes are also suitable to other pseudoscalar bound states. All codes are compiled within *Mathematica 5.0*.

## D.1 Codes for the Salpeter Eigenvalue Equation with $\gamma^0 \otimes \gamma^0$ Interaction Structure

*********************************************************************

(* input parameters:
"m1[p]" and "m2[p]" are constituent mass functions of the pseudoscalar bound state;
"Z1[p]" and "Z2[p]" are wave function renormalization function of quark propagator;
"x" is the number of matrix bases. *)

$$m1[p\_] = \frac{0.745}{1 + \frac{p^4}{0.744^4}} + 0.0055;$$

$$m2[p\_] = \frac{0.745}{1 + \frac{p^4}{0.744^4}} + 0.0055;$$

$$\text{Z1}[\text{p}_-] = 1 - \frac{0.545}{1 + \dfrac{\text{p}^2}{1.85508^2}};$$

$$\text{Z2}[\text{p}_-] = 1 - \frac{0.545}{1 + \dfrac{\text{p}^2}{1.85508^2}};$$

$$\lambda = 1;$$

$$\text{x} = 50;$$

$$\mu = 1;$$

(*main program *)

$$\text{phip0}[\text{s}_-, \text{p}_-, \mu_-] := \frac{1}{\sqrt{\pi\mu}\text{p}(\text{p}^2 + \mu^2)^{2+\text{s}}} * \sqrt{\frac{1}{2 + 3\text{s} + \text{s}^2}} * \text{Im}[(\text{p} + \mathtt{i}\mu)^{2\text{s}+3}(\text{p} - \mathtt{i}(3 + 2\text{s})\mu)]$$

(* here the $\mathtt{i}$ denotes the imaginary unit *)

$$\text{phip1}[\text{s}_-, \text{p}_-, \mu_-] := \mathtt{i}\sqrt{\frac{1}{\mu^3(1+\text{s})(2+\text{s})(3+\text{s})(4+\text{s})}} * \frac{1}{2\text{p}^2\sqrt{\pi}(\text{p}^2 + \mu^2)^3} * \text{Im}[\frac{(\text{p} - \mathtt{i}\mu)^{\text{s}+5}}{\text{p} + \mathtt{i}\mu^{\text{s}}}$$

$$* (3\text{p}^3 + 3\mathtt{i}\text{p}^2(5 + 2\text{s})\mu - \text{p}(5 + 2\text{s})^2\mu^2 - \mathtt{i}(5 + 2\text{s})\mu^3)]$$

$$\text{a}[\text{i}_-, \text{j}_-, \mu_-] := \text{NIntegrate}[\text{p}^2 * (\text{m1}[\text{p}]^2 + \text{p}^2) * \text{phip0}[\text{j}, \text{p}, \mu] * \text{phip0}[\text{i}, \text{p}, \mu], \{\text{p}, 0, \infty\}]$$

$$\text{a}[\text{x}_-, \mu_-] := \text{Table}[\text{a}[\text{i} - 1, \text{j} - 1, \mu], \{\text{i}, 1, \text{x}\}, \{\text{j}, 1, \text{x}\}]$$

$$\text{bu1j}[\text{u1}_-, \text{j}_-, \mu_-] := \text{NIntegrate}[\text{p}^2 * \text{Z1}[\text{p}]^2 * \sqrt{\text{m1}[\text{p}]^2 + \text{p}^2} * \text{phip0}[\text{j}, \text{p}, \mu] * \text{phip}[\text{u1}, \text{p}, \mu], \{\text{p}, 0, \infty\}$$

$$\text{bu1j}[\text{x}_-, \mu_-] := \text{Table}[\text{bu1j}[\text{u1} - 1, \text{j} - 1, \mu], \{\text{u1}, 1, \text{x}\}, \{\text{j}, 1, \text{x}\}]$$

$$\text{cju2}[\text{u2}_-, \text{j}_-, \mu_-] := \text{NIntegrate}[\frac{\text{p}^2 * \text{Z1}[\text{p}]^2 * \text{m1}[\text{p}]}{\sqrt{\text{m1}[\text{p}]^2 + \text{p}^2}} * \text{phip0}[\text{u2}, \text{p}, \mu] * \text{phip0}[\text{j}, \text{p}, \mu], \{\text{p}, 0, \infty\}]$$

$$\text{cju2}[\text{x}_-, \mu_-] := \text{Table}[\text{cju2}[\text{u2} - 1, \text{j} - 1, \mu], \{\text{u2}, 1, \text{x}\}, \{\text{j}, 1, \text{x}\}$$

$$\text{du3j}[\text{u3}_-, \text{j}_-, \mu_-] := \text{NIntegrate}[\frac{\text{p}^3 * \text{Z1}[\text{p}]^2}{\sqrt{\text{m1}[\text{p}]^2 + \text{p}^2}} * \text{Conjugate}[\text{phip1}[\text{j}, \text{p}, \mu]] * \text{phip0}[\text{u3}, \text{p}, \mu], \{\text{p}, 0, \infty\}]$$

$$\text{eu4i}[\text{u4}_-, \text{i}_-, \mu_-] := \text{NIntegrate}[\text{p}^3 * \text{Conjugate}[\text{phip1}[\text{i}, \text{p}, \mu]] * \text{phip0}[\text{u4}, \text{p}, \mu], \{\text{p}, 0, \infty\}]$$

eu4i[x_, μ_] := Table[eu4i[u4 − 1, i − 1, μ], {u4, 1, μ}, {i, 1, x}]

fiu5[u5_, i_, μ_] := NIntegrate[p² * m1[p] * phip0[u5, p, μ] * phip[i, p, μ], {p, 0, ∞}]

fiu5[x_, μ_] := Table[fiu5[u5 − 1, i − 1, μ], {u5, 1, x}, {i, 1, x}]

$$v[n_-, u_-, a_-, b_-, beta_-, ell_-, μ_-] := \frac{a}{(2μ)^b} * Sqrt[\frac{n!u!}{Gamma[2ell + 2beta + n + 1]}$$

$$* \frac{1}{Gamma[2ell + 2beta + u + 1]}] * Sum[Sum[\frac{(−1)^{s+r}}{s!r!} * Binomial[n + 2beta + 2ell, n − r]$$

$$*Binomial[u + 2beta + 2ell, u − s] * Gamma[s + r + b + 1 + 2beta + 2ell], \{s, 0, u\}, \{r, 0, n\}]]$$

v1[x_, a_, b_, beta_, ell_, μ_] := Table[v[n − 1, u − 1, a, b, beta, ell, μ], {n, 1, x}, {u, 1, x}]

a = a[x, μ]

b = bu1j[x, μ];

c = cju2[x, μ];

d = du3j[x, μ];

e = eu4i[x, μ];

f = fiu5[x, μ];

Vo = v1[x, λ, 1, 1, 0, μ];

Vl = v1[x, λ, 1, 1, 1, μ];

Msquared = 4 * a + 2 * b . Vo + 2 * c . Vo . f + c .Vo . c . Vo + 2 * Conjugate[d] . Vl . Transpose[e]

        +Conjugate[d] . Vl . Transpose[d] . Vo;

Print["mass eigenvalues"]

Mmatr = Chop[Sqrt[Eigenvalues[Msquared]]]

eigenvec = Chop[Eigenvectors[Msquared]];

Phip[p_] := Table[phip0[s − 1, p, 1], {s, 1, 50}]

MPhip[p_] := eigenvec . Phip[p]

Print["radial Salpeter function $\Phi_2$(p) in momentum space"]

MPhipvx[p_] := Part[eigenvec . Phip[p], x]

MPhipvx1[p_] := Part[eigenvec . Phip[p], x − 1]

MPhipvx2[p_] := Part[eigenvec . Phip[p], x − 2]

Print["Salpeter component function $\Phi_2$(p) of the ground state in momentum space"]

p1 = Plot[MPhipvx[p], {p, 0, 7}, PlotStyle → {Thickness[0.003], RGBColor{[1, 0, 0]}},
    PlotRange → {{0, 1.5}, {−4, 20}}]

Print["Salpeter component function $\Phi_2$(p) of the first excited state in momentum space"]

p2 = Plot[MPhipvx1[p], {p, 0, 7}, PlotStyle → {Thickness[0.003], Dashing[{0.015}],
    {RGBColor{[0, 1, 0]}}, PlotRange → {{0, 1.5}, {−4, 20}}]

Print["Salpeter component function $\Phi_2$(p) of the second excited state in momentum space"]

p3 = Plot[MPhipvx2[p], {p, 0, 7}, PlotStyle → {Thickness[0.003], Dashing[{0.03}],
    RGBColor{[0, 0, 1]}}, PlotRange → {{0, 1.5}, {−4, 20}}]

Show[p1,p2,p3]

Print["Salpeter component function $\Phi_2$(r) in configuration space"]

phir[i_, $\mu$_, r_] := Sqrt[$\dfrac{(2\mu)^3 i!}{\text{Gamma}[3 + i]}$] ∗ Exp[−$\mu$r] ∗ LaguerreL[i, 2, 2$\mu$r]

Phir[r_] := Table[phir[i − 1, $\mu$, r], {i, 1, x}]

pr1[r_] := N[Part[eigenvec . Phir[r], x]]

pr2[r_] := N[Part[eigenvec . Phir[r], x − 1]]

pr3[r_] := N[Part[eigenvec . Phir[r], x − 2]]

Print["Salpeter component function $\Phi_2(r)$ of the ground state in configuration space"]

pr1 = Plot[pr1[r], {r, 0, 16}, PlotStyle → {Thickness[0.003], RGBColor[1, 0, 0]},
    PlotRange → {{0, 16}, {−0.1, 0.4}}]

Print["Salpeter component function $\Phi_2(r)$ of the first excited state in configuration space"]

pr2 = Plot[−pr2[r], {r, 0, 16}, PlotStyle → {Thickness[0.003], Dashing[{0.015}],
    RGBColor[0, 1, 0]}, PlotRange → {{0, 16}, {−0.1, 0.4}}]

Print["Salpeter component function $\Phi_2(r)$ of the second excited state in configuration space"]

pr3 = Plot[pr3[r], {r, 0, 16}, PlotStyle → {Thickness[0.003], Dashing[{0.03}],
    RGBColor[0, 0, 1]}, PlotRange → {{0, 16}, {−0.1, 0.4}}]

Show[pr1, pr2, pr3]

*********************************************************************************

# D.2   Codes for Calculation of the Pseudoscalar Bound State

The numerical calculations of the mass eigenvalue for pseudoscalar bound state in this work are performed by *Mathematica 5.0*. The following *Mathematica* codes are compiled to solve the Salpeter eigenvalue equations with an intanton interaction for the pseudoscalar $u\bar{d}/d\bar{u}$ bound state within Koll's model [20, 21].


*********************************************************************

Print["Exact-propagator instantaneous Bethe-Salpeter equation with an instanton induced interaction"]
Print["u$\bar{\text{d}}$, d$\bar{\text{u}}$"]
(* input parameters:
"m1[p]" and "m2[p]" are u- and d-quark mass function respectively;
"Z1[p]" and "Z2[p]" are renormalization wave function for u- and d-quark propagator respectively;
"ac" and "bc" denote the parameters in the potential $V(r) = a_c + b_c \cdot r$;
"x" is the number of matrix bases used here. *)

91

$$\text{m1}[\text{p}_-] = \frac{0.745}{1 + \dfrac{\text{p}^4}{0.744^4}} + 0.0055;$$

$$\text{m2}[\text{p}_-] = \frac{0.745}{1 + \dfrac{\text{p}^4}{0.744^4}} + 0.0055;$$

$$\text{Z1}[\text{p}_-] = 1 - \frac{0.545}{1 + \dfrac{\text{p}^2}{1.85508^2}};$$

$$\text{Z2}[\text{p}_-] = 1 - \frac{0.545}{1 + \dfrac{\text{p}^2}{1.85508^2}};$$

$$\text{ac} = -1.135;$$

$$\text{bc} = 0.256525;$$

$$\text{x} = 50;$$

$$\mu = 1;$$

(*main program *)

$$\text{phip0}[\text{s}_-, \text{p}_-, \mu_-] := \frac{1}{\sqrt{\pi\mu}\text{p}(\text{p}^2 + \mu^2)^{2+\text{s}}} * \sqrt{\frac{1}{2 + 3\text{s} + \text{s}^2}} * \text{Im}[(\text{p} + \mathtt{i}\mu)^{2\text{s}+3}(\text{p} - \mathtt{i}(3 + 2\text{s})\mu)]$$

(* here the $\mathtt{i}$ denotes the imaginary unit *)

$$\text{phir0}[\text{s}_-, \text{r}_-, \mu_-] := \sqrt{\frac{(2\mu)^3\text{s}!}{\text{Gamma}[3 + \text{s}]}} * \text{Exp}[-\mu\text{r}] * \text{Sum}[(-1)^\text{t} * \text{Binomial}[2 + \text{s}, \text{s} - \text{t}] * \frac{(2\mu\text{r})^\text{t}}{\text{t}!},$$
$$\{\text{t}, 0, \text{s}\}]$$

$$\text{C}_\theta[\text{p}_-] := \text{Sqrt}[\frac{\sqrt{\text{m1}[\text{p}]^2 + \text{p}^2} * \sqrt{\text{m1}[\text{p}]^2 + \text{p}^2} + \text{p}^2 + \text{m1}[\text{p}] * \text{m2}[\text{p}]}{2\sqrt{\text{m1}[\text{p}]^2 + \text{p}^2} * \sqrt{\text{m1}[\text{p}]^2 + \text{p}^2}}]$$

$$\text{a}[\text{i}_-, \text{j}_-, \mu_-] := \text{NIntegrate}[\text{p}^2 * (\sqrt{\text{m1}[\text{p}]^2 + \text{p}^2} + \sqrt{\text{m2}[\text{p}]^2 + \text{p}^2})^2 * \text{phip0}[\text{j}, \text{p}, \mu] * \text{phip0}[\text{i}, \text{p}, \mu],$$
$$\{\text{p}, 0, \infty\}] \quad \text{(* here and in the following, the i is an index symbol *)}$$

$$\text{a}[\text{x}_-, \mu_-] := \text{Table}[\text{a}[\text{i} - 1, \text{j} - 1, \mu], \{\text{i}, 1, \text{x}\}, \{\text{j}, 1, \text{x}\}]$$

$$\text{b}[\text{i}_-, \text{j}_-, \mu_-] := \text{NIntegrate}[\text{p}^2 * (\sqrt{\text{m1}[\text{p}]^2 + \text{p}^2} + \sqrt{\text{m2}[\text{p}]^2 + \text{p}^2}) * \text{Z1}[\text{p}] * \text{Z2}[\text{p}] * \text{C}_\theta[\text{p}]$$
$$*\text{phip0}[\text{j}, \text{p}, \mu] * \text{phip0}[\text{i}, \text{p}, \mu], \{\text{p}, 0, \infty\}]$$

$b[x\_, \mu\_] := Table[b[i - 1, j - 1, \mu], \{i, 1, x\}, \{j, 1, x\}]$

$c[i\_, j\_, \mu\_] := NIntegrate[p^2 * C_\theta[p] * phip0[j, p, \mu] * phip0[i, p, \mu], p, 0, \infty]$

$c[x\_, \mu\_] := Table[c[i - 1, j - 1, \mu], \{i, 1, x\}, \{j, 1, x\}]$

$v[n\_, u\_, a\_, b\_, beta\_, ell\_, \mu\_] := \dfrac{a}{(2\mu)^2} * Sqrt[\dfrac{n!u!}{Gamma[2ell + 2beta + n + 1]}$

$\quad *Gamma[2ell + 2beta + u + 1])] * Sum[Sum[\dfrac{(-1)^{s+r}}{s!r!} * Binomial[n + 2beta + 2ell, n - r]$

$\quad *Binomial[u + 2beta + 2ell, u - s] * Gamma[s + r + b + 1 + 2beta + 2ell], \{s, 0, u\}, \{r, 0, n\}]]$

$v1[x\_, a\_, b\_, beta\_, ell\_, \mu\_] := Table[v[n - 1, u - 1, a, b, beta, ell, \mu], \{n, 1, x\}, \{u, 1, x\}]$

$vlu1u2[u1\_, u2\_, \mu\_] := NIntegrate[r^2 * \dfrac{1}{(2.12845\sqrt{\pi})^3} * Exp[\dfrac{-r^2}{2.12845^2}] * phir0[u2, r, \mu] * phir0[u1, r, \mu],$

$\quad \{r, 0, \infty\}]$

$vlu1u2[x\_, \mu\_] := Table[vlu1u2[u1 - 1, u2 - 1, \mu], \{u2, 1, x\}, \{u1, 1, x\}]$

$A = a[x, \mu];$

$b = b[x, \mu];$

$b = c[x, \mu];$

$vo = ac * IdentityMatrix[x] + v1[x, bc, 1, 1, 0, \mu];$

$vl = vlu1u2[x, \mu];$

$Msquared = A + 2 * b . vo . c - 16 * 1.62 * b . vl . c;$

$Print["mass\ eigenvalues"]$

$Mmatr = Chop[Sqrt[Eigenvalues[Msquared]]] \qquad (*the\ mass\ eigenvalues*)$

$eigenvec = Chop[Eigenvectors[Msquared]];$

$Phip[p\_] := Table[phip0[s - 1, p, 1], \{s, 1, 50\}]$

$MPhip[p\_] := eigenvec . Phip[p]$

$Print["eigenfunctions\ in\ momentum\ space"]$

MPhipvx[p_] := Part[eigenvec . Phip[p], x]

MPhipvx1[p_] := Part[eigenvec . Phip[p], x − 1]

MPhipvx2[p_] := Part[eigenvec . Phip[p], x − 2]

Print["eigenfunction of the ground state in momentum space"]

p1 = Plot[MPhipvx[p], {p, 0, 7}, PlotStyle → {Thickness[0.003], RGBColor{[1, 0, 0]}},

    PlotRange → {{0, 4}, {−3, 16}}]

Print["eigenfunction of the first excited state in momentum space"]

p2 = Plot[MPhipvx1[p], {p, 0, 7}, PlotStyle → {Thickness[0.003], Dashing[{0.015}],

    {RGBColor{[0, 1, 0]}}, PlotRange → {{0, 4}, {−3, 16}}]

Print["eigenfunction of the second excited state in momentum space"]

p3 = Plot[MPhipvx2[p], {p, 0, 7}, PlotStyle → {Thickness[0.003], Dashing[{0.03}],

    RGBColor{[0, 0, 1]}}, PlotRange → {{0, 4}, {−3, 16}}]

Show[p1,p2,p3]

Print["eigenfunctions in configuration space"]

phir[i_, μ_, r_] := Sqrt[$\frac{(2μ)^3 i!}{\text{Gamma}[3 + i]}$] ∗ Exp[−μr] ∗ LaguerreL[i, 2, 2μr]

Phir[r_] := Table[phir[i − 1, μ, r], {i, 1, x}]

pr1[r_] := N[Part[eigenvec . Phir[r], x]]

pr2[r_] := N[Part[eigenvec . Phir[r], x − 1]]

pr3[r_] := N[Part[eigenvec . Phir[r], x − 2]]

Print["eigenfunction of the ground state in configuration space"]

pr1 = Plot[pr1[r], {r, 0, 20}, PlotStyle → {Thickness[0.003], RGBColor[1, 0, 0]},

    PlotRange → {{0, 14}, {−0.2, 0.7}}]

Print["eigenfunction of the first excited state in configuration space"]

pr2 = Plot[pr2[r], {r, 0, 20}, PlotStyle → {Thickness[0.003], Dashing[{0.015}],

RGBColor[0, 1, 0]}, PlotRange → {{0, 14}, {−0.2, 0.7}}]]

Print["eigenfunction of the second excited state in configuration space"]

pr3 = Plot[pr3[r], {r, 0, 20}, PlotStyle → {Thickness[0.003], Dashing[{0.03}],

RGBColor[0, 0, 1]}, PlotRange → {{0, 14}, {−0.2, 0.7}}]]

Show[pr1, pr2, pr3]

*********************************************************************************

Running this code, the mass eigenvalues and plots of eigenfunction in momentum- and configuration-space for the pseudoscalar bound state $u\bar{d}/d\bar{u}$ will be obtained. In the case of free-propagator, one just needs to change the input parameters, i.e. replace the quark mass functions by the corresponding constituent quark masses and at the same time set $Z1[p] = Z2[p] = 1$. This code is also suitable to handle other pseudoscalar quark-antiquark bound states, such as pseudoscalar meson $u\bar{s}/s\bar{u}, u\bar{c}/c\bar{u}, s\bar{c}/c\bar{s}$ and so on - one needs to employ the quark mass functions and the wave function renormalization functions listed in table 4.2.

# Appendix E

# Plots of Eigenfunctions in Momentum Space

## E.1 Plots of Eigenfunctions of the Reduced Salpeter Equation
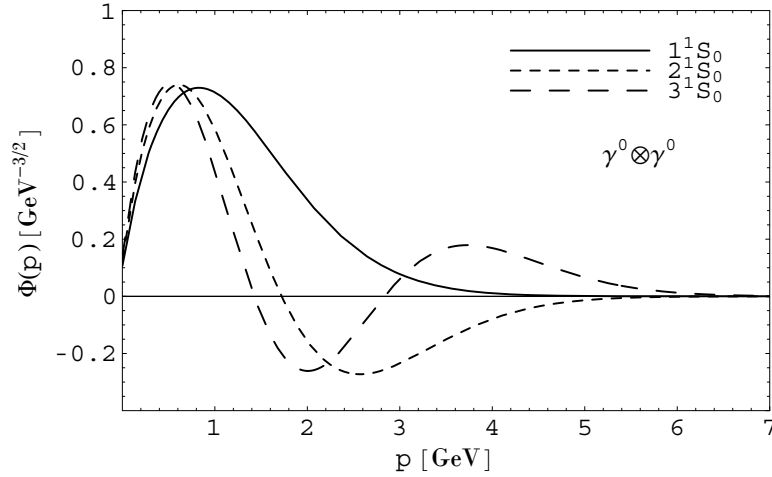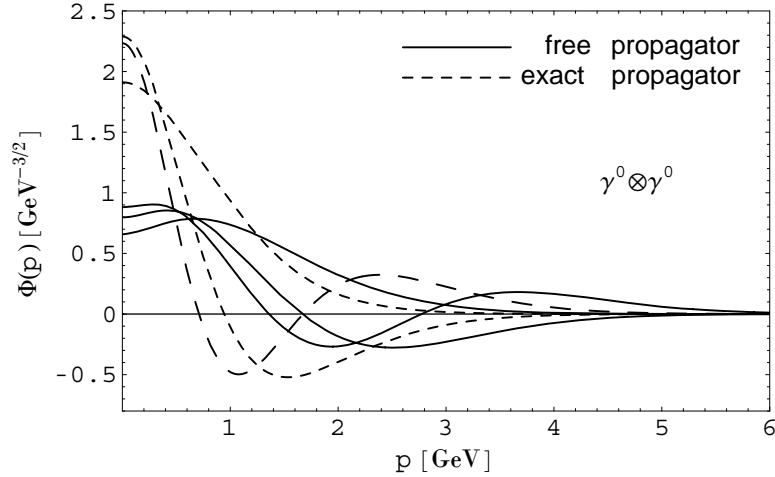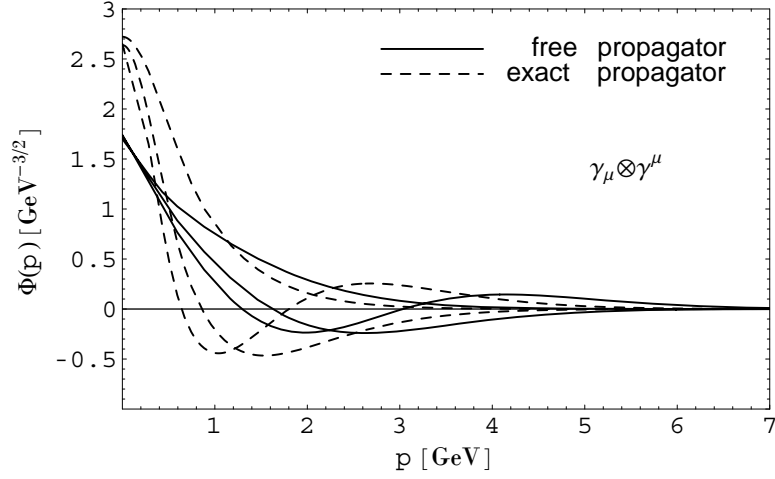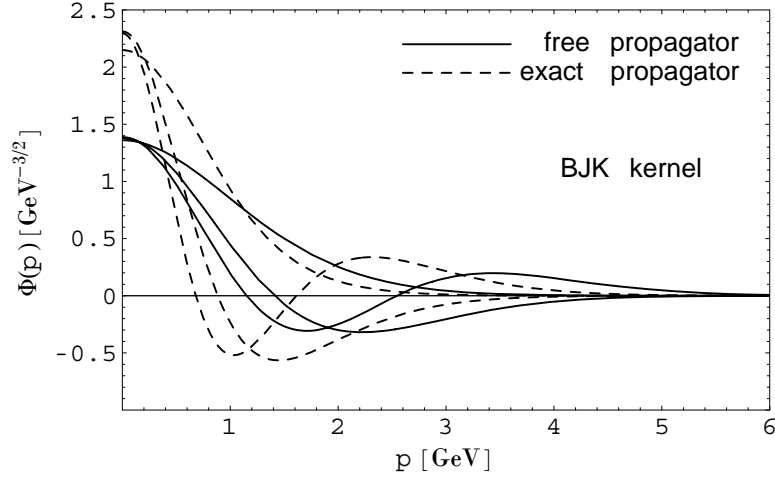


Figure E.1: Eigenfunctions of the reduced Salpeter equation for the three lowest states with vanishing constituent mass $m_1 = m_2 = 0\,GeV$ for time-component Lorentz-vector structure $\Gamma \otimes \Gamma = \gamma_0 \otimes \gamma_0$ with harmonic oscillator potential $V(r) = r^2$.
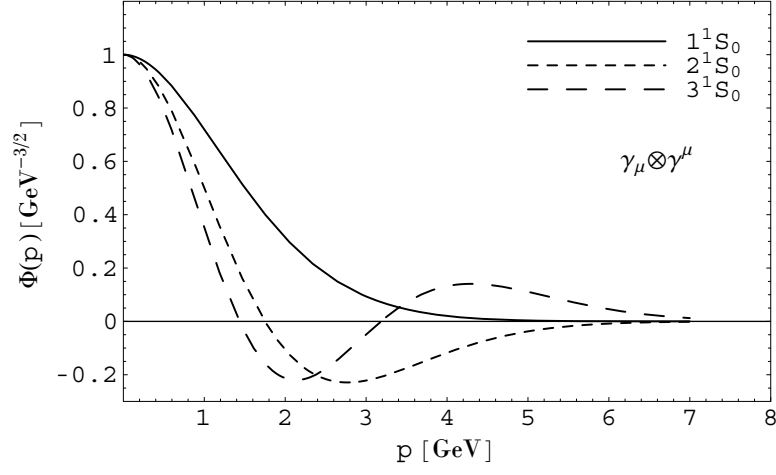
Figure E.2: Eigenfunctions of the reduced Salpeter equation for the three lowest states with vanishing constituent mass $m_1 = m_2 = 0 GeV$ for Lorentz-vector structure $\Gamma \otimes \Gamma = \gamma_\mu \otimes \gamma^\mu$ with harmonic oscillator potential $V(r) = r^2$.
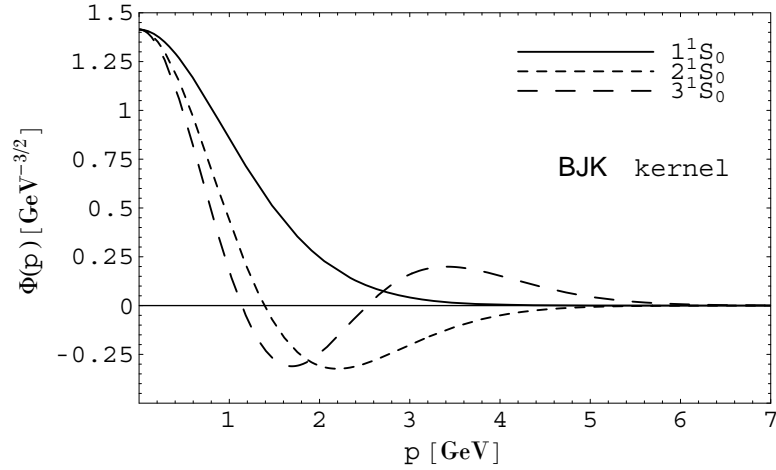


Figure E.3: Eigenfunctions of the reduced Salpeter equation for the three lowest states with vanishing constituent mass $m_1 = m_2 = 0 GeV$ for Böhm-Joos-Krammer (BJK) structure $\Gamma \otimes \Gamma = \frac{1}{2}(\gamma_\mu \otimes \gamma^\mu + \gamma_5 \otimes \gamma_5 - 1 \otimes 1)$ with harmonic oscillator potential $V(r) = r^2$.
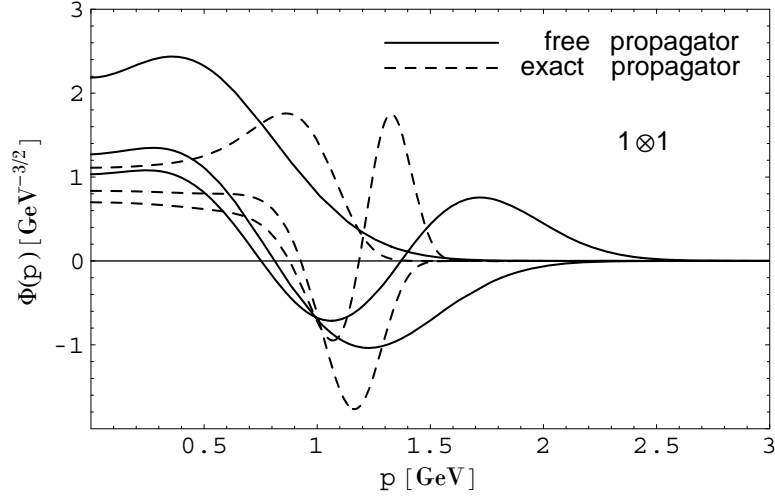
Figure E.4: Eigenfunctions of the reduced Salpeter equation for the three lowest states with light-quark constituent mass $m_1 = m_2 = 0.336 GeV$ (for free-propagator) and renormalization mass function and wave-function renormalization function (3.3), (3.4) (for exact-propagator), with harmonic oscillator potential $V(r) = r^2$, for Lorentz-scalar structure $\Gamma \otimes \Gamma = 1 \otimes 1$.



Figure E.5: Eigenfunctions of the reduced Salpeter equation for the three lowest states with light-quark constituent mass $m_1 = m_2 = 0.336 GeV$ (for free-propagator) and renormalization mass function and wave-function renormalization function (3.3), (3.4), with harmonic oscillator potential $V(r) = r^2$, for time-component Lorentz-vector structure $\Gamma \otimes \Gamma = \gamma_0 \otimes \gamma_0$.

Figure E.6: Eigenfunctions of the reduced Salpeter equation for the three lowest states with light-quark constituent mass $m_1 = m_2 = 0.336 GeV$ (for free-propagator) and renormalization mass function and wave function renormalization function (3.3), (3.4), with harmonic oscillator potential $V(r) = r^2$, for Lorentz-vector structure $\Gamma \otimes \Gamma = \gamma_\mu \otimes \gamma^\mu$.



Figure E.7: Eigenfunctions of the reduced Salpeter equation for the three lowest states with light-quark constituent mass $m_1 = m_2 = 0.38 GeV$ (for free-propagator) and renormalization mass function and wave function renormalization function (3.3), (3.4), with harmonic oscillator potential $V(r) = r^2$, for Böhm-Joos-Krammer (BJK) structure $\Gamma \otimes \Gamma = \frac{1}{2}(\gamma_\mu \otimes \gamma^\mu + \gamma_5 \otimes \gamma_5 - 1 \otimes 1)$.

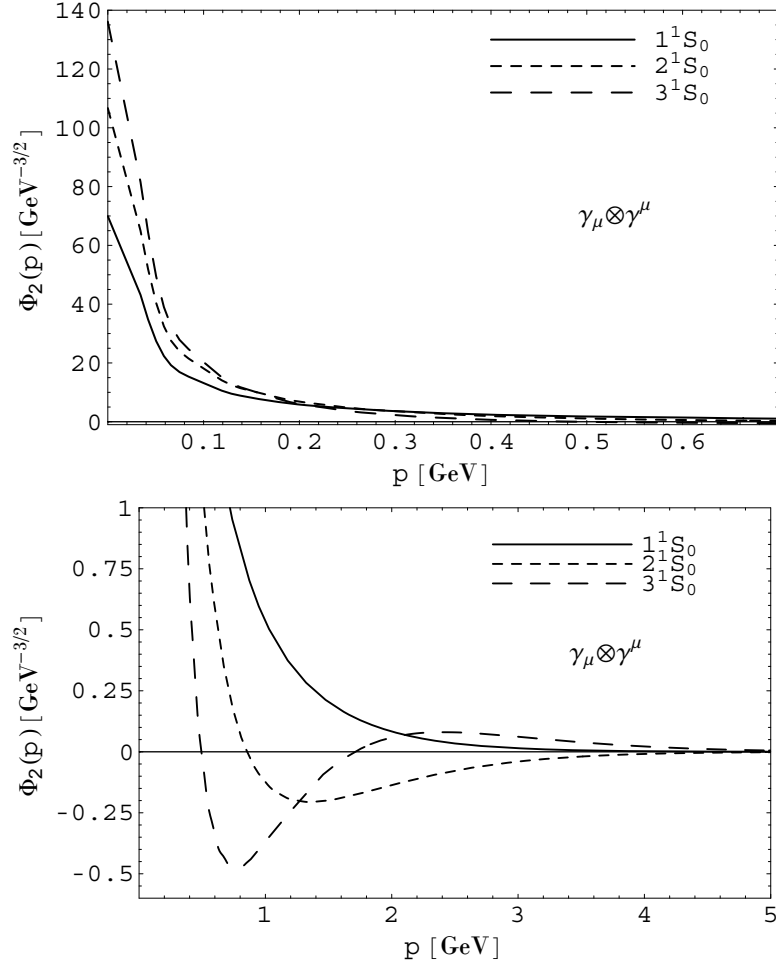## E.2 Plots of Eigenfunctions of the Full Salpeter Equation
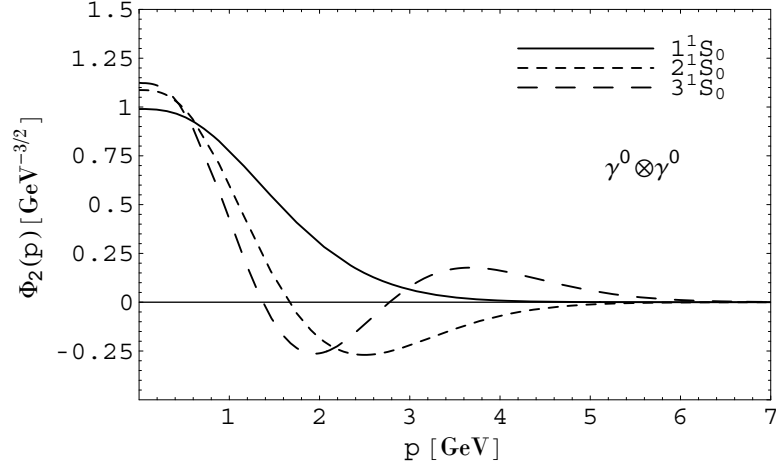


Figure E.8: Salpeter component functions $\Phi_2(p)$ of the free-propagator full Salpeter equation for the three lowest bound states with vanishing constituent mass $m_1 = m_2 = 0 GeV$ for time-component Lorentz-vector structure $\Gamma \otimes \Gamma = \gamma_0 \otimes \gamma_0$ with harmonic oscillator potential $V(r) = r^2$.
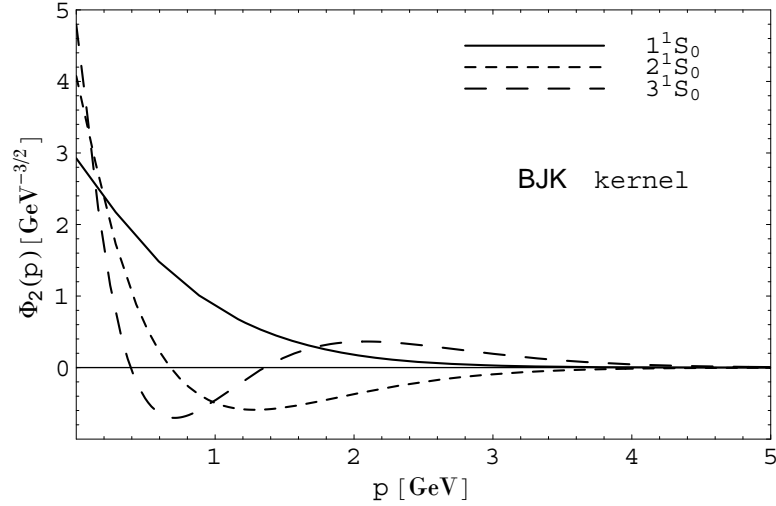


Figure E.9: Salpeter component functions $\Phi_2(p)$ of the free-propagator full Salpeter equation for the three lowest bound states with vanishing constituent mass $m_1 = m_2 = 0 GeV$ for Böhm-Joos-Krammer (BJK) structure $\Gamma \otimes \Gamma = \frac{1}{2}(\gamma_\mu \otimes \gamma^\mu + \gamma_5 \otimes \gamma_5 - 1 \otimes 1)$ with harmonic oscillator potential $V(r) = r^2$.

Figure E.10: Salpeter component functions $\Phi_2(p)$ of the free-propagator full Salpeter equation for the three lowest bound states with vanishing constituent mass $m_1 = m_2 = 0\,GeV$ for Lorentz-vector structure $\Gamma \otimes \Gamma = \gamma_\mu \otimes \gamma^\mu$ with harmonic oscillator potential $V(r) = r^2$. These two figures are the same but with a different scale.
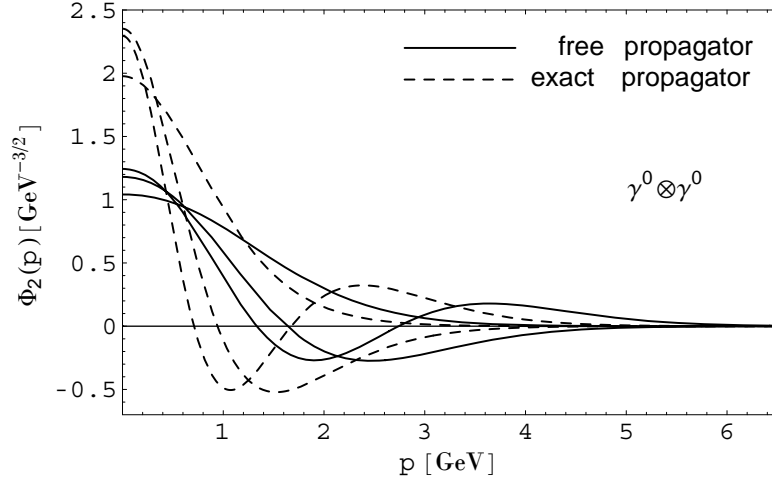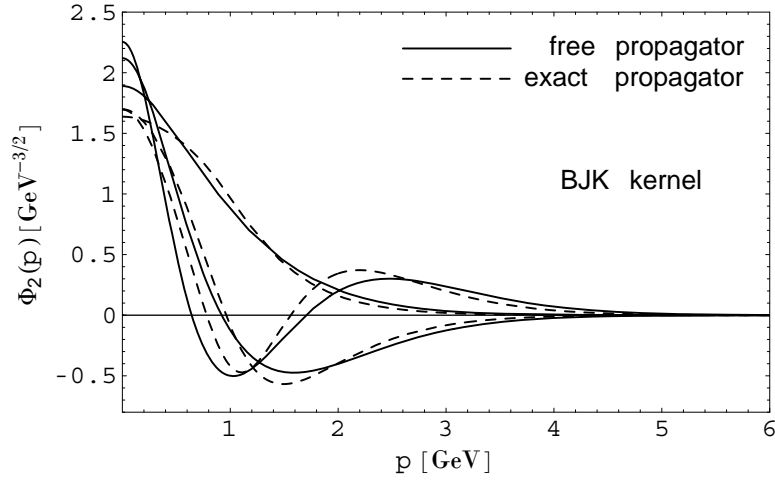
Figure E.11: Salpeter component functions $\Phi_2(p)$ of the free-propagator full Salpeter equation (full lines) and exact-propagator instantaneous Bethe-Salpeter equation (dashed lines) for the three lowest bound states with light-quark constituent mass $m_1 = m_2 = 0.336 GeV$ (for free-propagator) and renormalization mass function and wave-function renormalization function (3.3), (3.4) (for exact-propagator), with harmonic oscillator potential $V(r) = r^2$, for time-component Lorentz-vector structure interaction kernel $\Gamma \otimes \Gamma = \gamma_0 \otimes \gamma_0$.
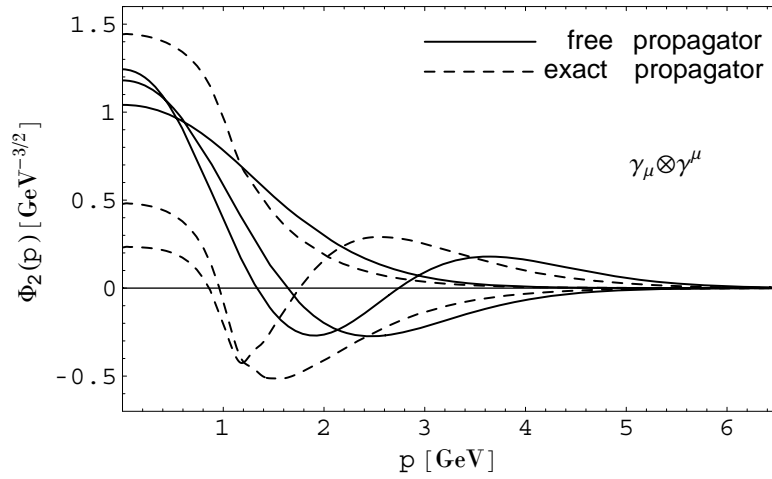


Figure E.12: Salpeter component functions $\Phi_2(p)$ of the free-propagator full Salpeter equation (full lines) and exact-propagator instantaneous Bethe-Salpeter equation (dashed lines) for the three lowest bound states with light-quark constituent mass $m_1 = m_2 = 0.336 GeV$ (for free-propagator) and renormalization mass function and wave-function renormalization function (3.3), (3.4) (for exact-propagator), with harmonic oscillator potential $V(r) = r^2$, for Lorentz-vector structure $\Gamma \otimes \Gamma = \gamma_\mu \otimes \gamma^\mu$.

Figure E.13: Salpeter component functions $\Phi_2(p)$ of the free-propagator full Salpeter equation (full lines) and exact-propagator instantaneous Bethe-Salpeter equation (dashed lines) for the three lowest bound states with light-quark constituent mass $m_1 = m_2 = 0.38 GeV$ (for free-propagator) and renormalization mass function and wave-function renormalization function (3.3), (3.4) (for exact-propagator), with harmonic oscillator potential $V(r) = r^2$, for Böhm-Joos-Krammer (BJK) structure $\Gamma \otimes \Gamma = \frac{1}{2}(\gamma_\mu \otimes \gamma^\mu + \gamma_5 \otimes \gamma_5 - 1 \otimes 1)$.

# E.3 Plot of Eigenfunctions of the Full Salpeter Equation for Mesons
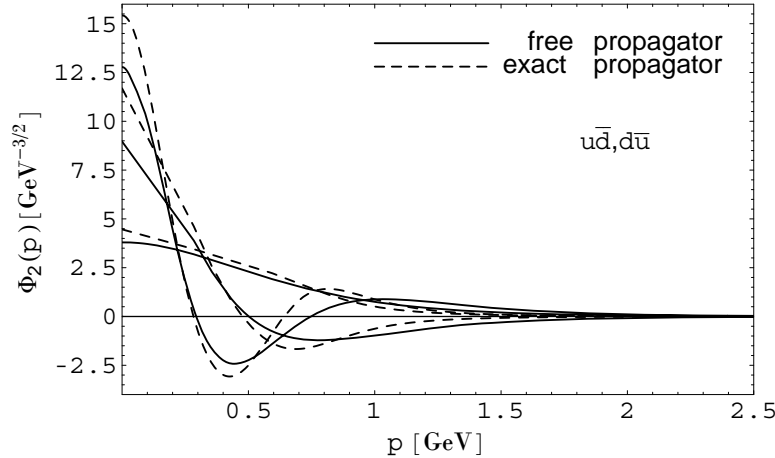


Figure E.14: Salpeter component functions $\Phi_2(p)$ of the three lowest states of instanton-induced Salpeter equation for $u\bar{d}/d\bar{u}$ with free propagator (full lines) and exact propagator (dashed lines) in momentum space.
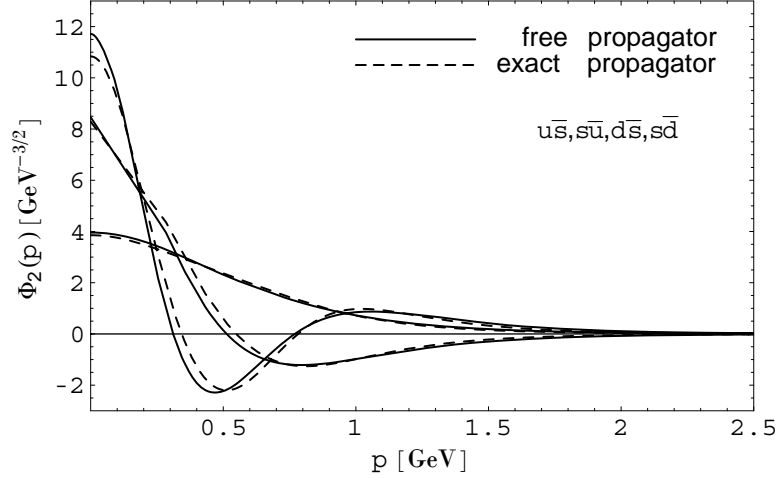
104

Figure E.15: Salpeter component functions $\Phi_2(p)$ of the three lowest states of instanton-induced Salpeter equation for $u\bar{s}/s\bar{u}$; $d\bar{s}/s\bar{d}$ with free propagator (full lines) and exact propagator (dashed lines) in momentum space.
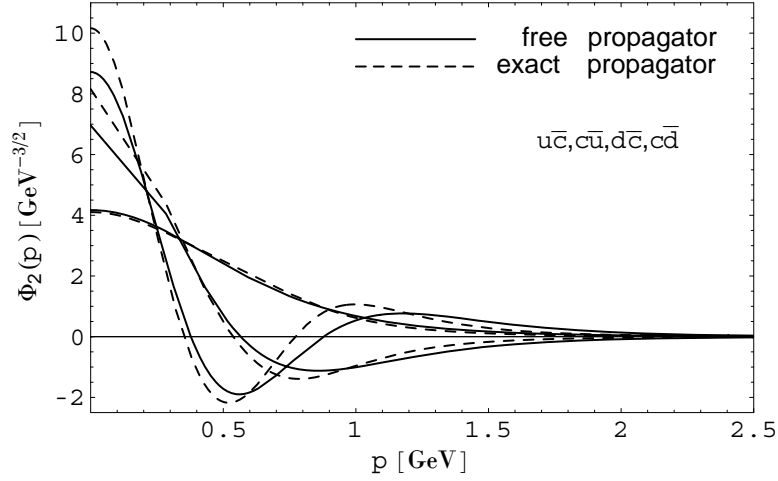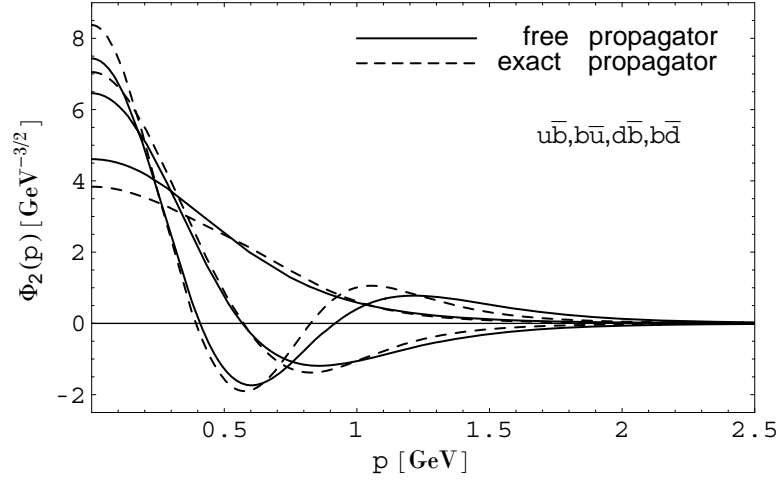


Figure E.16: Salpeter component functions $\Phi_2(p)$ of the three lowest states of instanton-induced Salpeter equation for $u\bar{c}/c\bar{u}$; $d\bar{c}/c\bar{d}$ with free propagator (full lines) and exact propagator (dashed lines) in momentum space.

Figure E.17: Salpeter component functions $\Phi_2(p)$ of the three lowest states of instanton-induced Salpeter equation for $u\bar{b}/b\bar{u}$; $d\bar{b}/b\bar{d}$ with free propagator (full lines) and exact propagator (dashed lines) in momentum space.
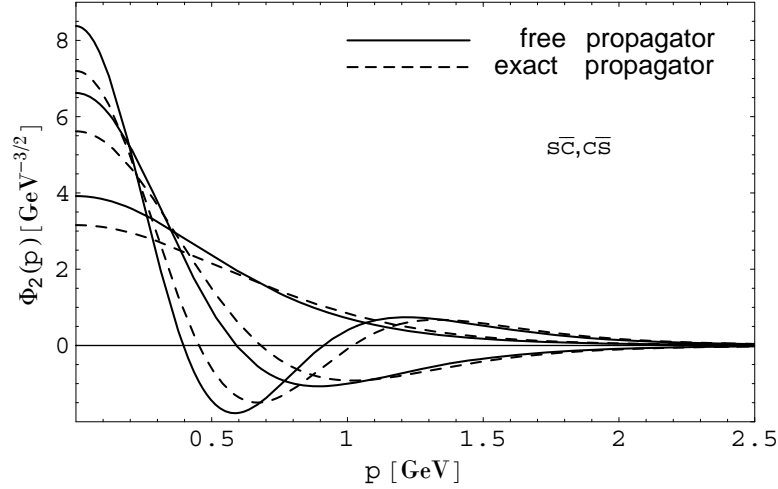


Figure E.18: Salpeter component functions $\Phi_2(p)$ of the three lowest states of instanton-induced Salpeter equation for $s\bar{c}/c\bar{s}$ with free propagator (full lines) and exact propagator (dashed lines) in momentum space.
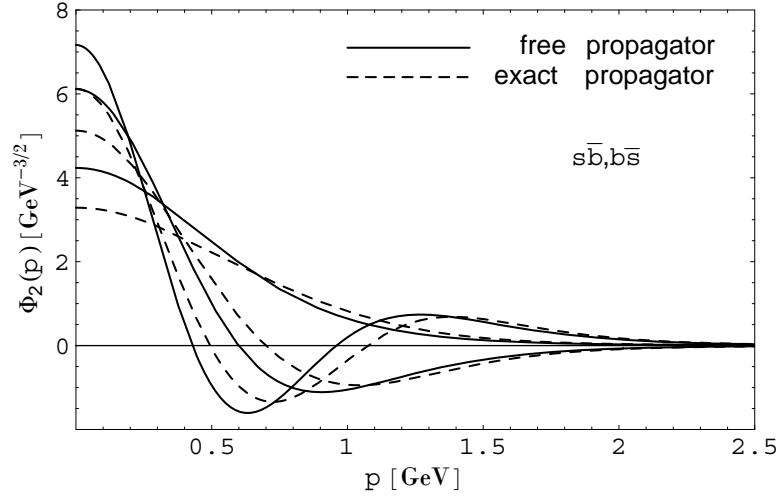
Figure E.19: Salpeter component functions $\Phi_2(p)$ of the three lowest states of instanton-induced Salpeter equation for $s\bar{b}/b\bar{s}$ with free propagator (full lines) and exact propagator (dashed lines) in momentum space.
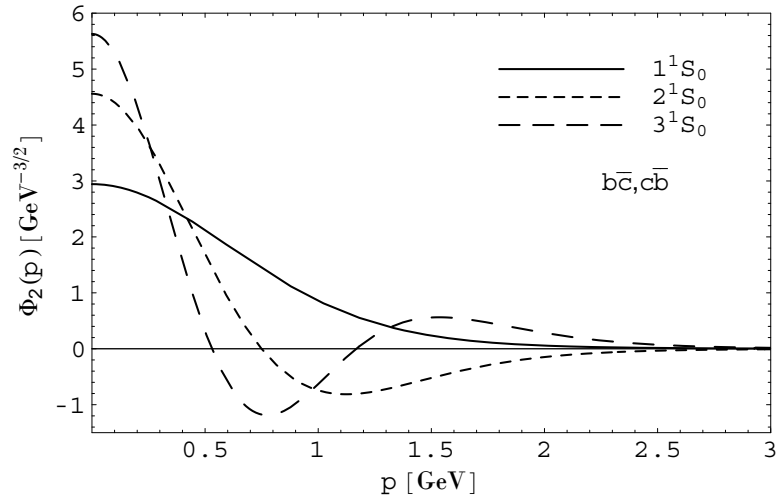


Figure E.20: Salpeter component functions $\Phi_2(p)$ of the three lowest states of instanton-induced Salpeter equation for $b\bar{c}/c\bar{b}$ in momentum space.
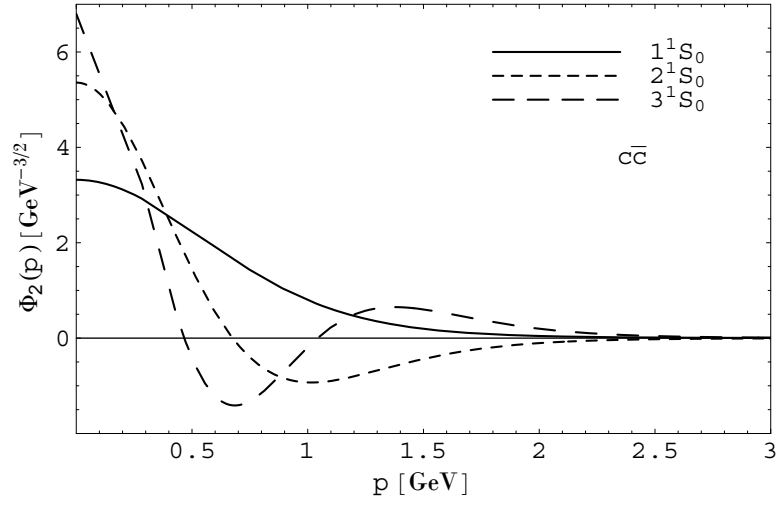
Figure E.21: Salpeter component functions $\Phi_2(p)$ of the three lowest states of instanton-induced Salpeter equation for $c\bar{c}$ in momentum space.
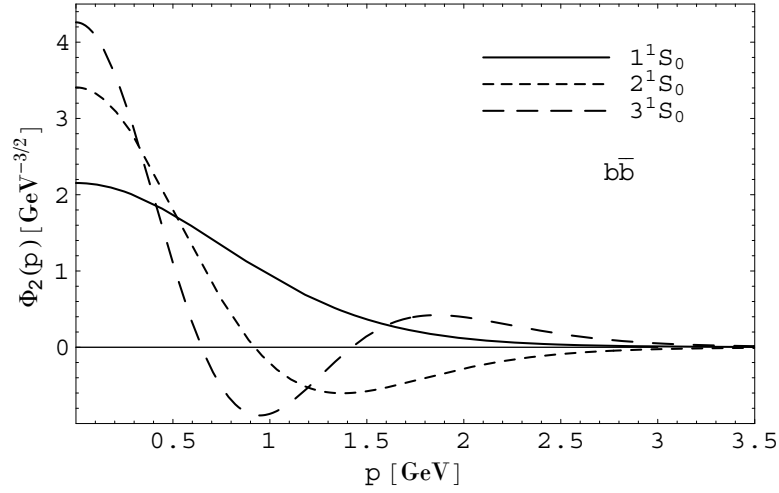


Figure E.22: Salpeter component functions $\Phi_2(p)$ of the three lowest states of instanton-induced Salpeter equation for $b\bar{b}$ in momentum space.

# Bibliography

[1] M. Gell-Mann, Phys. Lett. **8** (1964) 214.

[2] G. Zweig, CERN Reports Nos. CERN TH **401** and **402** (1964).

[3] L. I. Schiff, Phys. Rev. Lett. **17** (1966) 612.

[4] E. E. Salpeter and H. A. Bethe, Phys. Rev. **84** (1951) 1232.

[5] J. Schwinger, Proc. Natl. Acad. Sci. **37** (1951) 455.

[6] H. Kita, Prog. Theor. Phys. **7** (1952) 217.

[7] E. E. Salpeter, Phys. Rev. **87** (1952) 328.

[8] J.-F. Lagaë, Phys. Rev. D **45** (1992) 305.

[9] J.-F. Lagaë, Phys. Rev. D **45** (1992) 317.

[10] Y. Nambu, Prog. Theor. Phys. **5** (1950) 614.

[11] A. B. Henriques, B. H. Kellett, and R. G. Moorhouse, Phys. Lett. B **64** (1976) 85.

[12] S. Jacobs, M. G. Olsson, and C. J. Suchyta III, Phys. Rev. D **35** (1987) 2448.

[13] W. Lucha, H. Rupprecht, and F. F. Schöberl, Phys. Rev. D **45** (1992) 385.

[14] W. Lucha and F. F. Schöberl, J. Phys. G: Nucl. Part. Phys. **31** (2005) 1133, hep-th/0507281.

[15] C. H.  Llewellyn Smith, Ann. Phys. **53** (1969) 521.

[16] A. Le Yaouanc, L. Oliver, S. Ono, O. Pene, and J. C. Raynal, Phys. Rev. D **31** (1985) 137.

[17] M. G. Olsson, S. Veseli, and K. Williams, Phys. Rev. D **52** (1995) 5141, hep-ph/9503477.

[18] M. G. Olsson, S. Veseli, and K. Williams, Phys. Rev. D **53** (1996) 504, hep-ph/9504221.

[19] W. H. Blask, U. Bohn, M. G. Huber, B. C. Metsch, and H. R. Petry, Z. Phys. A **337** (1990) 327.

[20] M. Koll, R. Ricken, D. Merten, B. C. Metsch, and H. R. Petry, Eur. Phys. J. A **9** (2000) 73-94, hep-ph/0008220;
M. Koll, *Electroweak processes with light mesons in a relativistic quark model*, Ph. D. Thesis, University of Bonn (2001).

[21] R. Ricken, M. Koll, D. Merten, B. C. Metsch, and H. R. Petry, Eur. Phys. J. A **9** (2000) 221-244;
R. Ricken, *Properties of light mesons in a relativistic quark model*, Ph. D. Thesis, University of Bonn (2001).

[22] D. Merten, R. Ricken, M. Koll, B. Metsch, and H. Petry, Eur. Phys. J. A **13** (2002) 477;
D. Merten, *Hadron form factors and decays*, Ph. D. Thesis, University of Bonn (2002).

[23] W. Lucha, K. Maung Maung, and F. F. Schöberl, Phys. Rev. D **63** (2001) 056002, hep-ph/0009185.

[24] J. Parramore and J. Piekarewicz, Nucl. Phys. A **585** (1995) 705, nucl-th/9402019.

[25] M. Böhm, H. Joos, and M. Krammer, Nucl. Phys. B **51** (1973)397.

[26] F. Gross and J. Milana, Phys. Rev. D **43** (1991) 2401.

[27] C. Alabiso and G. Schierholz, Nucl. Phys. B **110** (1976) 81.

[28] C. Alabiso and G. Schierholz, Nucl. Phys. B **126** (1977) 461.

[29] G. C. Wick, Phys. Rev. **96** (1954) 1124.

[30] R. E. Cutkosky, Phys. Rev. **96** (1954) 1135.

[31] H. Pagels, Phys. Rev. D **15** (1977) 2991.

[32] T. Hofsäss and G. Schierholz, Phys. Lett. B **76** (1978) 125.

[33] R. Roth, Nucl. Phys. B **154** (1979) 21.

[34] M. Böhm, Nucl. Phys. B **91** (1975) 494.

[35] P. Maris and C. D. Roberts, Phys. Rev. C **56** (1997) 3369, nucl-th/9708029.

[36] P. Maris and C. D. Roberts, in: Proc. of the IVth Int. Workshop on *Progress in Heavy Quark Physics*, edited by M. Beyer, T. Mannel, and H. Schröder (University of Rostock, Rostock, 1998), p. 159, nucl-th/9710062.

[37] W.-M. Yao et al. (Particle Data Group), J. Phys. G **33** 1 (2006) and 2007 partial update for the 2008 edition.

[38] W. Lucha, F. F. Schöberl, and D. Gromes, Phys. Rep. **200** (1991) 127.

[39] W. Lucha and F. F. Schöberl, Int. J. Mod. Phys. A **7** (1992) 6431.

[40] P. Maris and P. C. Tandy, Phys. Rev. C **60** (1999) 055214, nucl-th/9905056.

[41] P. Maris, Nucl. Phys. A **663** (2000) 621, nucl-th/9908044.

[42] C. D. Roberts and S. M. Schmidt, Prog. Part. Nucl. Phys. **45** (2000) S1, nucl-th/0005064.

[43] C. D. Roberts, nucl-th/0007054.

[44] R. Alkofer and L. von Smekal, Phys. Rep. **353** (2001) 281, hep-ph/0007355.

[45] P. Maris, in: Proc. of the Int. Conf. on *Quark Confinement and the Hadron Spectrum IV*, edited by W. Lucha and K. Maung Maung (World Scientific, New Jersey/London/Singapore/Hong Kong, 2002), p. 163, nucl-th/0009064.

[46] P. Maris and P. C. Tandy, nucl-th/0109035.

[47] P. Maris, A. Raya, C. D. Roberts, and S. M. Schmidt, Eur. Phys. J. A **18** (2003) 231, nucl-th/0208071.

[48] M. S. Bhagwat, M. A. Pichowsky, and P. C. Tandy, Phys. Rev. D **67** (2003) 054019, hep-ph/0212276.

[49] P. C. Tandy, Prog. Part. Nucl. Phys. **50** (2003) 305, nucl-th/0301040.

[50] P. Maris and C. D. Roberts, Int. J. Mod. Phys. E **12** (2003) 297, nucl-th/0301049.

[51] M. S. Bhagwat, M. A. Pichowsky, C. D. Roberts, and P. C. Tandy, Phys. Rev. C **68** (2003) 015203, nucl-th/0304003.

[52] C. D. Roberts, Lect. Notes Phys. **647** (2004) 149, nucl-th/0304050.

[53] A. Krassnigg and C. D. Roberts, Fizika B **13** (2004) 143, nucl-th/0308039.

[54] A. Krassnigg and C. D. Roberts, Nucl. Phys. A **737** (2004) 7, nucl-th/0309025.

[55] R. Alkofer, W. Detmold, C. S. Fischer, and P. Maris, Phys. Rev. D **70** (2004) 014014, hep-ph/0309077.

[56] A. Krassnigg and P. Maris, J. Phys. Conf. Ser. **9** (2005) 153, nucl-th/0412058.

[57] L. J. Nickish, L. Durand, and B. Durand, Phys. Rev. D **30** (1984) 660.

[58] L. Durand and A. Gara, J. Math. Phys. **31** (1990) 2237.

[59] S. Jacobs, M. G. Olsson, and C. J. Suchyta III, Phys. Rev. D **33** (1986) 3338.

[60] S. Jacobs, M. G. Olsson, and C. J. Suchyta III, Phys. Rev. E **34** (1986) 3536.

[61] L. C. Hostler and W. W. Repko, Ann. Phys. (N.Y.) **130** (1980) 329.

[62] J. Parramore, H.-C. Jean, and J. Piekarewicz, Phys. Rev. C **53** (1996) 2449, nucl-th/9510024.

[63] W. Lucha, K. Maung Maung, and F. F. Schöberl, in: Proc. of the Int. Conf. on *Quark Confinement and the Hadron Spectrum IV*, edited by W. Lucha and K. Maung Maung (World Scientific, New Jersey/London/Singapore/Hong Kong, 2002), p. 340, hep-ph/0010078.

[64] W. Lucha, K. Maung Maung, and F. F. Schöberl, Phys. Rev. D **64** (2001) 036007, hep-ph/0011235.

[65] W. Lucha and F. F. Schöberl, Int. J. Mod. Phys. A **17** (2002) 2233, hep-ph/0109165.

[66] P. Maris, Phys. Rev. D **50** (1994) 4189.

[67] J. Resag and C. R. Münz, Nucl. Phys. A **590** (1995) 735, hep-ph/9407033.

[68] G. Zöller, S. Hainzl, C. R. Münz, and M. Beyer, Z. Phys. C **68** (1995) 103, hep-ph/9412355.

[69] E. Klempt, B. C. Metsch, C. R. Münz and H. R. Petry, Phys. Lett. B **361** 160, hep-ph/9507449.

[70] C. R. Münz, J. Resag, B. C. Metsch, H. R. Petry, Phys. Rev. C **52** (1995) 2110, nucl-th/9406035.

[71] C. R. Münz, Nucl. Phys. A **609** (1996) 364, hep-ph/9601206.

[72] R. Alkofer, W. Detmold, C. S. Fischer, and P. Maris, Nucl. Phys. Proc. Suppl. **141** (2005) 122, hep-ph/0309078.

[73] P. O. Bowman, U. M. Heller, D. B. Leinweber, M. B. Parappilly, A. G. Williams, and J.-B. Zhang, Phys. Rev. D **71** (2005) 054507, hep-lat/0501019.

[74] *Handbook of Mathematical Functions*, edited by M. Abramowitz and I. A. Stegun (Dover, New York, 1964).

[75] T. Babutsidze, T. Kopaleishvili, and A. Rusetsky, Phys. Lett. B **426** (1998) 139, hep-ph/9710278.

[76] T. Babutsidze, T. Kopaleishvili, and A. Rusetsky, Phys. Rev. C **59** (1999) 976, hep-ph/9807485.

[77] T. Kopaleishvili, Phys. Part. Nucl. **32** (2001) 560, hep-ph/0101271.

[78] T. Babutsidze, T. Kopaleishvili, and D. Kurashvili, Georgian Electronic Scientific J.: Phys. **1** (2004) 20, hep-ph/0308072.

[79] W. Lucha and F. F. Schöberl, Phys. Rev. A **56** (1997) 139, hep-ph/9609322.

[80] R. Ricken, M. Koll, D. Merten, and B. C. Metsch, Eur. Phys. J. A **18** (2003) 667.

[81] A. Gara, B. Durand, L. Durand and L. J. Nickisch, Phys. Rev. D **40** (1989) 843.

[82] A. Gara, B. Durand, and L. Durand, Phys. Rev. D **42** (1990) 1651; *ibid.* **43** (1991) 2447 (erratum).

113

[83] M. Beyer, U. Bohn, M. G. Huber, B. C. Metsch, and J. Resag, Z. Phys. C **55** (1992) 307.

[84] G. 't Hooft, Phys. Rev. D **14** (1976) 3432.

[85] M. A. Shifman, A. I. Vainshtein, and V. I. Zakharov, Nucl. Phys. B **163** (1980) 46.

[86] H. R. Petry, H. Hofestädt, S. Merk, K. Bleuler, H. Bohr, and K. S. Narain, Phys. Lett. B **159** (1985) 363.

[87] J. Resag, C. R. Münz, B. C. Metsch, H. R. Petry, Nucl. Phys. A **578** (1994) 397;
J. Resag, *Analysis of the instantaneous Bethe-Salpeter equation and its application to $q\bar{q}$ bound states*, Ph. D. Thesis, University of Bonn (1994).

[88] W. Lucha and F. F. Schöberl, Int. J. Mod. Phys. A **14** (1999) 2309, hep-ph/9812368.

[89] W. Lucha and F. F. Schöberl, Fizika B **8** (1999) 193, hep-ph/9812526.

[90] W. Lucha and F. F. Schöberl, Recent Res. Devel. Physics **5** (2004) 1423, hep-ph/0408184.

[91] W. Lucha and F. F. Schöberl, preprint HEPHY-PUB 844/07 (2007), arXiv:0707.1440 [hep-ph], to appear in the Proceedings of *QCD @ Work 2007, International Workshop on Quantum Chromodynamics - Theory and Experiment*, Martina Franca, Italy, June 16-20, 2007.

[92] H. Pietschmann, *Formulae and Results in Weak Interactions* (Springer-Verlag, Wien, New york, 1974).

[93] D. Lurie, *Particles and Fields* (Interscience, New York, 1968).

[94] Z.-F. Li, W. Lucha, and F. F. Schöberl, Mod. Phys. Lett. A **21** (2006) 1657.

[95] Z.-F. Li, W. Lucha, and F. F. Schöberl, Phys. Rev. D **76** (2007) 125028.

[96] Z.-F. Li, W. Lucha, and F. F. Schöberl, arXiv:0712.2947 [hep-ph].

[97] T. Murota, Prog. Theor. Phys. **69** (1983) 181.

[98] A. Le Yaouanc, L. Oliver, S. Ono, O. Pène, and J.-C. Raynal, Phys. Rev. D **31** (1985) 137.

[99] D. Lurié, A. J. MacFarlane, and Y. Takahashi, Phys. Rev. **140** (1965) 1091.

[100] C. Long, Phys. Rev. D **30** (1984) 1970.

[101] C. R. Münz, J. Resag, B. C. Metsch, and H. R. Petry, Nucl. Phys. A **578** (1994) 418.

[102] T. Feldmann, P. Kroll, and B. Stech, Phys. Rev. D **58** (1998) 114006.

# Acknowledgements

First of all, I would like to thank my supervisor Prof. Dr. Franz Schöberl for his guidance and help. I thank Prof. Herbert Pietschmann for introducing me into our institute. I also thank Dr. Wolfgang Lucha for his helpful discussion.

I am grateful to the Institute of Theoretical Physics at University of Vienna for giving the pleasant and inspiring working environment. I thank for Dr. Dmitri Melikhov's friendship and for Prof. Dr. Walter Grimus's lecture. It is also my pleasure to thank my colleagues, especially Mr. Helmut Kübök. With his help I finished the relevant paperwork.

Last, but certainly not least, I thank my family for their encouragement and support.

# Curriculum Vitae

**Name:**        Zhifeng Li

**Date of birth:**    10-05-1977

**Place of birth:**   Shanxi, China

**Degrees:**       B.S., Applied Physics, Chongqing University, China, 1999;
M.S., Theoretical Physics, Chongqing University, China, 2003;
Ph.D. Study, Theoretical Physics, University of Vienna,
Austria, starting from Nov. 2004.

### Reports:

**1.** Mar. 20, 2006, "Exact-Propagator Instantaneous Bethe-Salpeter Equation for Quark-Antiquark Bound States", in the Institute of Theoretical Physics, Chinese Academy of Sciences, Beijing, China.

**2.** Mar. 26, 2007, "Analyzing the Instantaneous Bethe-Salpeter Equation with Exact Propagators for Quark-Antiquark Bound States", in the Institute of Nuclear Physics, Vienna University of Technology, Austria.

**3.** Oct. 10, 2008, "Pseudoscalar Fermion-Antifermion Bound States–Analyzing the Salpeter Equation", in the Department of Physics, Chongqing University, China.

### Conferences:

**1.** Sept. 27-29, 2005, 55. Jahrestagung der Österreichischen Physikalischen Gesellschaft, Vienna, Austria.

**2.** Sept. 16, 2006, the 6th symposium of the Chinese Scholars in Austria, with poster: Exact-propagator instantaneous Bethe-Salpeter equation for quark-antiquark bound states.

**3.** Dec. 01-03, 2006, the 3rd Vienna Central European Seminar, University of Vienna, Austria, with poster: Eigenvalue Spectrum of the Reduced Salpeter Equation

with Harmonic Interaction by Solving the Corresponding Differential Equation.

**4.** Nov. 29 - Dec. 2, 2007, the 4th Vienna Central European Seminar, University of Vienna, Austria, with poster: Stability in the instantaneous Bethe-Salpeter formalism: reduced exact-propagator bound-state equation with harmonic interaction.

**Publications:**

**1.** Zhi-Feng Li, Jin-Jin Liu, Wolfgang Lucha, Wen-Gan Ma, Franz F. Schöberl, **Relativistic Harmonic Oscillator.** Journal of Mathematical Physics **46**, (2005) 103514, hep-ph/0501268;

**2.** Zhi-Feng Li, W. Lucha, Franz F. Schöberl, **Exact-Propagator Instantaneous Bethe-Salpeter Equation for Quark-Antiquark Bound States.** Mod. Phys. Lett. A **21** (2006) 1657, hep-ph/0510372;

**3.** Zhi-Feng Li, W. Lucha, Franz F. Schöberl, **Stability in the instantaneous Bethe-Salpeter formalism: Harmonic-oscillator reduced Salpeter equation.** Phys. Rev. D **76** (2007) 125028, arXiv:0707.3202 [hep-ph];

**4.** Zhi-Feng Li, W. Lucha, Franz F. Schöberl, **Stability in the instantaneous Bethe-Salpeter formalism: Reduced exact-propagator bound-state equation with harmonic interaction.** J.Phys.G **35** (2008) 115002, arXiv:0712.2947 [hep-ph].